OSCILLATORY FLOW AND HEAT TRANSFER CHARACTERISTICS IN A PIPE AND A PACKED COLUMN

A DISSERTATION SUBMITTED TO THE GRADUATE DIVISION OF THE UNIVERSITY OF HAWAII IN PARTIAL FULFILLMENT OF THE REQUIREMENTS FOR THE DEGREE OF

DOCTOR OF PHILOSOPHY

IN

MECHANICAL ENGINEERING

AUGUST 1995

By

Tianshou Zhao

Dissertation Committee:

Ping Cheng, Chairperson
Beei-Huan Chao
Ronald H. Knapp
Lloyd H. Hihara
Clark C. K. Liu

ACKNOWLEDGMENTS

I would like to express my most sincere gratitude to my advisor, Professor Ping Cheng, for introducing me to the study of the interesting field of oscillatory fluid flow and the associated heat transfer phenomena. Without his forceful encouragement, constructive criticism and enthusiastic guidance, this work would not have been possible.

Special thanks are extended to Professors Beei-Huan Chao, Ronald H. Knapp, Lloyd H. Hihara and Clark C. K. Liu, for serving on my thesis committee and offering suggestions for improving this thesis.

I would like to thank the Mechanical Engineering Department at the University of Hawaii for providing financial support which enables me to complete my Ph. D program. Appreciation is expressed to Drs. Patrick E. Phelan, Mehrdad Ghasemi Nejhad, and Chao-Yang Wang for their very kind help during my studies. I am also grateful to Mr. Benjsmin L. Respicio and Northrup H. Castle, Jr., for their help in the construction of the experimental apparatus. Special thanks go to my officemates, Oliver Easterday and Jocelyn Bayliss, for their assistance during this work.

I want to thank my parents and my brothers for their constant support and encouragement beginning from my first grade of elementary school to Ph. D. Finally, very special thanks go to my lovely wife and daughter, for without their love, patience and understanding, this work would not have been possible.

ABSTRACT

The fluid flow and heat transfer characteristics in a pipe subjected to a periodically oscillatory and reversing flow have been investigated numerically and experimentally. An examination of the governing equations and boundary conditions shows that the governing similarity parameters for the oscillatory flow in a pipe of finite length are the kinetic Reynolds number, the dimensionless oscillation amplitude of the fluid, and the length to diameter ratio of the pipe. An experimental study on the onset of turbulence found that the changes in the sign of the pressure gradient are directly responsible for the occurrence of instability in an oscillatory and reversing pipe flow. Friction coefficients of a fully developed laminar oscillating and reversing pipe flow were investigated analytically and experimentally. The numerical simulation of a sinusoidally oscillatory and reversing flow in a pipe of finite length shows that, at any instant of time, there exist three flow regimes in the pipe: an entrance regime, a fully developed regime, and an exit regime. Based on the numerical results, a correlation equation of the space-cycle averaged friction coefficient was obtained. For forced heat convection in an oscillatory flow, it was found that the Prandtl number is the additional similarity parameter, besides the kinetic Reynolds number, the dimensionless oscillation amplitude of the fluid, and the length to diameter ratio of the heated pipe. The numerical results of the associated heat transfer problem reveal that annular effects also exist in the temperature profiles of an oscillatory flow at high kinetic Reynolds numbers near the entrance and exit locations of the pipe. The space-cycle averaged Nusselt numbers of air oscillating in a pipe heated at constant temperature and uniform heat flux were obtained based on either the numerical results or the experimental data. The related problem of pressure drop in an oscillatory flow through a woven-screen packed column has also been investigated experimentally.

TABLE OF CONTENTS

ACKNOWLEDGMENTS....iii

ABSTRACT....iv

LIST OF TABLES....viii

LIST OF FIGURES....ix

NOMENCLATURE....xiv

1. INTRODUCTION....1

   1.1 Background....1

   1.2 Review of Literature....2

   1.3 Objectives of Present Investigation....8

2. GOVERNING EQUATIONS AND NUMERICAL METHOD USED....11

   2.1 Similarity Parameters for an Oscillatory and Reversing Flow....11

   2.2 Similarity Parameters for Forced Heat Convection in an Oscillatory Flow....15

   2.3 Numerical Method....16

3. EXPERIMENTAL APPARATUS AND INSTRUMENTATION....18

   3.1 Air Pump and Sinusoidal Motion Mechanism....18

   3.2 Measurement of Fluid Flow Characteristics....18

   3.3 Measurement of Heat Transfer Characteristics....19

   3.4 Data Acquisition System....20

   3.5 Calibration....21

4. THE ONSET OF TURBULENCE....23

   4.1 Introduction....23

   4.2 Results and Discussion....24

4.3 Summary....27

5. LAMINAR AND TURBULENT FULLY-DEVELOPED OSCILLATORY FLOWS....29

5.1 Introduction....29

5.2 The Friction Coefficient of Laminar Flow....30

5.2.1 Analytical Solution....30

5.2.2 Experimental Investigation....35

5.2.3 Comparison of Theory and Experiments....36

5.3 The Friction Coefficient of Turbulent Flow....39

5.4 Summary....39

6. LAMINAR DEVELOPING OSCILLATORY FLOW....41

6.1 Introduction....41

6.2 Formulation....41

6.3 Results and Discussion....43

6.3.1 Velocity Profiles....43

6.3.2 Friction Coefficient....45

6.4 Summary....49

7. LAMINAR OSCILLATORY HEAT TRANSFER IN A PIPE WITH CONSTANT WALL TEMPERATURE....51

7.1 Introduction....51

7.2 Formulation....52

7.3 Results and Discussion....53

7.3.1 Temperature Distributions....54

7.3.2 Heat Flux....56

7.4 Summary....61

8. LAMINAR OSCILLATORY HEAT TRANSFER IN A PIPE WITH CONSTANT HEAT FLUX....62

8.1 Introduction....62

8.2 Experimental Investigation....63

8.3 Numerical Simulation....63

8.4 Results and Discussion....65

8.4.1 Temperature Distributions....64

8.4.2 Space-Cycle Averaged Nusselt Number....67

8.5 Summary....69

9. OSCILLATORY PRESSURE DROPS THROUGH A WOVEN-SCREENPACKED COLUMN....70

9.1 Introduction....70

9.2 Experimental Details....73

9.3 Results and Discussion....76

9.3.1 Temporal Variations of Pressure Drop....77

9.3.2 Maximum Pressure Drop Factor....78

9.3.3 Cycle-Averaged Pressure Drop Factor....79

9.4 Summary....81

10. CONCLUDING REMARKS....83

10.1 Summary and Conclusions....83

10.2 Future Work....85

APPENDIX A BLOCK DIAGRAM OF THE DATA ACQUISITION AND PROCESSING SOFTWARE....145

APPENDIX B MEASUREMENT UNCERTAINTIES....146

REFERENCES....147

LIST OF TABLES

Table		Page
9.1	Properties of tested stainless steel wire screens used in the experiment....	74
9.2	Experimental conditions for the tested cases.....	77
9.3	Comparison of the pressure drop predicted by Eqs. (9.1) and (9.19).....	82

LIST OF FIGURES

Figure		Page
2.1	Schematic diagram of the flow geometry	86
2.2	Control volumes	87
3.1	Apparatus of the measurement of fluid flow characteristics	88
3.2	Apparatus of the measurement of heat transfer characteristics	89
4.1a	Temporal axial velocity variations of a laminar flow for A_o= 57.5 and Re_ω = 66.6	90
4.1b	Temporal axial velocity variations of a laminar flow for A_o= 21.4 and Re_ω =302.2	91
4.2a	Temporal axial velocity variations at the onset of transition to turbulence: A_o= 97 and Re_ω = 66.6	92
4.2b	Temporal axial velocity variations at the onset of transition to turbulence: A_o= 47.3 and Re_ω =302.2	93
4.3	Temporal axial velocity variations of a turbulent flow for A_o= 97.1 and Re_ω = 302.2	94
4.4a	Temporal variations of axial velocity and pressure drop at the onset of transition to turbulence: A_o= 97.1 and Re_ω = 66.6	95
4.4b	Temporal variations of axial velocity and pressure drop at the onset of transition to turbulence: A_o= 47.3 and Re_ω = 302.2	96
4.5	Correlation equation of the critical dimensionless oscillation amplitude of fluid A_o and the kinetic Reynolds number Re_ω	97
5.1	F_ω and δ versus the kinetic Reynolds number Re_ω	98

5.2 Comparison of the ensemble-averaged traces of the cross-sectional mean velocity at the inlet and the assumed sinusoidal inlet mean velocity variation.....99

5.3 Typical variations of the ensemble-averaged pressure drops for Re_ω =144.1 and 324.3 at A_o=26.42.....100

5.4a Comparison of the instantaneous friction coefficient of the fully developed flow between analytical and experimental results for Re_ω=64 and 208.2 atA_o=16.5.....101

5.4b Comparison of the instantaneous friction coefficient of the fully developed flow between analytical and experimental results for A_o=16.5 and 26.42 at Re_ω=256.1.....102

5.5 Comparison of the cycle-averaged friction coefficient between analytical solution and experimental data.....103

5.6 The accuracy of the predication equation of the cycle-averaged friction coefficient.....104

5.7 Correlation equation of the cycle-averaged friction coefficient in terms of A_o and Re_ω for oscillatory turbulent flow.....105

5. 8 Comparison of the correlation equations of the cycle-averaged friction coefficient between the oscillatory laminar flow and turbulent flow.....106

6.1 Transient velocity profiles at different locations along the pipe for A_o=10, Re_ω=100 and L/D=20.....107

6.2a Effects of Re_ω on the centerline axial velocity variations along axial location in the entrance region at ϕ=90°.....108

6.2b Variations of the centerline velocity along the tube at different instants of times for A_o=10, Re_ω=100 and L/D=20.....109

6.2c Transient centerline axial velocity near the exit for A_o=10, Re_ω=100, and L/D=20.....110

6.3a Comparison of the instantaneous friction coefficient of the fully developed flow between numerical and analytical solutions.....111

6.3b Variations of the friction coefficient along the tube at different instants for A_o=30, Re_ω=196 and L/D=30 112

6.3c The end effect and the end length 113

6.3d Effects of A_o and Re_ω on variations of the cycle-averaged friction coefficient along the axial location in the left end of the pipe 114

6.4 Correlation equation for end length in terms of A_o 115

6.5 Correlation equation for the space-cycle averaged friction coefficient in the end region 116

7.1a Temporal temperature variations at X=6.2 and at different radial positions for A_o=15, Re_ω=64, and L/D=40 117

7.1b Temporal velocity variations at X=6.2 and at different radial positions for A_o=15, Re_ω=64, and L/D=40 117

7.2a Temporal temperature variations at X=6.2 and at different radial positions for A_o=15, Re_ω=250, and L/D=40 118

7.2b Temporal velocity variations at X=6.2 and at different radial positions for A_o=15, Re_ω=250, and L/D=40 118

7.3a Development of temperature profiles at X=4.5 for A_o=15, Re_ω=64, and L/D=40 119

7.3b Development of temperature profiles at X=4.5 for A_o=15, Re_ω=250, and L/D=40 120

7.4a Development of temperature profiles at X=15 for A_o=15, Re_ω =250, and L/D=40 121

7.4b Development of temperature profiles at X=15 for A_o=35, Re_ω=250, and L/D=40 122

7.5 Variations of the centerline temperature along the axial position at different phase angles for A_o=15, Re_ω =180, and L/D= 40 123

7.6a Temporal variations of the local instantaneous Nusselt number at different axial locations for A_o=15, Re_ω =64, and L/D=40.....124

7.6b Temporal variations of the local instantaneous Nusselt number at different axial locations for A_o=15, Re_ω=250, and L/D=40.....125

7.7 Effects of the dimensionless oscillation amplitude of fluid $A_o$and the kinetic Reynolds number Re_ω on the cycle-averaged local Nusselt number at L/D=40.....126

7.8 Effects of the dimensionless oscillation amplitude of fluid A_o and the kinetic Reynolds number Re_ω on space-averaged instantaneous Nusselt number for L/D=40.....127

7.9 Effects of length/diameter of the pipe on the cycle-averaged local Nusselt number for A_o=25 and Re_ω =180.....128

7.10 Correlation equation of the space-cycle averaged Nusselt number for air in terms of A_o and Re_ω at L/D=40.....129

7.11 Correlation equation of the space-cycle averaged Nusselt number for air in terms of A_o, Re_ω and L/D.....130

8.1a Temporal fluid temperature variations in the left and right mixing chambers for A_o=15.3, Re_ω =120.1, and L/D=44.8.....131

8.1b Temporal fluid temperature variations in the left and right mixing chambers for A_o=34.9, Re_ω=120.1, and L/D=44.8.....132

8.2 Effects of the dimensionless oscillation amplitude of fluid A_o on the temporal fluid temperature variations in the left mixing chamber for Re_ω=120.1 and L/D=44.8.....133

8.3 Variations of the centerline temperature along the axial position at different phase angles for A_o=15.3, Re_ω=150.6, and L/D= 44.8.....134

8.4 Effects of the dimensionless oscillation amplitude of fluid A_o and the kinetic Reynolds number Re_ω on the cycle-averaged wall temperature at L/D=44.8.....135

8.5 A correlation equation based on the experimental data for the cycle-space averaged Nusselt number....136

8.6 The accuracy of the correlation equation....137

9.1 Schematic diagram of experimental apparatus....138

9.2a Woven-screens....139

9.2b Mesh unit geometry....139

9.3 Typical variations of the ensemble-averaged pressure drop for $(A_o)_{D_h}$ =843.38 and at $(Re_\omega)_{D_h}$ =0.01005, 0.03770, and 0.05529....140

9.4 Typical variations of the ensemble-averaged pressure drop for $(Re_\omega)_{D_h}$ =0.04524 and at $(A_o)_{D_h}$ =614.73, 843.38, and 1143.25....141

9.5 A correlation equation of the maximum pressure drop factor in terms of $(A_o)_{D_h}$ and $(Re_\omega)_{D_h}$ 142

9.6 Comparison of the present correlation equation of the maximum pressure drop factor with that obtained by Tanaka et al. (1990)....143

9.7 A correlation equation of the cycle-averaged pressure drop factor in terms of $(A_o)_{D_h}$ and $(Re_\omega)_{D_h}$ 144

NOMENCLATURE

A	function defined in Eq. (5.5)
A_m	cross-sectional area of the packed column
A_o	dimensionless oscillation amplitude of fluid defined in Eq.(2.9)
$(A_o)_{D_h}$	dimensionless oscillation amplitude of fluid based on the hydraulic diamter defined in Eq. (9.10)
A_p	amplitude of the imposed pressure gradient in Eq. (5.3)
B	function defined in Eq. (5.6)
C_1	constant defined in Eq. (5.9a)
C_2	constant defined in Eq. (5.9b)
c_f	friction coefficient defined in Eq. (5.11)
$c_{f,exp}$	measured friction coefficient defined in Eq. (5.19)
$c_{f,exp,j}$	measured friction coefficient at jth time interval
$c_{f,\infty}$	analytical friction coefficient defined in Eq. (5.13)
$\bar{c}_f$	cycle-averaged friction coefficient defined in Eq. (5.12)
$\bar{c}_{f,exp}$	measured cycle-averaged friction coefficient defined in Eq. (5.21)
$\bar{c}_{f,l}$	cycle-averaged friction coefficient of a laminar flow
$\bar{c}_{f,t}$	cycle-averaged friction coefficient of a turbulent flow
$\bar{c}_{f,\infty}$	cycle-averaged friction coefficient defined in Eq. (5.14)
$(\bar{c}_f)_m$	space-cycle averaged friction coefficient defined in Eq. (6.6)
$(\bar{c}_{f,e})_m$	space-cycle averaged friction coefficient within the end length, defined in Eq. (6.7b)
D	diameter of the pipe
D_h	hydraulic diameter defined in Eq. (9.4)
D_w	wire diameter of screens

Δp	pressure drops
Δp_{max}	maximum pressure drop in one cycle
Δp_{st}	pressure drops of steady flow
$\Delta \tilde{p}$	ensemble-averaged pressure drop
$\Delta \bar{p}$	cycle-averaged pressure drop
$(\Delta \bar{p})_{pre}$	predicted cycle-averaged pressure drop
$(\Delta p_{st})_{pre}$	pressure drops of steady flow
f_{max}	the maximum pressure drop factor defined in Eq. (9.5)
f_{st}	the pressure drop factor of the steady flow defined in Eq. (9.2)
$\bar{f}$	the cycle-averaged pressure drop factor defined in Eq. (9.18)
F_{ω}	expression defined in Eqs. (5.15a) and (5.16a)
h	instantaneous heat transfer coefficient
k	thermal conductivity of the fluid
L	distance of the two taps of the pressure transducer
L_e	dimensional end length
n	number of stacked screens
N	number of cycles to be ensemble averaged
N_i	number of sampling intervals in one cycle
Nu	local instantaneous Nusselt number defined in Eq. (7.5)
$\overline{Nu}$	space-cycle averaged Nusselt number defined in Eq. (7.11)
$\overline{Nu}_{\tau}$	space-averaged Nusselt number defined in Eq. (7.9)
$\overline{Nu}_{X}$	cycle-averaged Nusselt number defined in Eq. (7.10)
p, P	dimensional and dimensionless pressure of the fluid
Pr	Prandtl number of the fluid
q_w	heat flux at the wall

r, R	dimensional and dimensionless radial coordinates
$(Re_\delta)_{cri}$	critical Reynolds number based on the Stokes layer thickness
Re_{max}	Reynolds number
$(Re_{max})_{D_h}$	Reynolds number based on the hydraulic diamter defined in Eq. (9.6)
Re_ω	kinetic Reynolds number
$(Re_\omega)_{cri}$	critical kinetic Reynolds number
$(Re_\omega)_{D_h}$	kinetic Reynolds number based on the hydraulic diamter defined in Eq. (9.14)
t, τ	dimensional and dimensionless time
t'	time, together with ω in Eq. (5.3), denoting the externaly imposed pressure gradient
T, θ	dimensional and dimensionless temperature
T_i	dimensional inlet fluid temperature
T_c, θ_c	dimensional and dimensionless centerline temperature of the fluid
$T_{m,l}$, $\theta_{m,l}$	dimensional and dimensionless temperature of the fluid in the left mixing chamber
$T_{m,r}$, $\theta_{m,r}$	dimensional and dimensionless temperature of the fluid in the right mixing chamber
T_w, θ_w	dimensional and dimensionless wall temperature of the pipe
$\overline{T}_w$, $\overline{\theta}_w$	dimensional and dimensionless space-cycle averaged wall temperature of the pipe
u, U	dimensional and dimensionless axial velocity
u_m, U_m	dimensional and dimensionless cross-sectional mean velocity
$\tilde{u}_m$	ensemble-averaged cross-sectional mean velocity
$(u_m)_p$	area-averaged fluid velocity in the packed column

u_{max}	maximum cross-sectional mean velocity
$(u_{max})_P$	maximum area-averaged fluid velocity in the packed column
$\vec{V}$	velocity vector
V_{pis}	the swept volume of the piston
x, X	dimensional and dimensionless axial distance
x_{max}	dimensional maximum fluid displacement
$(x_{max})_P$	maximum fluid displacement in the packed column
x_p	fluid displacement in the packed column

Greek Symbols

α	thermal diffusivity of fluid
δ	phase difference defined in Eqs. (5.15b) and (5.16b)
δ_f	the Stokes layer thickness
δ_t	thermal boundary layer thickness
Γ	phase difference defined in Eq. (5.7b)
λ	Stokes number defined in Eq. (2.6)
Λ	ratio of the radius to the viscous boundary layer thickness
ϕ	phase angle
φ	porosity
ρ	density of fluid
τ_w	shearing stress at the wall
$\bar{\tau}_w$	cycle-averaged wall shearing stress
μ	kinematic viscosity of fluid
ν	kinematic viscosity of fluid

ω	oscillatory frequency

Subscripts

∞	fully-developed flow
c	centerline
e	end length
exp	measured data
f	friction
i	*i*th cycle or inlet
j	*j*th sampling interval
l	left side or laminar flow
m	cross-sectional mean value
max	maximum value
p	packed column
r	right side
τ	function of time
w	wall of the pipe
x	function of positions

CHAPTER 1

INTRODUCTION

1.1 Background

In recent years, a great deal of efforts have been devoted to the development of Stirling-cycle machines such as Stirling engines and miniature pulse tube cryocoolers for military and space applications. The Stirling engine is a prospective power source for future space missions because it can be operated using solar energy. The miniature pulse tube cryocooler is an ideal device for the cooling of infrared detectors in night vision and missile guidance systems, as well as for infrared sensors aboard satellites; this is owing to their high reliability and relatively free of vibration and noise as discussed by Radebaugh (1991).

For an optimum design of Stirling-cycle machines, it is important to predict accurately heat transfer and frictional loss in the heat exchangers (heater, regenerator and cooler). Until recently, the flow frictional loss and heat transfer correlations used in the design of these heat exchangers were based on unidirectional steady flow conditions, which are unrealistic since Stirling machines operate under oscillatory flow conditions. Thus, there is a need for more realistic predictions of the fluid flow and heat transfer characteristics of an oscillatory and reversing flow in a heated pipe. It should be noted that the nomenclature of the oscillatory reversing flow in this study means a periodical flow with zero mean velocity in one cycle while the nomenclature of the pulsating flow refers to an unidirectional steady mean flow superimposed by a unsteady periodical flow component. The present work will focus on the basic transport phenomena of an

oscillatory and reversing flow and the associated heat transfer characteristics in a pipe and in a woven-screens packed column.

1.2 Review of Literature

In this section, the existing literature on oscillatory and reversing flow in a pipe and associated heat transfer characteristics will be reviewed. Previous research efforts concerning pressure drops through a packed column subjected to a periodically reversing flow will also be discussed.

Laminar Oscillatory Flow in a Pipe

The problem of oscillatory flow in a pipe under the influence of periodical pressure fluctuations has been studied by many researchers both analytically and experimentally. Richardson and Tyler (1929) were among the first to measure the velocity distribution in an oscillatory pipe flow, and discovered the so-called "annular effect", i.e., the maximum axial velocity in a fast oscillatory flow occurs near the wall rather than at the center of the pipe as in the case of unidirectional steady flow in a pipe. Subsequently, Sexl (1930), Womersley (1955) and Uchida (1956) verified the "annular effect" by performing analyses of both sinusoidal and non-sinusoidal motions of a fully-developed oscillatory flow in a pipe. Similar analyses were carried out by Drake (1965) for an oscillatory flow in a rectangular channel, and by Siegel (1987) and Gedeon (1986) for flow between parallel plates. Most recently, Akhaven et al. (1991) experimentally verified Uchida's analytical solution (1956) by measuring velocity profiles of an oscillating flow of water in a pipe.

Relatively few papers have been reported on the study of a hydrodynamically developing oscillatory flow in tubes of finite length. Peacock and Stairmand (1983) hypothesized that the entrance length in a laminar oscillating flow would be shorter than in a unidirectional steady flow. They speculated that the velocity profiles of an oscillatory flow may not change much in the entrance region because the velocity profiles of an oscillatory flow tend to be flatter than those of a steady flow. Chayrreyon (1984), based on observations made by Golaberg (1958) about steady flows, suggested that entrance length may vary over a cycle and proposed a time dependent entrance length. Roach and Bell (1988) performed experiments on pressure drop and heat transfer in both an empty tube and a packed tube under the imposed conditions of a rapidly reversing flow. They reported higher friction factors but could not find frequency dependence in their pressure drop and heat transfer data. Wu, et al. (1990) obtained some data for the friction factor in a gap heat exchanger, and presented their data graphically as a function of the Reynolds number. Taylor and Aghili (1984) measured pressure drops in an oscillating flow of water in a pipe of a finite length at relatively low frequencies. Their data indicate an increase of the friction coefficient over that of unidirectional steady flow. However, they did not have sufficient data to investigate the effects of frequency on the friction coefficient.

Onset of Turbulence

The onset of turbulence in an oscillatory flow has been given a considerable amount of attention in the past. Hino et al. (1976) studied transition by means of hot wire measurements. They found that there was a laminar-like flow during the acceleration phase of the half cycle whereas a turbulent-like flow existed during the deceleration phase. A correlation equation for predicting the transition to turbulence

was first given by Sergeev (1966), who used flow visualization to identify transition in an oscillating pipe flow. Ohmi et al. (1982) performed experiments on forced oscillations of a gas in a straight pipe. They found that velocity profiles during the laminar phase of cycle agree well with the Uchida's analytical solution for a laminar fully-developed oscillatory flow, and that the velocity profiles during the turbulent flow regime agree well with the 1/7th-power law of a steady turbulent pipe flow. They determined a correlation equation for the prediction of transition based on whether the observed velocity profiles are in agreement with the 1/7th-power law. Park and Baird (1970) reported transition flow during free oscillations of a liquid in an U-tube. Iguchi et al. (1983) experimentally studied free oscillations in a U-tube and determined that transition occurred when the velocity profile deviated from the Uchida-type laminar profile. Using hot-wires, Seume (1988) experimentally studied the transition in an oscillatory flow pipe with parameter ranges corresponding with the heat exchangers of Stirling engines and cryocoolers. Recently, Cooper et al (1993) presented a review of literature on oscillating flows.

Turbulent Oscillatory Flow

In this section, we shall focus our attention upon the turbulence structure characteristics of an oscillatory flow. In this regard, the most detailed work was given by Hino et al. (1983). Using a laser-Doppler velocimeter and hot-wire anemometers, Hino et al. (1983) experimentally investigated a reciprocating oscillatory turbulent flow in a rectangular duct. They found that at large fluid displacements and frequencies, the turbulence structure of the oscillating flow was substantially different from that of a steady flow. In the accelerating phase, turbulence was triggered near the wall but was suppressed and could not develop. On the other hand, with the beginning of flow

deceleration, turbulence grows explosively and violently and was maintained by the bursting type of motion. They stated that the turbulence-energy production became exceedingly high in the decelerating phase, but that also the turbulence is reduced to a very low level at the end of the decelerating phase and in the accelerating stage of the reversal flow. They pointed out that although there exists a great degree of difference between the ensemble-averaged characteristics of the oscillatory flow and those of the steady wall turbulence, its basic processes such as ejection, sweep and interactions directed towards and away from the wall are the same as those of the steady flow near the wall. Other studies on turbulence structure characteristics of pulsating flows can be found in the work by Ramaprian et al. (1983), Mao and Hanratty (1986), and Gerrard (1971).

Oscillatory Heat Transfer

The related problem of oscillatory heat transfer in a heated pipe subjected to a periodically reversing flow has important applications to the design of heat exchangers and pulse tubes in Stirling machines and cryocoolers. Simon and Seume (1988) presented an excellent survey of literature on this subject, and pointed out important differences in fluid flow and heat transfer between steady and oscillatory flows. Iwabuchi and Kanzaka (1982) experimentally investigated heat transfer of an oscillatory flow in a test facility which was designed to obtain data for a specific prototype engine; they presented their heat transfer data in terms of the piston speed (rpm), mean pressure and phase difference between the opposing pistons, but did not attempt to correlate their heat transfer data of oscillatory heat transfer in terms of dimensionless parameters. Hwang and Dybbs (1983) graphically presented their oscillatory heat transfer data in terms of Nusselt number versus Reynolds number at selected oscillating

amplitudes. Kurzweg (1985) and Gedeon (1986) analyzed the enhancement of axial heat transfer due to an oscillatory flow between two parallel plates. Siegel (1987) obtained an analytical solution for heat transfer of a pulsating flow in a channel with uniform heat flux; his analysis showed that the effect of flow oscillation is to reduce the heat transfer coefficient. Roach and Bell (1988) designed and constructed a test facility for the study of heat transfer in a packed tube under conditions of rapidly reversing flows. Since their experimental results did not show frequency dependence in either pressure drop or heat transfer, they correlated the cycle-averaged Nusselt number in terms of the Reynolds number as in the case of a steady flow. Wu et al. (1990) investigated oscillating flow resistance and heat transfer in a gap heat exchanger of a cryocooler. They found that the value of the cycle-averaged Nusselt number is constant at a value of about 9, and that it is independent of the oscillatory frequency over a wide range of the Reynolds number. Cooper et al. (1994) experimentally investigated convective heat transfer from a heated surface of a rectangular duct subjected to a periodically reversing flow. They found that the heat transfer rate increases with the increase of the oscillatory frequency and the tidal displacement.

Pressure Drops in a Packed Column

Abundant data have been obtained for the pressure drop in a packed column consisting of a stack of screens under unidirectional steady flow conditions. For example, Tong and London (1957) presented correlation equations for pressure drop in a steady flow through screens which have been widely used for the design of regenerators in Stirling machines. Walker and Vasishta (1971) obtained experimental data for pressure drop through dense-mesh wire screens. Later, Miyabe et al. (1982) presented further experimental data for flow through stacked screens. Chen and Griffin

(1983) obtained an empirical equation based on the Tong and London (1957) data. Until recently, the correlation equation of pressure drops used in the design of a regenerator was simply based on the aforementioned unidirectional steady flow. It is apparent that these steady correlations do not correctly predict the pressure drop in a regerenator of Stirling-cycle machines, which operate under oscillatory and reversing flow conditions. For example, it was found by Matini (1978) and Rix (1984) that good agreement between simulated and measured pressure drops can be achieved only if the friction coefficient provided by Tong and London (1957) is arbitrarily adjusted by a constant that takes on a value ranging between 3 and 5. Thus, there is a need for obtaining a more accurate correlation equation for the pressure drop in regenerators under oscillatory and reversing flow conditions.

Relatively little research has been performed on the study of pressure drops in a packed column subjected to an oscillatory and reversing flow. Roach and Bell (1988) performed experiments on pressure drop and heat transfer in a packed tube under rapidly reversing flow conditions. They reported higher friction factors but could not determine frequency dependence in pressure drop. Tanaka et al. (1990) experimentally investigated the fluid flow and heat transfer characteristics of a Stirling engine regenerator packed with wire screens and sponge metals under oscillating flow conditions. They successfully obtained a correlation equation of the friction factor in terms of the Reynolds number as defined by the maximum flow velocity and the hydraulic diameter. Unfortunately, their experiments were performed with a fixed fluid displacement, and thus their data are not suitable for general use.

From the preceeding review of the literature, it is evident that the studies of the oscillatory flow and associated heat transfer in a pipe and in a packed column are still in its infancy, and much work remains to be done.

1.3 Objectives of the Present Investigation

The objectives of the present study are:

1. To investigate the mechanism for transition to turbulence in an oscillatory flow. The criterion for the onset of turbulence in an oscillatory and reversing flow will be obtained.
2. To investigate the fluid flow characteristics of a laminar oscillatory flow in a pipe of finite length.
3. To investigate frictional losses of both oscillatory laminar and turbulent pipe flows.
4. To investigate the heat transfer characteristics in a pipe subjected to a periodically oscillatory and reversing flow.
5. To investigate pressure drops through a woven-screen packed column subjected to a periodically reversing flow.

Results obtained from the aforementioned investigations will enhance our understanding of oscillatory flow and its associated heat transfer characteristics in a pipe. The information will be useful for the design of heat exchangers in a Stirling engine or a pulse-tube cryocooler. Both numerical and experimental investigations will be carried out in the present work.

This dissertation consistis of ten chapters: the problem statement and solution techniques will be described in Chapter 1. In Chapter 2, the mathematical problem will be formulated and the similarity parameters for fluid flow and heat transfer will be identified. The numerical method for solving the hydrodynamically and thermally developing pipe flow will also be described briefly. In Chapter 3, the experimental apparatus and instrumentation for investigating the oscillatory flow and heat transfer behaviors will be discussed. Chapter 4 reports on the results of experimental investigation into transition mechanisms and presents a correlation equation for the prediction of the onset of turbulence in an oscillatory and reversing flow. Chapter 5 presents an analytical expression of the friction coefficient of a laminar fully-developed oscillatory pipe flow and a comparison against experimental data. The experimental data on friction coefficients of a turbulent fully-developed oscillatory flow will also be presented and compared against those for a laminar flow. In Chapter 6, a numerical solution of a laminar hydrodynamically developing oscillatory pipe flow will be presented. The difference in the fluid flow characteristics between an oscillatory flow and an unidirectional steady flow will be discussed. The friction coefficient of the oscillatory flow in a pipe of finite length as determined from the numerical solution will be also presented. Chapter 7 deals with a numerical solution of oscillatory laminar forced convection in a pipe heated at constant wall temperature. The difference between the temperature distribution of an oscillatory flow and that of steady flow will be discussed. In Chapter 8, the results generated from the experimental data and the numerical solution for oscillatory heat transfer in a pipe heated at uniform heat flux will be examined. A correlation equation of the space-cycle averaged Nusselt number for air in terms of appropriate similarity parameters will be obtained. Chapter 9 will present the measurement of pressure drops across a woven-screen packed tube subjected to a periodically reversing flow. Chapter 10 will summarize the important findings and

conclusions of the present study. Suggestions for further research on oscillatory and reversing flows in a pipe and a packed column will also be addressed.

CHAPTER 2

GOVERNING EQUATIONS AND NUMERICAL METHOD USED

The mathematical problem of an oscillatory and reversing flow and associated heat transfer characteristics in a pipe will be formulated in this chapter. The relevant similarity parameters governing the fluid flow and heat transfer will be chosen and their significance will be discussed. The numerical method employed in the present study will also be briefly described.

2.1 Similarity Parameters for an Oscillatory and Reversing Flow

The schematic diagram of the flow geometry for the present experimental investigation and numerical simulation of the problem of oscillatory and reversing flow and associated heat transfer in a pipe (with diameter D) are shown in Fig. 2.1. It is assumed that the fluid is incompressible with constant thermophysical properties, and the oscillatory motion of the fluid is driven by a sinusoidal displacer which was designed such that the fluid displacement x_m varies according to

$$x_m = \frac{x_{max}}{2}(1 - \cos\omega t) \tag{2.1}$$

where the fluid displacement x_m is defined by assuming the fluid moves as a plug flow at a mean velocity u_m, with the maximum fluid displacement x_{max} being adjusted by changing the stroke of an air pump which will be described shortly. In Eq. (2.1), ω is

the oscillation angular frequency and t is time. Differentiating Eq. (2.1) with respect to time gives the cross-sectional mean velocity u_m

$$u_m = u_{max} \sin\phi \tag{2.2}$$

where the maximum cross-sectional mean velocity u_{max} is related to the maximum fluid displacement x_{max} by

$$u_{max} = \frac{x_{max}\omega}{2} \tag{2.3}$$

and the crank phase angle ϕ is related to the dimensionless time τ by $\tau = \omega t = 2\pi(i-1)+\phi$, with i being the number of cycles.

If the dimensionless coordinates, velocity, and pressure are defined as (X,R)=(x/D,r/D), U=u/u_{max}, V=v/u_{max}, $P = p/\rho u_{max}^2$ (where x, r, p, and u are the corresponding dimensional quantities, ρ is the density), the governing dimensionless conservation equations of mass and momentum for an incompressible periodically reversing flow are given by

$$\nabla \cdot \vec{V} = 0 \tag{2.4}$$

$$Re_\omega \frac{\partial \vec{V}}{\partial \tau} + Re_{max}[(\vec{V}\cdot\nabla)\vec{V} + \nabla P] = \nabla^2 \vec{V} \tag{2.5}$$

where $Re_\omega = \frac{\omega D^2}{\nu}$ is the kinetic Reynolds number with ν being the kinematic viscosity of the fluid and $Re_{max} = \frac{u_{max} D}{\nu}$ is the Reynolds number. Thus, Seume (1988) used

Re_ω and Re_{max} as the similarity parameters to characterize an oscillatory and reversing flow in a pipe. Other investigators have used different similarity parameters. For example, Hino et al. (1976) used the Reynolds number Re_{max} and the Stokes number λ as the similarity variables, which is related to the kinetic Reynolds number by

$$\lambda = \frac{D}{2}\sqrt{\frac{\omega}{\nu}} = \frac{1}{2}\sqrt{Re_\omega} \tag{2.6}$$

Ohmi (1982) used the Reynolds number Re_{max} and the pipe radius to viscous boundary layer thickness ratio Λ (where $\Lambda = R/\delta_f$ with $\delta_f = \sqrt{2\nu/\omega}$ being the Stokes layer thickness) as the similarity parameters. It should be noted that the similarity parameters Re_ω (or λ), Re_{max}, and Λ are all dependent on the oscillatory frequency. Although any two of these parameters can be used for the correlation of experimental data to characterize the fluid dynamics aspect of an oscillatory and periodically reversing flow, these choices of similarity parameters will not be able to isolate the effect of the oscillatory frequency. Thus, another choice of parameters should be attempted for the correlation of experimental data. To this end, we note that the Reynolds number Re_{max}, with the aid of Eq.(2.3), can be written as

$$Re_{max} = \frac{x_{max}\omega D}{2\nu} \tag{2.7}$$

Eq.(2.7) can be rewritten as

$$Re_{max} = \frac{A_o}{2}Re_\omega \tag{2.8}$$

where

$$A_o = \frac{x_{max}}{D} \tag{2.9}$$

is the dimensionless oscillation amplitude of fluid. Substituting Eq. (2.8) into Eq.(2.5) yields

$$\frac{\partial \vec{V}}{\partial \tau} + \frac{A_o}{2}[(\vec{V}\cdot\nabla)\vec{V} + \nabla P] = \frac{1}{Re_\omega}\nabla^2\vec{V} \tag{2.10}$$

Eq. (2.10) shows that for a given dimensionless oscillation amplitude of fluid A_o, the kinetic Reynolds number Re_ω in an oscillatory flow plays the same role as that of the Reynolds number in a unidirectional flow. The kinetic Reynolds number Re_ω in the momentum equation given by Eq. (2.10) describes the relative importance of both the inertial force and the frictional force. It can be speculated that at low Re_ω the frictional force is more important and a parabolic velocity profile could be formed. At high Re_ω however, the inertial force becomes more dominent and viscous effects are confined to a thin oscillating boundary layer so that the central core behaves like a plug flow as shown in Uchida's velocity solution.

Eqs. (2.4) and (2.10) show that A_o and Re_ω are the two alternative similarity parameters for an incompressible periodically reversing flow. Since the amplitude of fluid displacement and the oscillatory frequency are independent of each other, this choice of similarity parameters for the correlation of experimental data will be able to demonstrate the effects of amplitude of fluid displacement and oscillatory frequency separately.

It should be recognized that for a pipe of finite length, the length ratio L/D will be an additional parameter which enters the mathematical problem through the inlet and outlet boundary conditions as will be discussed in Chapters 7 and 8. Therefore, we can conclude that the governing similarity parameters for the fluid flow in a pipe of finite length subjected to a sinusoidally oscillatory flow are the kinetic Reynolds number Re_ω, the dimensionless oscillation amplitude of fluid A_o, and the length to diameter ratio of the pipe L/D.

2.2 Similarity Parameters for Forced Heat Convection in an Oscillatory Flow

The energy equation in dimensionless form is

$$Re_\omega Pr[\frac{\partial\theta}{\partial\tau} + Re_{max}(\vec{V}\cdot\nabla)\theta] = \nabla^2\theta \tag{2.11}$$

which can be written in term of the dimensionless fluid displacement to give

$$\frac{\partial\theta}{\partial\tau} + \frac{A_o}{2}(\vec{V}\cdot\nabla)\theta = \frac{1}{Re_\omega Pr}\nabla^2\theta \tag{2.12}$$

where $Pr = \frac{\nu}{\alpha}$ is the Prandtl number with α being the thermal diffusivity of fluid and $\theta = \frac{T - T_i}{T_w - T_i}$ (for the case heated at constant temperature T_w) or $\theta = \frac{kT}{q_w D}$ (for the case heated at constant heat flux q_w) with T_i being the inlet fluid temperature. Thus, for the problem of oscillatory heat transfer, the Prandtl number is the additional similarity parameter. It follows from Eq. (2.12) that the kinetic Reynolds number Re_ω together with the Prandtl number Pr, controls the thickness of the thermal boundary layer. It

can be also speculated that for a given fluid with a specific Prandtl number, the heat transfer rate of an oscillatory flow increases with Re_ω because the thermal boundary layer becomes thinner with the increase of Re_ω.

2.3 Numerical Method

Numerical solutions to the simultaneously developing oscillatory flow mechanics and the associated heat transfer problems, described by Eqs. (2.4), (2.10) and (2.12), subject to the corresponding boundary conditions specified for the individual problems in the later chapters, will be obtained based on a control-volume method detailed by Patankar (1980). In this procedure, the domain is discretized into a series of control volumes. A typical control volume is shown in Fig. 2.2, where the dashed lines denote the boundaries of the control volumes with a grid point (denoted by a dot) located at the geometrical center of each control volume (shaded area), and the solid lines being the grid lines. It can be seen that a given grid point communicates with the four neighboring grid points through the four faces of the control volume. Although most variables in the program are stored in the grid point locations, the velocity components U or V normal to each interface is stored at the center of the interface (see Fig. 2.2). The partial differential equations are expressed in an integral manner over the control volume, and a power law variation (Patankar, 1980) is assumed in each coordinate direction, leading to a system of algebraic equations that can be solved in an iterative manner. Pressure-velocity interlinkages are handled by the SIMPLER formulation as described by Patankar (1980).

Because of the extremely thin boundary layer encountered at high kinetic Reynolds numbers and large velocity gradients in the inlet region of the tube, a non-

uniform grid was deployed. A grid independent solution for each group of Re_ω A_o, and L/D will be established by reducing the grid size until a convergance criterion is satisfied. Different criteria will be used for different problems to be solved in Chapters 5-8. The choice of 181 grid points in the axial direction and 51 points in the radial direction was found to provide grid independence for the results reported in this work. For each case, 180 time steps were used in one cycle and transient behaviors were recorded until a steady periodic state was reached. Numerical computations were carried out on a Sun SPARC 10 Workstation.

CHAPTER 3

EXPERIMENTAL APPARATUS AND INSTRUMENTATION

This chapter describes the experimental apparatus and instrumentation employed for the measurements of the oscillatory fluid flow and the associated heat transfer characteristics. The calibration procedures for the different sensors such as hot-wire probes, pressure transducers and thermocouples are also explained.

3.1 Air Pump and Sinusoidal Motion Mechanism

In the present study, the sinusoidal oscillatory and reversing motion of air in the pipe was created by a double acting reciprocating piston pump connected to a crank shaft and yoke sinusoidal mechanism designed by Tang (1992). The apparatus is shown in the bottom of Figs. 3.1 and 3.2. The air pump (74 mm in diameter and 116 mm in length) driven by a 1 kW DC motor, was designed to create identical flow conditions to either end of the test section. The stroke of the piston can be adjusted from 0 to 70 mm, with a speed from 7 to 570 rpm, which is equivalent to 0.12 to 9.5 Hz.

3.2 Measurements of Fluid Flow Characteristics

Measurements of fluid flow characteristics were carried out in the horizontal test rig shown in Fig. 3.1. The oscillating motion of flow was induced by the air pump and its sinusoidal mechanism, as described in the previous section. The working fluid (air)

moved reversibly and periodically in the test section, which was made of a long copper tube, 94.5 cm in length and 1.35 cm in diameter. At the two ends of the test section, two velocity straightening chambers (made of fine screens) were connected to ensure that a uniform flow was entering the test section. The test section was connected to the two ends of the pump by flexible tubes.

A differential pressure transducer, (Validyne, Model DP15), having a high natural frequency (>5000 Hz), and a carrier demodulator (Validyne, Model CD15) were employed to measure pressure drops along the pipe. Since it was intended for measuring pressure drops in the fully-developed flow region in this work, the pressure transducer taps were installed at locations far removed from the entrance regions of the pipe. As shown in Fig. 3.1, the two ends of the pressure transducer were separated at a distance of L (L=68 cm) in the central portion of the pipe. To study the onset of turbulence of the oscillatory pipe flow, a miniature straight hot-film probe (TSI, Model 1260A-10) with a manual traverse positioning mechanism was installed at the mid-section of the pipe to measure the instantaneous axial velocities at different radial positions. Another miniature hot-film probe was installed between the two velocity straighteners at the left side of the test section (see Fig. 3.1) to measure the cross-sectional mean velocity. These two hot-film probes were connected to a hot-wire anemometer (TSI, IFA 100).

3.3 Measurements of Heat Transfer Characteristics

The above described experimental setup was modified to allow for the measurements of oscillatory heat transfer characteristics. As shown in Fig. 3.2, a heated test section, made of a long copper tube with 60.5 cm in length and 1.35 in

diameter (i.e., L/D = 44.8), is located in the central part of the horizontal test rig. Each end of the test section was connected by two mixing chambers, made of fine plastic screens, to two identical coolers having the same inside diameter as the test section and 40 cm in length. The test section was heated uniformly by a wrapped-around insulated flexible heater (manufactured by Omega), which was connected to a filtered DC power supply (Model PS-5, EPSCD). The two coolers were fabricated out of two concentric tubes with tap water as the coolant. The other end of each cooler was connected to a velocity straightener.

Because both the geometry and the imposed hydrodynamic and thermal boundary conditions were symmetric with respect to the mid-section of the heated tube, the sensors were installed only in the left-hand side of the test rig. Five foil T-type thermocouples (manufactured by RdF) were used to measure wall temperatures, two on the cooler wall and the other four were on the wall of the heated tube. Centerline fluid temperatures inside the heated tube were measured by four mini-needle T-type thermocouples (manufactured by Omega). To measure inlet and outlet fluid temperatures in the heated tube, two fine thermocouples (0.001" in diameter) were carefully installed inside the two mixing chambers.

3.4 Data Acquisition System

Analog to digital conversions were carried out by a Metrabyte DAS-20 A/D board, giving 100,000 samples per second with 12-bit precision. A 4-channel simultaneous sample and hold front end for the A/D board (SSH-4) was employed, which was capable of securing the 4-channel signals to be sampled simultaneously. A high speed data acquisition streaming-to-disk package (STREAMER, Metrabyte) was

employed to collect and store signals, which allows A/D conversions from the data acquisition board to be directly stored on a hard disk at the maximum sample rate.

For the measurements of the fluid flow characteristics, the crank angle ϕ was monitored by an optical shaft encoder (Lucas Ledex, Model LD23) with a half degree resolution, which can also provide a top dead center (TDC) signal for data acquisition purposes. A similar angle shaft encoder, but equipped with a two-degree resolution, was used for the measurements of heat transfer characteristics.

3.5 Calibrations

In order to estimate and control the measurement system errors, calibrations were carried out before the test. The A/D converter board was calibrated first by using a high accuracy standard voltage signal source following the manufacturer's instructions. After calibration, the differences among the channels were identified.

Hot-film probes were calibrated by using a static calibrator (Model 1125, TSI). When making calibrations, a standard velocity was provided by this calibrator, and the corresponded voltage of a hot-film probe was sampled by the data acquisition system, including the electric bridge, the signal conditioner and the A/D converter board. Since the velocities provided by the calibrator were nominal values at the standard conditions, the velocities in the measurement applications were corrected based on the actual conditions.

The differential pressure transducer was calibrated before the installation. The transducer calibration was carried out using a pressure calibrator (DPI 601, Omega).

In the test temperature range, all thermocouples were calibrated by a block calibrator (CL 730, Omega) which is equipped with ±0.1 °C resolution and ±0.4 °C accuracy. To accelerate the data reduction process, a tenth order curve was fitted for the data given in the calibration run table.

CHAPTER 4

THE ONSET OF TURBULENCE

This chapter presents an experimental study on the onset of turbulence in an oscillatory and reversing flow of air in a pipe. A correlation equation in terms of the appropriate similarity parameters for the prediction of the onset of turbulence will be obtained in this chapter. The physical reason for the onset of periodically turbulent bursts, followed by relaminarization in the same cycle, will be examined.

4.1 Introduction

The transition from laminar to turbulent oscillatory and reversing flow must be understood and characterized before frictional losses and heat transfer can be determined quantitatively. A considerable amount of work has been performed to study transition to turbulence in an oscillatory flow as discussed by Sergeev (1966), Park and Baird (1970), Hino et al. (1976), and Ohmi et al. (1982), etc. Past measurements show that a laminar-like flow exists during the acceleration phase of the half cycle whereas a turbulent-like flow exists during the deceleration phase. A number of correlation equations for predicting the onset of turbulence in an oscillatory flow have been proposed. However, due to inappropriate selections of similarity parameters, the effect of oscillation frequency on the transition could not be identified. Furthermore, little information is known about the physical reason for the onset of turbulent bursts followed by relaminarization in the same cycle. In view of these facts, it was decided first to conduct a series of experiments on transition from laminar to

turbulent oscillatory pipe flow, which will be helpful for subsequent study of frictional losses and the associated heat transfer in an oscillatory and reversing flow.

As discussed in Section 3.2, a hot-wire anemometer was employed to observe the temporal axial velocity variations while a pressure transducer was used to measure the temporal variations of pressure drop along the pipe. In contrast to previous work, the similarity parameters chosen for the present study are the kinetic Reynolds number Re_ω and the dimensionless oscillation amplitude of the fluid A_o. As in the previous investigations, we found that transition to turbulence occurs only in the deceleration period of the cycle and above certain values of A_o and Re_ω. A correlation equation in terms of these two similarity parameters to predict transition to turbulence will be obtained. The physical reason for the occurrence of turbulence in a periodically reversing flow will be explained.

4.2 Results and Discussion

The experiment was performed with the test rig shown in Fig. 3.1, which was described in the previous chapter. Variations of the instantaneous axial velocities at different radial positions were sampled at the mid section of the pipe for different values of the dimensionless oscillation amplitude of fluid A_o and the kinetic Reynolds number Re_ω. Since the hot-wire anemometer cannot detect the direction of the fluid flow, velocities are presented as absolute values. Typical velocity traces in the laminar flow regime, transition, and turbulent flow regime are illustrated from Figs. 4.1 to 4.4. An instability diagram is presented in Fig. 4.5.

Experiments were first conducted for an oscillatory flow at low dimensionless oscillation amplitudes of the fluid and low kinetic Reynolds numbers. Figs. 4.1a and 4.1b illustrate typical temporal velocity variations at different radial positions for A_o = 57.5 and Re_ω = 66.6 as well as for A_o=21.4 and Re_ω=302.2 respectively. It is shown that at these small values of A_o and Re_ω the variations of the axial velocity are smooth, indicating that the flow is laminar everywhere. It is noted that the axial velocity at different radial positions varies sinusoidally with time; the axial velocity in the core also has a slight phase delay with respect to that near the wall.

When the values of A_o and Re_ω were increased to certain values, periodic turbulent bursts occurred near the wall. Figs. 4.2a and 4.2b show two examples of the temporal axial velocity variations at the centerline of the pipe and near the wall at the onset of turbulence. It should be noted from these figures that the velocity fluctuations near the wall are much stronger than in the centerline of the pipe. This finding implies that the instabilities were generated near the wall and the radial momentum transfer caused a lower level of velocity fluctuations along the centerline. This is because at high kinetic Reynolds numbers the annular effect becomes pronounced and there exist inflexion points in the velocity profile near the wall. Thus, if the kinetic Reynolds number exceeds a critical value at a given dimensionless fluid displacement, the fluid flow near the wall may first become unstable and eddies occur near the wall. These eddies are transferred to the core flow which cause small fluctuations. As in previous studies, we observed that the turbulence disappeared and the flow recovered to a laminar-like flow in the accelerating period during the following half cycle.

Fig. 4.3 illustrates an example of a fully turbulent flow situation at A_o= 97.1 and Re_ω = 302.2. It is shown that axial velocity fluctuations become much more significant

both near the wall and in the core flow as well. It is interesting to compare Fig. 4.2a with Fig. 4.3 where the dimensionless oscillation amplitude of fluid is fixed at A_o=97.1 and the kinetic Reynolds number is increased from Re_ω = 66.6 to 302.2. It is apparent that velocity fluctuations near the wall at a high kinetic Reynolds number are much larger than those at a lower kinetic Reynolds number. This is because the velocity gradient becomes steeper with the increase of the kinetic Reynolds number. Similarly, when comparing Figs. 4.2b and 4.3, where the kinetic Reynolds number is fixed at Re_ω = 302 while the dimensionless oscillation amplitude is increased from A_o = 47.1 to 97.1, we found that velocity fluctuations become larger with the increase of A_o.

Figs. 4.4a and 4.4b show temporal variations of the pressure drop and the axial velocity near the wall of the pipe at two different sets of A_o and Re_ω. The axial velocity and pressure signals were sampled simultaneously. It is shown that during the acceleration period for which a favorable pressure gradient exists in the flow direction, the flow is laminar. However, during the deceleration period for which an adverse pressure gradient exists, the flow becomes turbulent. It is important to note that the onset of the turbulence occurs whenever the pressure gradient changes signs from both positive to negative or from negative to positive. This finding has never be discussed in the literature.

To identify the conditions for which onset of turbulence occurs, experiments were first carried out for small dimensionless oscillation amplitudes and at low kinetic Reynolds numbers. At a given dimensionless oscillation amplitude of fluid A_o, the value of the kinetic Reynolds number Re_ω is gradually increased until velocity fluctuations appear near the wall but not in the core, as observed on the screen of the oscilloscope. A typical situation is presented in Figs. 4.4a and 4.4b as discussed earlier.

We then recorded the critical value of the kinetic Reynolds number at each dimensionless oscillation amplitude of fluid. It is found that the data for transition to turbulence as represented by solid circles in Fig. 4.5 is fitted well by the following algebraic expression:

$$(A_o)_{cri} = \frac{761}{\sqrt{(Re_\omega)_{cri}}} \tag{4.1}$$

or

$$\sqrt{2}\left(Re_\delta\right)_{cri} = A_0\sqrt{Re_\omega} = x_{max}\sqrt{\frac{\omega}{\nu}} = 761 \tag{4.2}$$

where $(Re_\delta)_{cri}$ is the Reynolds number based on the Stokes layer thickness δ. The parameter Re_δ is the critical transition parameter identified by Sergreev (1966) and Kurzweg et al. (1989). Note that Eq. (4.1) was obtained based on experimental data in the ranges of $8.05 \le A_0 \le 121.1$, and $23 \le Re_\omega \le 540$. There is experimental evidence that the critical value of $(Re_\delta)_{cri}$ depends on Re_ω at small values of A_o and Re_ω (Kurzweg et al., 1989). Eq. (4.2) is presented as a solid straight line in Fig. 4.5. where laminar and turbulent flows exist below and above this line. It is shown that the onset of turbulence in an oscillatory flow occurs at high dimensionless fluid displacements and high kinetic Reynolds numbers; the critical value of A_o decreases with the increase of Re_ω.

4.3 Summary

In this chapter, experiments were carried out for the study of the onset of turbulence in a periodically reversing pipe flow. As in the previous investigations, it is found that onset of turbulence occurs only in the deceleration period of the cycle. The

change in the sign of the pressure gradient is found to be directly responsible for the occurrence of instability in an oscillatory and reversing pipe flow. A correlation equation in terms of the kinetic Reynolds number and the dimeneionless fluid displacement for the onset of turbulence has been obtained.

CHAPTER 5

FULLY-DEVELOPED OSCILLATORY AND REVERSING FLOW

In this chapter, we shall first obtain an analytical expression for the friction coefficient of a fully developed laminar oscillatory and reversing pipe flow. We then compare this expression with experimental data in the laminar flow region. Experimental results for the friction coefficient of a fully-developed turbulent oscillatory and reversing flow in a long pipe will also be presented.

5.1 Introduction

The study of the frictional loss is one of the most important aspects of oscillatory fluid mechanics. Uchida (1956) obtained an analytical solution for the axial velocity distribution of a fully-developed laminar pulsating flow in a long straight pipe. Both sinusoidal and non-sinusoidal motions of fluid were considered by Uchida (1956). In the present study, an analytical expression for the friction coefficient of a laminar fully developed oscillating and reversing pipe flow is derived based on Uchida's solution (1956). Experiments were carried out to measure the pressure drop of laminar and turbulent oscillatory flows downstream of a long pipe at various frequencies and fluid displacements. Comparisons are made between the analytical solution and experimental data for the time-resolved and the cycle-averaged friction coefficient of the laminar fully-developed flow. It is shown that the analytical solution is in good agreement with the measured data. Based on the measured data of pressure drops and cross-sectional mean velocities, a correlation equation for the cycle-averaged friction coefficient of a cyclically turbulent oscillatory flow is obtained in terms of the two similarity

parameters: the kinetic Reynolds number Re_ω and the dimensionless oscillation amplitude of fluid A_o. Finally, a comparison of the cycle-averaged friction coefficient data measured in the laminar and turbulent oscillatory flow regimes will be made.

5.2 Friction Coefficient of a Laminar Flow

5.2.1 Analytical Solution

Consider a hydrodynamically fully-developed oscillatory flow in a pipe with diameter D. The dimensional governing conservation equations of mass and momentum are

$$\frac{\partial u}{\partial x} = 0 \tag{5.1}$$

$$\frac{\partial u}{\partial t} = -\frac{1}{\rho}\frac{\partial p}{\partial x} + \nu\left(\frac{\partial^2 u}{\partial r^2} + \frac{1}{r}\frac{\partial u}{\partial r}\right) \tag{5.2}$$

We now assume the oscillating motion of the fluid is driven by a sinusoidally varying pressure gradient given by

$$\frac{1}{\rho}\frac{\partial p}{\partial x} = A_p \cos \omega t' \tag{5.3}$$

where A_p and $\omega t'$ are the oscillation amplitude and the phase angle of the externally imposed pressure gradient. An exact solution for the axial velocity profile of a fully-developed oscillatory and reversing flow can be obtained from a modification of Uchida's analytical solution (1956) to give:

$$u = \frac{A_p D^2}{4\lambda^2 \nu}[B\cos\omega t' + (1 - A)\sin\omega t'] \tag{5.4}$$

where A and B are given respectively by

$$A = \frac{\text{ber}\,\lambda\,\text{bei}2\lambda R + \text{bei}\,\lambda\,\text{ber}2\lambda R}{\text{ber}^2\,\lambda + \text{bei}^2\,\lambda} \tag{5.5}$$

$$B = \frac{\text{ber}\,\lambda\,\text{ber}2\lambda R - \text{bei}\,\lambda\,\text{bei}2\lambda R}{\text{ber}^2\,\lambda + \text{bei}^2\,\lambda} \tag{5.6}$$

with $R = \frac{r}{D}$ being the dimensionless radial coordinate and λ being the Stokes number defined in Eq. (2.6). Integrating Eq. (5.4) over the cross section of the pipe yields the cross-sectional mean velocity in the same form as given by Eq. (2.2). For the case where the externally imposed pressure gradient is given by Eq.(5.3), it can be shown that the maximum cross-sectional mean velocity u_{max} is related to A_p by

$$u_{max} = \frac{A_p D^2 \sigma}{32\nu} \tag{5.7a}$$

while the phase angle ϕ is related to $\omega t'$ by

$$\phi = \frac{\pi}{2}(\omega t' - \Gamma) \tag{5.7b}$$

where

$$\sigma = \frac{8}{\lambda^3}\sqrt{(\lambda - 2C_1)^2 + 4C_2^{\,2}} \tag{5.8a}$$

$$\Gamma = \tan^{-1}\left[\frac{\lambda - 2C_1}{2C_2}\right] \tag{5.8b}$$

In Eq. (5.8), C_1 and C_2 are given by

$$C_1 = \frac{\text{ber}\,\lambda\,\text{bei}'\lambda - \text{bei}\,\lambda\,\text{ber}'\lambda}{\text{ber}^2\lambda + \text{bei}^2\lambda} \tag{5.9a}$$

$$C_2 = \frac{\text{ber}\,\lambda\,\text{ber}'\lambda + \text{bei}\,\lambda\,\text{bei}'\lambda}{\text{ber}^2\lambda + \text{bei}^2\lambda} \tag{5.9b}$$

where $\text{ber}'\lambda = \frac{d(\text{ber}\,\lambda)}{d\lambda}$, and $\text{bei}'\lambda = \frac{d(\text{bei}\,\lambda)}{d\lambda}$. It follows from Eqs. (5.4) and (5.7a) that the dimensionless axial velocity for a fully-developed oscillatory flow is given by

$$U = \frac{u}{u_{max}} = f(R, \tau, Re_\omega) \tag{5.10}$$

Eq. (5.10) shows that the dimensionless axial velocity of a fully-developed flow, at a given position and time, is a function of the kinetic Reynolds number only.

We now define the instantaneous friction coefficient c_f and the cycle-averaged friction coefficient $\bar{c}_f$ as

$$c_f = \frac{\tau_w}{\frac{1}{2}\rho u_{max}^2} = \frac{\mu(\frac{\partial u}{\partial r})_{r=D/2}}{\frac{1}{2}\rho u_{max}^2} \tag{5.11}$$

$$\bar{c}_f = \frac{1}{2\pi}\int_0^{2\pi}\sqrt{c_f^2}\,d\tau \tag{5.12}$$

where τ_w is the wall shearing stress and μ is the viscosity of the fluid. Eq. (5.11) is a function of time only for a fully-developed flow, but it depends on both position and time for a developing flow which will be disussed in the next chapter. An exact solution for the instantaneous and the cycle-averaged friction coefficients of a fully developed laminar oscillatory flow ($c_{f,\infty}$ and $\bar{c}_{f,\infty}$) can be obtained by differentiating Eq. (5.4) and substituting into Eqs.(5.11) and (5.12) to yield

$$c_{f,\infty} = \frac{32F_\omega}{A_o}\sin(\phi+\delta) \tag{5.13}$$

$$\bar{c}_{f,\infty} = \frac{64F_\omega}{\pi A_o} \tag{5.14}$$

with

$$F_\omega = \frac{\sqrt{C_1^2+C_2^2}}{16\sqrt{(\lambda-2C_1)^2+4C_2^2}} \tag{5.15a}$$

$$\delta = \tan^{-1}\left[\frac{\lambda-2C_1}{2C_2}\right] - \tan^{-1}\left[\frac{C_2}{C_1}\right] \tag{5.15b}$$

where A_o is given by Eq. (2.10), δ is the phase angle difference between the cross-sectional mean velocity u_m given by Eq. (2.2) and the wall shearing stress. It should be noted that both F_w and δ are functions of Re_ω only. It is interesting to note that although the velocity in a fully-developed oscillatory flow depends only on the kinetic

Reynolds number, the friction coefficients of a fully-developed oscillatory flow depend not only on the kinetic Reynolds number Re_ω , but also on the dimensionless oscillation amplitude of the fluid A_o as well. The instantaneous pressure coefficient can be either positive or negative during a cycle. The positive sign of the friction coefficient means that the fluid flow moves in the positive direction while the negative sign implies that it moves in the negative direction.

The values of F_ω and δ versus Re_ω given by Eqs.(5.15a) and (5.15b) are presented in Fig. 5.1. Since these expressions are complicated functions of Re_ω simplified expressions for these quantities are needed. For this purpose, the values of F_ω and δ computed from Eqs. (5.15a) and (5.15b) are fitted by the following algebraic expressions

$$F_\omega = \frac{0.16061}{(Re_\omega^{0.548} - 2.03946)} \tag{5.16a}$$

$$\delta = 0.647[1 - 1.015\exp(-0.019Re_\omega)] \tag{5.16b}$$

The values of F_ω and δ computed from the approximate expressions given by Eq. (5.16) and the exact solution given by Eq. (5.15) are in good agreement in the range of Re_ω from 10.4 to 400. The standard deviations are 3.3% for F_ω and 1.9% for δ with the maximum relative errors being 6.4% for F_ω and 2.8% for δ.

Substituting Eq. (5.16a) into Eq. (5.14) yields

$$\bar{c}_{f,\infty} = \frac{3.27192}{A_o(Re_\omega^{0.548} - 2.03946)} \tag{5.17}$$

which shows that the cycle-averaged friction coefficient is inversely proportional to both Re_ω and A_o.

5.2.2 Experimental Investigation

A differential pressure transducer was employed to measure the pressure drop in a laminar oscillatory and reversing flow downstream of a long pipe while a hot-film probe was used to measure the cross-sectional mean velocity. The details of the experimental setup have been described in Chapter 3. Since pressure drops were measured in the fully-developed flow region, the reduction of experimental data will be based on a hydrodynamically fully-developed flow whose momentum equation is given by Eq. (5.2). If Eq. (5.2) is first multiplied by $2\pi r dr$ and integrated over the cross section of the tube and then integrated with respect to x from x=0 to x=L, it becomes

$$\frac{\Delta p}{L} = \rho \frac{du_m}{dt} + \frac{4\tau_w}{D} \tag{5.18}$$

where we have assumed $\frac{\partial p}{\partial x}$ to be a constant. Substituting Eq. (5.18) into Eq. (5.11) and solving for $c_{f,exp}$ yields

$$c_{f,exp} = \frac{1}{2\rho u_{max}^2}\left[\Delta p \frac{D}{L} - \rho D \frac{du_m}{dt}\right] \tag{5.19}$$

where Δp and u_m can be measured by a differential pressure transducer and a hot-wire anemometer, respectively. These data were analyzed using an ensemble-averaged

procedure. The ensemble-averaged pressure drop $\Delta\tilde{p}$ and the axial cross-sectional mean velocity $\tilde{u}_m$ are defined as

$$\Delta\tilde{p}(\phi) = \frac{1}{N}\sum_{i=1}^{N} \Delta p_i[\phi + 2\pi(i-1)] \tag{5.20a}$$

$$\tilde{u}_m(\phi) = \frac{1}{N}\sum_{i=1}^{N} u_{m,i}[\phi + 2\pi(i-1)] \tag{5.20b}$$

where N is the total numbers of cycles to be ensemble averaged and was typically set to be 100 in this study.

The measured cycle-averaged friction coefficient $\bar{c}_{f,exp}$ is defined as

$$\bar{c}_{f,exp} = \frac{1}{N_i}\sum_{j=1}^{N_i} \sqrt{c^2_{f,exp,j}} \tag{5.21}$$

where N_i is the total number sampling intervals in a cycle, and $c_{f,exp,j}$ is the measured data from Eq. (5.19) at *j*th time interval.

5.2.3 Comparison of Theory and Experiments

In this section, we shall compare the analytical results of the instantaneous and cycle-averaged friction coefficients given by Eq.(5.17) for a laminar oscillatory fully-developed flow with experimental data on pressure drop downstream of a long pipe for $A_o \leq 26.42$, and with values of Re_ω ranging from 23.1 to 395. In these ranges of parameters, the flow is laminar as observed in Chapter 4.

Fig 5.2 shows a comparison of the cross-sectional mean velocity u_m given by Eq. (2.2) and the measured ensemble-averaged velocity at the inlet of the tube at Re_ω= 208.2 for A_o= 16.5 and 22.51. It is shown that for the smaller value of A_o (A_o =16.5) the measured velocity is in good agreement with the assumed cross-sectional mean velocity of the analytical solution. For higher values of A_o (A_o =22.51 for example), however, the measured velocities deviated slightly from the sinusoidal curve at certain instances of time. Uncertainty in the ensemble-averaged velocity is about 2.5%. It is worth mentioning that the velocity shown in the figure is the absolute value since the hot-wire probe could not detect the flow direction.

Typical variations of the measured instantaneous pressure drop during a complete cycle at A_o=26.42 for Re_ω=144.1 and Re_ω=324.3 are illustrated in Fig 5.3. It is seen that the pressure drop increases with the kinetic Reynolds number at a fixed value of dimensionless oscillation amplitude of the fluid. There are two reasons for the increase of the pressure drop under these conditions. First, the increase of the kinetic Reynolds number leads to more significant "annular effect", and thus the radial velocity gradients adjacent to the pipe wall become steeper; consequently, the friction force increases with the increase of the kinetic Reynolds number. Secondly, the inertia component in the momentum balance increases with the increase of the kinetic Reynolds number.

Fig 5.4a shows typical variations of the instantaneous friction coefficient c_f during a complete cycle at A_o=16.5 for Re_ω=64 and Re_ω=208.2 while Fig 5.4b shows those at Re_ω=256.1 for A_o=16.5 and A_o=26.42. The circlar symbols represent the measured data $c_{f,exp}$ while the solid lines represent the analytical solutions $c_{f,\infty}$, given by

Eq. (5.12a), at the same corresponding conditions. Generally, the temporal friction coefficient varies sinusoidally with time and its amplitude decreases with either the increase of the kinetic Reynolds number at a fixed value of the dimensionless oscillation amplitude of the fluid (shown in Fig. 5.4a), or the increase of the dimensionless oscillation amplitude of the fluid at a fixed value of the kinetic Reynolds number (shown in Fig, 5.4b). Comparing the analytical solution with the measured data, we can see that the analytical solution is in a fairly good agreement with the experimental data.

A comparison of the cycle-averaged friction coefficient of the measured data $\bar{c}_{f,exp}$ and the analytical solution $\bar{c}_{f,\infty}$ given by Eq. (5.14) for A_o=16.5, 22.51, and 26.42 is presented in Fig. 5.5. The symbols represent the measured data while the solid line represents the analytical solution. It is shown that the analytical solution is in good agreement with the experiment, with the maximum deviation from the analytical solution being 14.8%. The scatter of data may be attributed to the fact that fluctuations occurred in the measurements of pressure drops and cross-sectional mean velocities as shown in Figs. 5.2 and 5.3.

In order to assess the accuracy of Eq. (5.17) for the cycle-averaged friction coefficient of a laminar fully-developed oscillatory flow, the measured data and the values computed from Eq. (5.17) are presented in Fig 5.6. Any deviations of data from the inclined straight line indicates the inaccuracy of the predication equation. As shown in Fig. 5.6, Eq. (5.17) correlates the experimental data quite well, with the maximum relative deviation being 15%. Therefore, we concluded that Eq. (5.17) is a good correlation equation for the prediction of the cycle-averaged friction coefficient of oscillatory and reversing flow in a long pipe, and is valid in the present experimental range, i.e.: $A_o \leq 26.42$ and $23.1 \leq Re_\omega \leq 395$.

5.3 Friction Coefficient of a Turbulent Flow

The friction coefficient of a cyclically turbulent oscillatory flow $\bar{c}_{f,t}$ was also measured. The range of the dimensionless fluid displacement A_o and the kinetic Reynolds number Re_ω covered in this study is illustrated in Fig. 4.5. Forty-three experimental runs, represented by the triangular symbols above the solid line in Fig. 4.5, were performed to investigate the friction coefficient in the turbulent flow regime. The measured data are shown in Fig. 5.7, where the cycle-averaged friction coefficient multiplied by the dimensionless oscillation amplitude of the fluid A_o is plotted against the kinetic Reynolds number Re_ω. It was found that the following algebraic equation fits the measured data with a maximum relative error of 14.8%:

$$\bar{c}_{f,t} = \frac{1}{A_o}\left(\frac{76.6}{Re_\omega^{1.2}} + 0.40624\right) \tag{5.22}$$

The correlation equations of the cycle-averaged friction coefficient for the laminar and turbulent flow given by Eqs. (5.17) and (5.22) respectively are compared in Fig. 5.8. It is evident that the value of $\bar{c}_f(A_o)$ for the turbulent flow is significantly higher than that of the laminar flow for the same given kinetic Reynolds number.

5. 4 Summary

In this chapter, it was shown that a sinusoidally oscillatory and reversing flow in a long pipe is governed by two similarity parameters: the dimensionless oscillation

amplitude of fluid and the kinetic Reynolds number. Analytical expressions of the instantaneous and cycle-averaged friction coefficients for a fully developed laminar oscillating and reversing pipe flow have been obtained in terms of these two parameters. These simple equations for the friction coefficients of a laminar oscillatory and reversing flow are shown in good agreement with measured data. Based on the measurement of pressure drops and cross-sectional mean velocities, a correlation equation for the cycle-averaged friction coefficient of a cyclically turbulent flow has also been obtained. A comparison of the cycle-average friction coefficients of the turbulent flow and laminar flow has been made.

CHAPTER 6

DEVELOPING LAMINAR OSCILLATORY FLOW

The preceding chapter is concerned with the friction coefficient at a location far downstream from the pipe entrance region where a fully developed flow has been established. However, an oscillatory flow in a pipe of finite length is more frequently encountered in real situations where the entrance length cannot be ignored. In this chapter, we shall obtain a numerical solution for a laminar hydrodynamically developing oscillatory and reversing flow in a pipe with a finite length.

6.1 Introduction

A hydrodynamically developing oscillatory and reversing flow in a short pipe occurs more frequently in engineering applications, such as in internal combustion engines, Stirling engines, cryocoolers and other periodical processes in thermal and chemical systems. In this chapter, we shall obtain a numerical simulation of an incompressible, laminar, hydrodynamically developing flow, which oscillates periodically and reversingly in a short pipe. The purposes of this study are to gain insights into this complicated flow phenomena, and to develop a correlation equation for the prediction of the friction coefficient of a laminar oscillating flow in a short pipe.

6.2 Formulation

Consider an incompressible, laminar, viscous fluid oscillates periodically and reversibly in a pipe (with diameter D and a finite length L) which is connected between

two large reservoirs as shown in Fig. 2.1. We assume that the fluid in the reservoir is undergoing an oscillatory motion which is driven by a sinusoidal displacer. Under this situation, the cross-sectional mean velocity u_m in the pipe is given by Eq. (2.2); the governing dimensionless conservation equations of mass and momentum for the periodically reversing pipe flow are given by Eqs. (2.4) and (2.10).

Boundary conditions adopted in the present numerical analysis are those no-slip occuring at that the tube wall and the axial velocity at the inlet (X=0) is as specified by Eq. (2.2). Thus, the dimensionless axial velocity at the inlet of the pipe (X= 0) during the first each half cycle is

$$U(0,R,\tau) = \sin\phi \qquad 0 \le \phi \le 180^{\circ} \tag{6.1}$$

The corresponding outflow condition at the outlet of the tube (X=L/D) is given by

$$\frac{\partial U}{\partial X}(L/D,R,\tau) = 0 \qquad 0 \le \phi \le 180^{\circ} \tag{6.2}$$

It is relevant to note that the inlet and outlet conditions change at each half-cycle as the fluid flow reverses its direction periodically. Thus, for a oscillatory and periodically reversing hydrodynamically developing flow, the similarity parameters are A_{o},, Re_{ω} and L/D.

A numerical solution to Eqs. (2.4) and (2.10) subject to the boundary conditions (6.1) and (6.2) was carried out based on a control-volume method detailed in Chapter 2. A grid independence solution for each group of Re_{ω}, A_o and L/D was established by reducing the grid size until the computed instantaneous friction coefficient in the fully

developed region was within 1% of the analytical solution given by Eq. (5.13). The choice of 181 grid points in the axial direction and 31 points in the radial direction was found to provide grid independence for the results reported in this study. For each case, 180 time steps were used in one cycle and transient behaviors were recorded until a steady periodic state was reached.

6.3 Results and Discussion

Computations were carried out for pipes with L/D=20 and 30, with values of A_o ranging from 8 to 30, and Re_ω from 15 to 400. As shown in Chapter 4, the oscillatory flow is laminar within these ranges of the parameters. The results of these computations at steady periodic states are presented in Figs. 6.1-6.5.

6.3.1 Velocity Profiles

Typical transient velocity profiles during a cycle at different locations along the pipe length for A_o=10 and Re_ω=100 are illustrated in Fig. 6.1. The fluid enters the pipe as a plug flow from the left (X=0) during the first half cycle ($0 \le \phi \le 180^\circ$), and a viscous boundary layer caused by wall friction forms at the inlet and grows in thickness downstream. Because of viscous and inertial effects, velocity profiles downstream (X= 0.8) change from a rectangular shape to a parabola-like shape with velocity overshoot occurring near the walls, i.e., the so-called annular effect becomes pronounced. At the instant when the cross-sectional mean velocity of fluid is zero ($\phi = 0^\circ$), the velocity near the wall is positive while the core flow remains in the negative x-direction due to the inertia effect from the previous half cycle. During the second half cycle ($180^\circ \le \phi \le 360^\circ$), the fluid flow reverses its direction and repeats the behavior similar

to those in the first half cycle. It should be added that unlike a unidirectional laminar steady flow, the viscous layers in an oscillatory flow may not coalesce at the fully developed region because velocity near the wall and in the core is out of phase due to the inertial effect (at high Re_ω). Further downstream (at X=10 for this particular case) the velocity profile ceases to change with the axial position which is defined to be hydrodynamically fully developed. It is interesting to note that as the fluid moves toward the exit (X=19.2), the shape of the velocity profile begins to change with the axial location again. This can be seen by comparing the velocity profiles at X = 19.2 with the fully-developed velocity profiles at X = 10. The change of the velocity profile with the axial location near the exit is caused by the fact that the flow reverses its direction. We shall call this the "exit effect".

Fig. 6.2a shows that the effect of the kinetic Reynolds number on centerline velocity variations along the pipe at $\phi = 90^\circ$ near the entrance ($0 \le X \le 10$). For slow oscillations (Re_ω= 23 and 41), the centerline velocity increases asymptotically with distance to the fully developed value, which is similar to that of a unidirectional steady flow. For fast oscillations (Re_ω= 64, 100, and 196), the centerline velocity increases to a maximum value and then decreases before the fully developed region is reached. This is owing to the fact that annular effects occur in a fast oscillatory flow.

Fig. 6.2b illustrates the variations of the centerline velocity along the pipe at different phase angles ϕ for a fast oscillating flow (A_o=10 and Re_ω=100). This figure clearly shows that there are three flow regions at any instants of time: an entrance region where the centerline axial velocity either increases or decreases with the axial location, a fully-developed region where the centerline axial velocity remains unchanged,

and an exit region where the centerline velocity either increases or decreases with distance.

As explained earlier, the entrance length reflects the development of the velocity profile from a plug flow to a fully-developed shape due to wall friction and inertial effects. It can also be seen from Fig. 6.2b that at some instants of time (such as $\phi = 45^{\circ}$ 90° and 135° during the first half cycle) the centerline velocity increases before the fully developed region is reached. The plug flow at the inlet becomes parabolic at some distance from the inlet, and the annular effect appears downstream (see Fig. 6.1).

To investigate the exit effect, we focus our attention to the centerline velocity variations in the exit regime (near X= 20) at $\phi = 180^{\circ}$ as shown in Fig. 6.2b. At this instant of time, the centerline velocity near the exit begins to decrease from the fully-developed value to zero at the exit due to the fluid flow reversing its direction. However, at other instants of time, the centerline velocity near the exit is not zero and may be in fact higher than the fully-developed value because of the inertial effect as shown in Fig. 6.2b. This exit effect is clearly shown in Fig. 6.2c, where the axial centerline velocities at both X = 18.4 and 20 may be higher or lower than the fully developed value depending on the particular instant of time. It is relevant to point out that the slope of the centerline velocity variation with time at the exit (X=20) is discontinuous at $\phi = 180^{\circ}$ as shown in Fig. 6.2c. This is because the axial centerline velocity at the exit reverses its direction at $\phi = 180^{\circ}$.

6.3.2 Friction Coefficients

The instantaneous local friction coefficient $c_f(X,\tau)$ has been defined in Eq. (5.11). The cycle-averaged local friction coefficient $\bar{c}_f$ can be defined as

$$\bar{c}_f(X) = \frac{1}{2\pi}\int_0^{2\pi}\sqrt{c_f^2(X,\tau)}d\tau \qquad (6.3)$$

Fig. 6.3a shows a comparison of the numerical results of the instantaneous friction coefficient at large X (i.e., a fully-developed flow) for A_o=8 at Re_ω=64 and 324 and the exact solution for a fully developed flow given by Eq. (5.12). The curves indicate that the agreement between the numerical results and the analytical solution is excellent.

The variations of the instantaneous friction coefficient along the pipe at different phase angles ϕ for A_o=30 and Re_ω=196 are illustrated in Fig. 6.3b. It is shown that during the first half cycle ($0 \le \phi \le 180^\circ$) as the fluid flowing through the tube from the left to the right, the friction coefficient decreases asymptotically from the maximum value at the inlet of the pipe and practically becomes independent of the axial positions downstream in the fully developed region. The drastic decrease of the instantaneous friction coefficient in the entrance regime is owing to the change in the velocity profile from rectangular to parabola-like shape. The variation of the instantaneous friction coefficient is relatively small in the exit region (near X = 30) for most of the time. But near the flow reversing period ($\phi = 180^\circ$) the variation of the friction coefficient becomes much more significant in the exit region. During the second half cycle ($180^\circ \le \phi \le 360^\circ$), the behavior is repeated in the reverse direction.

A typical variation of the cycle-averaged friction local coefficient $\bar{c}_f$ along the pipe is illustrated in Fig. 6.3c. It is seen that the cycle-averaged local friction coefficient

is symmetrical with respect to the middle of the pipe. It should be noted that the drastic increase in the value of the cycle-averaged local friction coefficient at either end of the pipe is owing to the end effects (i.e., a combination of the entrance and the exit effects) with the entrance effect being predominant. We shall henceforth call the length from the inlet to the fully- developed flow regime (or from the fully-developed flow regime to the outlet) as the end length. The end effect and the end length are shown in Fig. 6.3c.

The variations of the cycle-averaged local friction coefficient $\bar{c}_f$ along the left hand side of the pipe ($0 \le X \le 10$) for different A_o and Re_w are presented in Fig. 6.3d. For comparison purposes, the analytical values computed from Eq. (5.15) are represented by half-solid circles in this figure. It is noted that the numerical solution in the fully-developed region is in excellent agreement with the analytical solution as discussed earlier.

End Length

The end length L_e for an oscillatory and reversing flow is determined based on the following criterion:

$$\frac{\bar{c}_f(X) - \bar{c}_{f,\infty}}{\bar{c}_{f,\infty}} = 0.01 \qquad (6.4)$$

Eq. (6.4) implies that the end length at the present work is a time-averaged value. Fig. 6.3d shows that the end length increases significantly with the increase of A_o but remains relatively constant with the change of $\phi = 180^o$. It was found that the change of

the end length is less than 3% for the range of Re_ω computed. Thus, we can conclude that the end length is only sensitive to A_o, but not to Re_ω for the range of the kinetic Reynolds number considered. The results of numerical calculations of the end length as a function of A_o can be fitted by the following algebraic equation

$$L_e / D = 0.246A_o + 1.22 \tag{6.5}$$

A comparison of Eq. (6.5) with the results of the numerical solution is shown in Fig. 6.4.

Space-Cycle Averaged Friction Coefficient

The space-cycle averaged friction coefficient $(\bar{c}_f)_m$ of a pipe with a length L is

$$(\bar{c}_f)_m = \frac{1}{L}\int_0^L \bar{c}_f(x)dx \tag{6.6}$$

Eq. (6.6) can be integrated over the two end regions and the fully developed region as indicated in Fig. 6.3c to give

$$(\bar{c}_f)_m = \frac{2L_e}{L}(\bar{c}_{f,e})_m + \frac{L-2L_e}{L}\bar{c}_{f,\infty} \tag{6.7a}$$

with

$$(\bar{c}_{f,e})_m = \frac{1}{L_e}\int_0^{L_e} \bar{c}_f(x)dx \tag{6.7b}$$

Eq. (6.7b) was computed for A_o= 8 to 30 and Re_ω=15 to 400 with L_e given by Eq. (6.5). The results of the computations are presented as a solid curve in Fig. 6.5, which can be correlated by the following expression

$$(\bar{c}_{f,e})_m = \frac{3.774}{A_o(Re_\omega^{0.543} - 2.20863)} \tag{6.8}$$

For comparison purposes, the value of $\bar{c}_{f,\infty}$, given by Eq. (5.15) for a fully-developed flow, is also plotted in Fig. 6.5 as dashed lines. It is shown that the spaced-cycle average friction coefficient in the end region given by the solid line is higher than that in the fully-developed flow region given by dashed lines.

6.4 Summary

In this chapter, the problem of a laminar incompressible periodically reversing flow in a pipe with a finite length was investigated numerically. For a sinusoidally oscillatory and reversing flow in a pipe with a finite length, it was shown that the three governing similarity parameters of the problem are: the kinetic Reynolds number Re_ω, the dimensionless oscillation amplitude A_o and the length to diameter ratio of the pipe L/D. At any instant of time, there exists three flow regimes in the pipe: an entrance regime, a fully developed regime, and an exit regime. The existence of the entrance regime is owing to the velocity profile changes from a rectangular shape to a parabola-like shape. The existence of the exit regime is because of the reversal of flow direction at the end of each half cycle. This phenomena is unique for a periodically oscillatory and reversing flow. Based on the numerical results, a correlation equation of the space-

cycle averaged friction coefficient for an incompressible, laminar, hydrodynamically developing oscillatory flow in a pipe with a finite length was obtained.

CHAPTER 7

LAMINAR OSCILLATORY HEAT TRANSFER IN A PIPE WITH CONSTANT WALL TEMPERATURE

In this chapter we shall obtain a numerical solution for the forced convection of a laminar oscillatory flow in a heated pipe at constant wall temperature. The purpose of this study is to gain physical insight on heat transfer characteristics in an oscillatory and periodically reversing flow.

7.1 Introduction

The problem of oscillatory heat transfer in a heated pipe subjected to a periodically reversing flow has important applications to the design of heat exchangers of Stirling-cycle machines. Most of the previous work is limited to analytical studies of a thermally fully-developed flow. For example, Gedeon (1980) and Kurzweg (1989) analyzed the enhancement of axial heat transfer in an oscillatory flow between two parallel plates. Siegel (1987) obtained an analytical solution for the heat transfer of a pulsating flow in a channel with uniform heat flux.

In this chapter, a numerical solution based on the control volume approach is obtained for laminar forced convection of a periodically reversing flow in a pipe heated at constant temperature. The effects of the kinetic Reynolds number, the dimensionless oscillation amplitude of fluid, and the length to diameter ratio of the pipe on both the temperature profiles and Nusselt numbers for air are illustrated. It will be shown that the annular effect also exists in temperature profiles at high kinetic Reynolds numbers near the entrance and exit of the pipe. As far as the author is aware, this is the first time

that annular effects in the temperature profiles of an oscillating flow are discussed. A correlation equation of the space-cycle averaged Nusselt number for a periodically reversing flow of air will be obtained in terms of the three similarity parameters, Re_ω, A_o and L/D. This correlation equation can be used for the design of heat exchangers in Stirling machines and cryocoolers.

7.2 Formulation

The problem under consideration is shown in Fig. 2.1, where an incompressible, laminar, viscous fluid oscillates in a heated pipe (with diameter D and a finite length L) which is connected between two large reservoirs at a constant but lower temperature T_i. The wall of the pipe is heated at a constant temperature T_w. The inlet axial velocity during the each half cycle is taken to be uniform over the cross section with periodical variations as given by Eq. (2.2). The governing dimensionless conservation equations of mass, momentum and energy for a periodically reversing pipe flow are given by Eqs. (2.4), (2.10) and (2.12). The numerical solution for the velocity field has already been presented in Chapter 6. The thermal boundary conditions for the problem under consideration are

$$\text{at } X=0, \qquad 0 \le R \le 0.5: \quad \theta(0,R,\tau) = 0 \tag{7.1}$$

$$\text{at } X=L/D, \qquad 0 \le R \le 0.5: \quad \theta(L/D,R,\tau) = 0 \tag{7.2}$$

$$\text{at } R=0, \qquad 0 \le X \le L/D: \quad \frac{\partial \theta}{\partial R} = 0 \tag{7.3}$$

at R=0.5, $\qquad 0 \le X \le L/D: \quad \theta(X, 0.5, \tau) = \theta_w = 1 \qquad (7.4)$

Thus, we can conclude from the governing equations and the boundary conditions that the similarity parameters for the problem of oscillatory heat transfer in a pipe subjected a periodically reversing flow are A_o, Re_ω, L/D, and Pr.

Numerical solutions to Eqs. (2.4), (2.10) and (2.12), subject to boundary conditions (6.1) to (6.2) and (7.1) to (7.4), were obtained by a control-volume-based method detailed by Patankar [13]. Because of the extremely thin thermal boundary layer at a high kinetic Reynolds number, a highly nonuniform grid was deployed. Extensive computations were performed to ensure grid independent solutions for different values of the kinetic Reynolds number. A grid independent solution for a particular set of parameters was established by reducing the grid size until the change in the space-cycle averaged Nusselt number $\overline{Nu}$ (see definition below) is smaller than 0.4%.

7.3 Results and Discussion

As mentioned earlier, the problem under consideration has four similarity parameters: A_o, Re_ω, L/D and Pr. Most of the computations were carried out for a laminar flow of air (Pr = 0.71) in a pipe with L/D=40. The frequency of oscillations were varied such that the range of Re_ω is from 10 to 400 and the range of dimensionless oscillation amplitude of the fluid is from 5 to a value less than the critical A_o for the onset of turbulence, which is given by Eq. (4.1). The results of the computations are presented in Figs. 7.1-7.11.

7.3.1 Temperature Distribution

Figs. 7.1a and 7.1b illustrate typical temporal variations of temperature and axial velocity of the fluid near the entrance of the pipe (X=6.2) for A_o =15 and Re_ω=64 at different radial positions during one cycle ($0° \le \phi \le 360°$). As shown in Fig 7.1a, during the first half cycle ($0° \le \phi \le 180°$) the fluid temperature near the entrance changes slowly when the phase angle is less than $\phi \cong 45°$, then it begins to drop rapidly due to colder fluid entering the pipe from the reservoir. The fluid temperature near the entrance starts to rise near the end of the first half cycle due to the warmer fluid exiting from the pipe. Similar trends are observed for a higher kinetic Reynolds number Re_ω=250 (Fig. 7.2a), with peaks and valleys occuring at different phase angles because the phase angles of the axial velocity change with Re_ω. From Figs. 7.1 and 7.2, it can be observed that at the centerline of the pipe, the phase difference between the axial velocity and temperature variations for Re_ω= 64 is about 52° while those at Re_ω = 250 is about 86°. At R = 0.47, the corresponding phase differences are 84° and 60°, respectively. It can be concluded that the phase difference between the velocity and temperature in the core flow region increases with the kinetic Reynolds number. But the phase difference near the wall region decreases with the increase of the kinetic Reynolds number. This is because the heat transfer rate is faster near the wall at higher kinetic Reynolds numbers, and consequently, the temperture near the wall responds more swiftly with respect to velocity variations.

Transient temperature profiles near the entrance of the pipe (X=4.5) for A_o= 15 at two different kinetic Reynolds numbers (Re_ω=64 and 250) are presented in Figs. 7.3a and 7.3b respectively. At these kinetic Reynolds numbers, annular effects exist in the velocity profiles (not shown). It is interesting to note that annular effects also exist

in the temperature profiles of an oscillatory flow as shown in Fig. 7.3. This annular effect becomes more pronounced as the kinetic Reynolds number is increased. A comparison between Figs. 7.3a and 7.3b shows that temperature gradients near the wall become steeper when the kinetic Reynolds number is increased.

Transient temperature profiles near the center of the heated pipe (X= 15) at a fixed value of Re_ω= 250 for two different dimensionless fluid displacements (A_o=15 and 25) are presented in Figs. 7.4a and 7.4b respectively. Fig. 7.4a shows that no annular effect exists at positions near the mid-section of the pipe although annular effect is clearly evident near the entrance of pipe (X= 4.5) as shown in Fig. 7.4b. In comparison of Figs. 7.3b and 7.4a, the temperature profiles are flatter near the mid-section of the heated pipe than near the entrance. These findings can be explained based on Eq. (2.12) as follows. At a position near the mid-section of the pipe, axial temperature gradients are small, as will be shown below shortly. Therefore, the second term in Eq. (2.12) is small and the forced convection effect becomes less significant. Thus, the transient development of temperature profiles near the mid-section of the pipe depends mainly on the diffusion mechanism. However, if the kinetic Reynolds number is fixed at 250 and the fluid displacement A_o is increased from 15 to 25, the convection term in Eq. (2.12) will become larger and will have some effect on the temperature profile. This point is illustrated in Fig. 7.4b where the variation of temperature along the radial direction becomes more significant across any instant of time.

Typical variations of the centerline temperature along the pipe at different phase angles for A_o=15 and Re_ω=180 are presented in Fig. 7.5. Because the pipe is heated at a constant temperature θ_w, the centerline temperature of the fluid increases

with the distance from the entrance or exit of the pipe with a maximum value occuring near the mid-section of the pipe. The fact that the fluid temperature variation is almost symmetric with respect to X suggests that heat conduction is predominant near the mid-section of the pipe. However, the location at which the maximum value of the fluid temperature occurs, depends on time and the dimensionless parameters A_o and Re_ω.

7.3.2 Heat Flux

The local instantaneous Nusselt number along the heated wall for an unsteady flow is defined as

$$Nu = \frac{h(X,\tau)D}{k} \tag{7.5}$$

where h is the local instantaneous heat transfer coefficient which is defined as

$$h(X,\tau) = \frac{q_w(X,\tau)}{\Delta T(X,\tau)} = \frac{-k(\partial T/\partial r)_{r=D/2}}{\Delta T} \tag{7.6}$$

where q_w is the heat flux at the pipe wall and ΔT is a thermal potential for the heat flux. For an unidirectional flow $\Delta T = T_w - T_b$ is the difference between the wall temperature and the local instantaneous bulk temperature $T_b(x,t)$ which is defined as

$$T_b(x,t) = \frac{\int_0^{D/2} u(r,x,t)T(r,x,t)rdr}{\int_0^{D/2} u(r,x,t)rdr} \tag{7.7}$$

The instantaneous bulk temperature given by Eq.(7.7) losts its physical significance in an oscillating and reversing flow because the cross-sectional mean velocity becomes zero twice in each cycle, which gives rise to an infinite value of the bulk temperature twice in a cycle. This will cause anomalies in evaluating the local instantaneous Nusselt number defined in Eqs. (7.6) and (7.7). For this reason, for a periodically reversing flow we choose $\Delta T = T_w - T_i$ which is the thermal potential for heat transfer from the heated wall of the pipe to the cold fluid at the entrance and the exit of the pipe. Substituting this temperature difference in Eq. (7.7) gives the following expression for the local instantaneous Nusselt number

$$Nu = -(\frac{\partial \theta}{\partial R})_{R=0.5} \tag{7.8}$$

It should be noted that the value of the local instantaneous Nusselt number is a function of the axial location X and the time τ. The cycle-averaged local Nusselt number $\overline{Nu}_X$, the space-averaged instantaneous Nusselt number $\overline{Nu}_\tau$, and the space-cycle averaged Nusselt number $\overline{Nu}$ are defined respectively as follows

$$\overline{Nu}_X = \frac{1}{2\pi}\int_0^{2\pi} Nu(X,\tau)d\tau \tag{7.9}$$

$$\overline{Nu}_\tau = \frac{1}{L/D}\int_0^{L/D} Nu(X,\tau)dX \tag{7.10}$$

and

$$\overline{Nu} = \frac{1}{2\pi}\int_0^{2\pi}\overline{Nu}_\tau d\tau = \frac{1}{L/D}\int_0^{L/D}\overline{Nu}_X dX = \frac{1}{2\pi L/D}\int_0^{2\pi L/D}\int_0^{} Nu(X,\tau)d\tau dX \tag{7.11}$$

The variations of the local instantaneous Nusselt number $\overline{Nu}$ along different dimensionless axial locations of the pipe for A_o=15 at Re_ω=64 and Re_ω=250 across a complete cycle are presented in Figs. 7.6a and 7.6b respectively. The solid lines represent locations in the entrance region while the dashed lines represent locations in the exit region. It should be noted that the phase difference between the entrance location and the corresponding exit location is ϕ=180°. Let us focus our attention first to the entrance region. Near the inlet at X=2 for example, the instantaneous Nusselt number increases with ϕ until it reaches a maximum value around ϕ=90°. This is because the colder fluid enters the entrance region with the cross-sectional mean velocity according to Eq. (2.2) which has a maximum velocity around ϕ=90°. Since the colder fluid enters with a decreasing velocity after ϕ>90°, the heat transfer rate begins to decrease after ϕ>90°. The heat transfer rate continues to decrease as the velocity of the entering fluid decreases to zero at about 180°. Subsequently, the fluid reverses its direction and the warmer fluid passes through the location at X=2; consequently, the heat transfer between the fluid and the pipe continues to decrease. The value of Nu decreases as the value of X is increased from the inlet to the mid-section of the pipe (X=20). Toward the middle of the pipe, the instantaneous Nusselt number becomes vanishingly small. Its value is almost symmetric with respect to ϕ with the maximum value occuring near ϕ=180°. A comparison of Figs. 7.6a and 7.6b shows that value of the Nusselt number increases as the kinetic Reynolds number is increased.

The effects of A_o and Re_ω on the cycle-averaged local Nusselt number $\overline{Nu}_X$ of air along the axial location are presented in Fig. 7.7. Generally, the cycle-averaged local Nusselt number $\overline{Nu}_X$ is symmetrical with respect of the mid-section of the pipe because of the symmetrical boundary conditions for both velocity and temperature for

the problem under consideration. A comparison of Case 1 (A_o=20, Re_ω=64) and Case 2 (A_o=20, Re_ω=250), shows that the value of $\overline{Nu}_x$ increases with the increase of Re_ω at a fixed value of A_o, which implies that the heat transfer rate increases with the increase of frequency at a given fixed oscillation amplitude of fluid. This is because the thermal boundary thickness δ_t in an oscillatory flow is

$$\delta_t \propto \left(\frac{1}{Re_\omega}\right)^{1/2} \tag{7.12}$$

which shows that the thermal boundary layer thickness becomes thinner with the increase of Re_ω. Consequently, the heat transfer rate increases with the value of Re_ω. Similarly, a comparison of Case 2 (A_o=20, Re_ω=250) and Case 3 (A_o=35, Re_ω=250) shows that the value of $\overline{Nu}_x$ increases with the increase of A_o for a fixed value of Re_ω, which implies that the heat transfer rate increases with the increase of oscillation amplitude of fluid at a given fixed value of frequency. This can be explained based on the energy equation (2.12). With fixed values of Re_ω and Pr, the convection term in Eq. (2.12) becomes more significant with the increasing value of A_o. Physically, a higher value of A_o means a larger amount of fluid is heated by the pipe during each cycle. It can also be observed from Fig. 7.7 that the heat transfer rate becomes vanishingly small at the middle of the heated pipe (X=20) for smaller A_o, because most of the fluid near the middle of the pipe never exits from the heated pipe.

The effects of A_o and Re_ω on the instantaneous space-averaged Nusselt number $\overline{Nu}_\tau$ for the three cases in Fig. 7.7 are illustrated in Fig. 7.8. Similarly, it is observed that the space-averaged heat transfer rate increases with the increase of either the dimensionless fluid displacement or the kinetic Reynolds number. It is interesting to

compare the temporal variation of the instantaneous space-averaged Nusselt number with the specified sinusoidal variation of the cross-sectional mean flow velocity given by Eq. (2.2). It is found that the phase difference between the cross-sectional mean velocity and the instantaneous space-averaged Nusselt number $\overline{Nu}_\tau$ is about 18^o for all cases. This is due to the fact that the instantaneous local Nusselt number in the entrance region predominates, as evidented in Figs 7.6a and 7.6b, which is out of phase with the cross-sectional mean velocity by approximately 18^o.

The effect of the length/diameter ratio L/D of the pipe on the local heat transfer rate for A_o=25 and Re_ω=180 is displayed in Fig. 7.9. As shown in this figure when L/D is increased from 25 to 50, the value of the cycle-averaged local Nusselt number $\overline{Nu}_x$ in the entrance region before X=5 remains the same while those in the middle region of the pipe increases with the descrease of L/D. Physically, the decrease of L/D at a fixed value of A_o means that the ratio of the fluid displacement to the length of the heated pipe becomes larger, and therefore a larger amount of heat is advected away from the heated pipe to the cooler reservoirs.

The cycle-space averaged Nusselt number $\overline{Nu}$ was computed according to Eq. (7.11) for A_o= 10 to 35 and Re_ω=10 to 400 at L/D=40. The results of these computations are presented as a solid line in Fig. 7.10. It is found that the solid line can be correlated by the following expression

$$\overline{Nu} = 0.00495 A_o^{0.9} Re_\omega^{0.656} \qquad (7.13)$$

Computations were then carried out for different values of L/D ranging from 10 to 120 for air (Pr=0.7) at the following three different sets of A_o and Re_ω: (i) A_o= 20, Re_ω=250, (ii) A_O= 25, Re_ω=180, and (iii) A_o= 35, Re_ω=100. It is found that the numerical results for the cycle-space averaged Nusselt number of air can be correlated by the following expression

$$\overline{Nu} = 0.00495 A_o^{0.9} Re_\omega^{0.656} [43.74 (D/L)^{1.18} + 0.06] \qquad (7.14)$$

A comparison of Eq. (7.14) against the numerical results is presented in Fig. 7.11.

7.4 Summary

The problem of oscillatory heat transfer in a periodically reversing flow is governed by four similarity parameters: the Prandtl number Pr, the kinetic Reynolds number Re_ω, the dimensionless oscillation amplitude of fluid A_o, and the length to diameter ratio of the heated tube L/D. A numerical solution to the conservation equations of mass, momemtum and energy has been obtained for an oscillatory and reversing flow of air in a pipe at constant wall temperature. The computed results reveal that annular effects also exist in temperature profiles of an oscillatory flow at high kinetic Reynolds numbers near the entrance and exit locations of the tube. It is found that for a fixed value of L/D and a specific Prandtl number, the space-cycle average heat transfer rate increases with both the parameters A_o and Re_ω. Although the value of L/D has a small effect on the local heat transfer rate near the entrance and exit of the pipe, its effect becomes significant on the space-cycle averaged heat transfer rate. Based on the nuermical solution, a correlation equation of the space-cycle averaged Nusselt number for air in terms of the three dimensionless parameters A_o, Re_ω and L/D has been obtained.

CHAPTER 8

LAMINAR OSCILLATORY HEAT TRANSFER IN A PIPE WITH CONSTANT HEAT FLUX

The preceding chapter is concerned with the numerical solution of laminar oscillatory heat transfer characteristics in a pipe heated at constant temperature. This chapter deals with laminar oscillatory transfer in a heated pipe with uniform heat flux, which is connected to two coolers at both ends as shown in Fig. 3.2. A numerical solution is carried out to study the heat transfer characteristics in the heated pipe. A correlation equation for the cycle-space averaged Nusselt number in terms of the appropriate similarity parameters is obtained. Experiments have been carried to verify the numerical solution.

8.1 Introduction

In this chapter, both experimental and numerical studies will be carried out for laminar oscillatory forced convection in a long pipe heated by uniform heat flux and subjected to a periodically reversing flow of air. Transient fluid temperature variations in the two mixing chambers adjacent to both ends of the heated pipe were measured and used as the thermal boundary conditions for the numerical simulation. The finite difference scheme based on a control volume method by Patankar (1980) was used for the numerical simulation of the hydrodynamically and thermally developing oscillatory flow in the pipe. The time-resolved centerline temperature and cycle-averaged wall temperature obtained from the numerical solution are presented and shown to be in good agreement with the experimental data. A correlation equation based on

experimental data is obtained for the cycle-averaged Nusselt number (in terms of the kinetic Reynolds number Re_ω and the dimensionless oscillation amplitude of fluid A_o) for oscillatory heat transfer in a long pipe subjected to a periodically reversing flow.

8.2 Experimental Investigation

The experimental apparatus and instrumentation for this study have been described in Chapter 3. Experiments were carried out for a laminar oscillatory flow of air (Pr = 0.71) in a heated pipe (with L/D=44.8) which is connected to two coolers at both ends. Because both the geometry and the imposed thermal boundary conditions were symmetric with respect to the mid-section of the heated pipe, the sensors were installed only in the left-hand side of the test rig. Five foil thermocouples were used to measure wall temperatures, two on the cooler wall and the other four were on the wall of the heated tube. Centerline fluid temperatures inside the heated tube were measured by four mini-needle T-type thermocouples. To measure inlet and outlet fluid temperatures in the heated tube, two fine thermocouples (0.001" in diameter) were carefully installed inside the two mixing chambers. The frequency and the stroke of oscillations were varied such that the range of Re_w was from 23.1 to 464.5 while the range of dimensionless oscillation amplitude of the fluid A_o was from 8.54 to 34.9 which was less than the critical value of A_o for the onset of turbulence according to Eq. (4.1).

8.3 Numerical Simulation

A numerical simulation of the experiments will now be carried out. The velocity field is identical to those presented in Chapter 6 and will not be repeated here. The

dimensionless energy equation is given by Eq.(2.12) with the dimensionless temperature defined as as $\theta = \frac{k_f T}{q_w D}$. The thermal boundary conditions for the problem under consideration are

$$\text{at X=0,} \qquad 0 \le R \le 0.5: \quad \theta(0, R, \tau) = \theta_{m,l} \tag{8.1}$$

$$\text{at X=L/D,} \qquad 0 \le R \le 0.5: \quad \theta(L/D, R, \tau) = \theta_{m,r} \tag{8.2}$$

$$\text{at R=0,} \qquad 0 \le X \le L/D: \quad \frac{\partial \theta}{\partial R} = 0 \tag{8.3}$$

$$\text{at R=0.5,} \qquad 0 \le X \le L/D: \quad \frac{\partial \theta}{\partial R} = 1 \tag{8.4}$$

where $\theta_{m,l}$ and $\theta_{m,r}$ are the transient fluid temperatures measured in the left and right mixing chambers. The similarity parameters for the present problem are the same as those considered in Chapter 7, i.e.: the dimensionless oscillation amplitude of fluid $A_o = \frac{X_{max}}{D}$, the kinetic Reynolds number $Re_\omega = \frac{\omega D^2}{\nu}$, the Prandtl number $Pr = \frac{\nu}{\alpha}$, and the length/diameter ratio L/D.

The computer program, used in the preceeding chapter for an oscillatory flow in a pipe at constant wall temperature with constant inlet and outlet fluid temperatures, was modified for the numerical simulation of the present problem with boundary conditions given by Eqs.(8.1)-(8.4). Extensive computations were carried out to ensure grid independent solutions for different values of the kinetic Reynolds number. A grid independence solution for a particular set of parameters was established by reducing the

grid size until the change in the wall temperature at the mid-section of the pipe is smaller than 0.4%.

8.4 Results and Discussion

8.4.1 Temperature Distributions

Figs. 8.1a and 8.1b illustrate typical temporal temperature variations measured at the left and right mixing chambers during one cycle at the same oscillatory frequency (Re_ω =120.1) for A_o= 34.9 and 15.3 respectively. These measurements were used as the thermal boundary conditions given by Eqs. (8.1) and (8.2). For A_o=34.9, as the piston moves from the left to right, the fluid temperature in the left mixing chamber continues to drop until the piston reverses its direction at the end of the first half cycle. For A_o=15.3, the fluid temperature in the left mixing chamber first starts to increase and then decreases to a minimum before it increases again. For the convenience of further discussion, the temperature history curves in the left mixing chamber and the corresponding temporal cross-sectional mean velocity variations for these two cases are presented in Fig. 8.2. The square symbols represent the case for A_o= 34.9 while the circle symbols represent those for A_o= 15.3. For the case of A_o= 34.9, when the fluid reverses its direction at the beginning of the cycle, the fluid temperature drops immediately due to the cooling effect of the fluid in the cooler. For the case of A_o=15.3, however, a different behavior occurs. In this case, the fluid temperature increases at the beginning of the cycle and starts to drop at about 45° of the crank angle. The reason for the different behaviors of temporal temperature variations between low and high values of A_o can be explained as follows. Consider the inlet fluid temperature at the beginning of the cycle as the fluid is reversing its direction. The fluid in the mixing chamber is

cooled by convection through the fluid coming from the cooler while, at the same time, it is heated by the fluid residing in the heated section by conduction. At a high value of A_o (A_o=34.9 for example) where the maximum cross-sectional mean velocity is high (as can be deduced from Eq. (2.2)), forced convection effects predominate. Therefore, the fluid temperature in the mixing chamber drops immediately when the fluid reverses its direction as colder fluid enters. However, for A_o=15.3 where the fluid velocity is small and axial heat conduction effect predominates at least initially, the fluid temperature at first begins to increase. Later in the cycle when the fluid velocity is increased, the fluid temperature starts to drop because the cooling effect of the fluid from the cooler begins to be felt.

Typical temporal variations of the centerline fluid temperature θ_c along different axial locations during one cycle for A_o=15.3 and Re_ω=150.6 are presented in Fig. 8.3. The triangle symbols represent the experimental data while the solid curves represent numerical solution. It is seen that the numerical solution is in fairly good agreement with the experimental data. Because both the geometry and imposed thermal boundary conditions are symmetric with respect to the mid-section of the heated pipe, only the behaviors of the temperature variations in the left-hand side of the test section ($X < 22.4$) are presented. As shown in this plot, during the first half cycle the fluid temperature near the left mixing chamber (X=1.4) begins to drop due to colder fluid entering from the cooler. The fluid temperature starts to rise near the end of the first half cycle due to warmer fluid exiting from the heater. The amplitude of the fluid temperature variations is at a maximum near the heater-cooler interface (X=0) and progressingly smaller as the mid-section of the heated tube ($X = 22.4$) is approached. At the mid-section of the heated tube (X=22.4), temporal variations of the fluid temperature are symmetric with respect to time.

Fig. 8.4 is a comparison between experimental and numerical results for the cycle-averaged wall temperature variations along the axial locations in the left side of the test section ($X < 22.4$) for four different cases. Again, the numerical solution is in good agreement with the experimental data. Generally, the cycle-averaged wall temperature progressingly increases with the axial location, with the minimum value occurring at the left mixing chamber and maximum value at the mid-section of the heated pipe. It can also be observed that the cycle-averaged wall temperature decreases with the increase of either the kinetic Reynolds number Re_ω or the dimensionless oscillation amplitude of fluid A_o.

8.4.2 The Space-Cycle Averaged Nusselt Number.

The space-cycle averaged Nusselt number is defined as

$$\overline{Nu} = \frac{q_w D}{k(\overline{\overline{T}}_w - \overline{\overline{T}}_m)} = \frac{1}{\overline{\overline{\theta}}_w - \overline{\overline{\theta}}_m} \tag{8.5}$$

where q_w is the measured heat flux; $\overline{\overline{T}}_w$ and $\overline{\overline{\theta}}_w$ are the dimensional and dimensionless space-cycle averaged wall temperature of the heated tube, with $\overline{\overline{\theta}}_w$ being computed from

$$\overline{\overline{\theta}}_w = \frac{1}{N_p}\sum_{i=1}^{N_p} \overline{\theta}_{w,i} \tag{8.6}$$

where $\overline{\theta}_{w,i}$ is the cycle-averaged local wall temperature and N_p is the number of positions in the test section at which the local wall temperatures were measured; $\overline{\overline{T}}_m$

and $\bar{\theta}_m$ are the dimensional and dimensionless cycle-averaged temperatures of the fluid measured in the left or right mixing chambers with $\bar{\theta}_m$ computed from

$$\bar{\theta}_m = \frac{1}{2\pi}\int_0^{2\pi}\theta_{m,l}d\tau = \frac{1}{2\pi}\int_0^{2\pi}\theta_{m,r}d\tau \tag{8.7}$$

The space-cycle averaged Nusselt number $\overline{Nu}$ was computed according to Eqs. (8.5) to (8.7) based on the experimental data for A_o= 8.54 to 34.9 and Re_ω=23.1 to 464.5 at L/D=44.8. The following correlation was obtained based on a least square fit of 53 experimental runs:

$$\overline{Nu} = 0.0199A_o^{0.85}Re_\omega^{0.58} \tag{8.8}$$

Eq. (8.8) with experimental data is presented in Fig. 8.5. Note that Eq. (8.8) indicates that the heat transfer rate increases with both the dimensionless oscillation amplitude of fluid A_o and the kinetic Reynolds number Re_ω. The increase in heat transfer is more sensitive to A_o than to Re_ω as indicated by the exponent of A_o being greater than that of Re_ω. To assess the accuracy of the correlation equation (8.8), the experimental data of the space-cycle averaged Nusselt number and the values computed according to Eq. (8.8) are presented in Fig. 8.6. Any deviations of data from the inclined straight line indicates the inaccuracy of the correlation equation. As shown in Fig. 8.6, Eq. (8.8) correlates the experimental data quite well.

8.5 Summary

In this chapter, experimental and numerical studies have been carried out for laminar oscillatory forced convection in a long tube heated by uniform heat flux and subjected to a periodically reversing flow of air. The numerical solutions for time-resolved centerline temperature and cycle-averaged wall temperature are shown to be in good agreement with the experimental data. Based on the experimental data, a correlation equation for the space-cycle averaged Nusselt number in terms of appropriate similarity parameters is obtained.

CHAPTER 9

OSCILLATORY PRESSURE DROPS THROUGH A WOVEN-SCREEN PACKED COLUMN

Previous chapters are concerned with the fluid flow and heat transfer characteristics in a empty tube subjected to oscillatory and reversing flow. This chapter deals with oscillatory pressure drop characteristics in packed columns (composed of three different sizes of woven screens) under a periodically reversing flow of air, which is of significance in the optimum design of regenerators of a Stirling engine or a cryocooler.

9.1 Introduction

The ability to predict pressure drops and heat transfer rates accurately in a regenerator is of crucial importance in the optimum design of a Stirling engine or a cryocooler. The literature review in the Chapter 1 shows that, in the past, the estimation of the pressure drop in a regenerator has been based on correlation equations for an unidirectional steady flow through a stack of screens. For example, Miyabe et al. (1982) obtained the following correlation equation for pressure drop of a steady flow through a stack of woven-screens:

$$f_{st} = \frac{33.6}{Re_\beta} + 0.337 \tag{9.1}$$

with

$$f_{st} = \frac{\Delta p_{st} / n}{\frac{1}{2}\rho (u_{st})_p^2} \tag{9.2}$$

$$Re_\beta = \frac{(u_{st})_p \beta}{\nu} \tag{9.3}$$

where Δp_{st} is the steady flow pressure drop, $\left(u_{st}\right)_p$ is the cross-sectional mean flow velocity in the packed column, n is the number of screens packed in the column, β is the distance between meshes, and Re_β is the Reynolds number based on β and $\left(u_{st}\right)_p$.

Since Stirling-cycle machines are operating under periodically reversing flow conditions, it is apparent that correlation equations based on a steady flow would not be able to predict accurately the pressure drop in a regenerator. Matini (1978) and Rix (1984), for example, found that good agreement between simulated and measured pressure drops can be achieved only if the friction coefficient provided by Tong and London (1957) is arbitrarily adjusted by a constant value of 3 to 5. Thus, there is a need for obtaining more accurate correlation equations for the pressure drop in a regenerator under cyclic flow conditions.

Relatively little research has been performed on the pressure drop in a packed column subjected to an oscillatory and reversing flow. Roach and Bell (1988) performed experiments on the pressure drop in a packed column under rapidly reversing flow conditions. They reported higher friction factors in an oscillatory flow but could not find frequency dependence in the pressure drop. Tanaka et al. (1990) experimentally investigated the fluid flow characteristics of a Stirling engine regenerator (made of wire screens or sponge metals) under the condition of an oscillating flow. They obtained the following correlation equation for the friction factor

$$f_{max} = \frac{198}{(Re_{max})_{Dh}} + 1.737 \tag{9.4}$$

with

$$f_{max} = \frac{\Delta p_{max} D_h}{\frac{1}{2}\rho (u_{max})_p^2 L} \tag{9.5}$$

$$(Re_{max})_{D_h} = \frac{(u_{max})_p D_h}{\nu} \tag{9.6}$$

where Δp_{max} is the maximum pressure drop in one cycle, $(u_{max})_p$ is the maximum cross-sectional mean flow velocity in the packed column, L is the length of the packed column, and D_h is the hydraulic diameter of the screens which is defined by Tanaka et al.(1990) as

$$D_h = \frac{\varphi D_w}{(1-\varphi)} \tag{9.7}$$

with φ being the porosity of the screens which is defined by Miyabe et al. (1982) as

$$\varphi = 1 - \frac{\pi D_w \sqrt{\ell^2 + D_w^2}}{4\ell^2} \tag{9.8}$$

It is relevant to note that Eq. (4) was determined based on experimental data for a fixed fluid displacement and is therefore not suitable for general use.

The objectives of the present work are: (1) to experimentally investigate pressure drops across a tube packed with stainless steel wire screens subjected to an oscillatory and reversing flow, and (2) to obtain a correlation equation of the pressure drop factor in terms of appropriate similarity parameters. In what follows, the experimental apparatus and the geometrical parameters of woven screens will first be described. The experimental data of pressure drops in a woven-screen packed column under cyclic flow conditions will then be presented, and a correlation equation for the friction factor will be obtained.

9.2 Experimental Details

Fig. 9.1 shows the test rig used to measure oscillatory pressure drops through a packed column, which was modified from the test rig for studying the fluid flow and heat transfer characteristics in an empty tube. The test section consisted of a packed column (33.3 mm inside diameter and 40 mm in length) with each of its end connected to a copper tube of the same diameter (33.3 mm in diameter and 150 mm in length), and through a converging nozzle to another copper tube of smaller diameter (13.5 mm in diameter). This test section was connected to the pump through a flexible tube. The other equipment and instrumentation were the same as those used to measure the pressure drop in a tube described in Chapter 3.

Packed Columns

The three packed columns, 33.3 mm in diameter and 40 mm in length, were made of stacks of stainless steel plainly-woven wire screens with three different mesh sizes. Fig. 9.2a shows the plane view of the wire screens used in this study while Fig. 9.2b illustrates the detailed construction of a mesh unit of the screens. The wire diameters D_w, pitch ℓ, the distance between meshes β, porosity φ, the number of

screens n, and hydraulic diameter D_h for the three mesh sizes of the wire screens are listed in Table 9.1. Wire diameter and pitch of the screens were provided by the manufacturer (Jelliff Corp). The hydraulic diameter D_h and the porosity φ of the packed column were determined by Eqs.(9.7) and (9.8) respectively.

Table 9.1 Properties of Stainless Steel Wire Screens used in this experiment

Mesh Size	Number of screens n	Wire Dia D_w (mm)	Pitch ℓ (mm)	Mesh distance β (mm)	Porosity φ	Hydraulic Dia D_h (mm)
100	194	0.102	0.254	0.152	0.662	0.199
150	300	0.066	0.170	0.104	0.673	0.136
200	341	0.058	0.127	0.069	0.602	0.089

Sinusoidal Motion of Air

The sinusoidal fluid displacement x_p in the packed column varies according to

$$x_p = \frac{(x_{max})_p}{2}(1-\cos\phi) \tag{9.9}$$

which was obtained from the fluid displacement in an empty tube given by Eq. (2.1). Thus the maximum fluid displacement in the empty tube x_{max} and in the packed column $(x_{max})_p$ are related by

$$(x_{max})_p = \frac{x_{max}}{\varphi} \tag{9.10}$$

Differentiating Eq. (9.6) with respect to time, we obtain the cross-sectional mean fluid velocity $(u_m)_p$

$$(u_m)_p = (u_{max})_p \sin\phi \tag{9.11}$$

where the maximum cross-sectional mean velocity $(u_{max})_p$ is related to the maximum fluid displacement by

$$(u_{max})_p = \frac{(x_{max})_p \omega}{2} \tag{9.12}$$

Similarity Parameters

When studying the friction coefficient of an oscillatory flow in a empty pipe in Chapter 5, we pointed out that the similarity parameters for an oscillatory flow in an empty tube are the dimensionless fluid displacement and the kinetic Reynolds number, and obtained a correlation of the friction coefficient in terms of these two similarity parameters. In view of the similarity in the friction coefficients of a steady flow in a bundle of tubes and in a packed column, it can be conjectured that the similarity parameters for an oscillatory flow in a bundles of tubes and in a packed column are also the same except that the diameter of the tube is replaced by the hydraulic diameter in the similarity parameters. It follows that the similarity parameters of an oscillatory flow in a packed column are the dimensionless fluid displacement and the kinetic Reynolds number which are defined respectively by

$$(A_o)_{D_h} = \frac{(x_{max})_p}{D_h} \tag{9.13}$$

$$(Re_\omega)_{D_h} = \frac{\omega D_h^2}{\nu} \tag{9.14}$$

With the aid of Eq. (9.9), we note that the Reynolds number $(Re_{max})_{D_h}$ in Eq. (9.3) can be expressed in terms of $(A_o)_{D_h}$ and $(Re_\omega)_{D_h}$ as

$$(Re_{max})_{D_h} = \frac{(A_o)_{D_h}}{2}(Re_\omega)_{D_h} \tag{9.15}$$

It follows that, if the Reynolds number $(Re_{max})_{D_h}$ is used as the parameter for the correlation equation of fluid flow characteristics in a sinusoidally oscillatory and reversing flow as was done by Tanaka et al. (1990), the effects of the fluid displacement and frequency of oscillation can not be isolated. Thus, in this study we shall use $(A_o)_{D_h}$ and $(Re_\omega)_{D_h}$ defined in Eqs.(9.13) and (9.14) as the two independent similarity parameters to correlate the pressure drop data of an oscillatory flow in a packed column.

9.3 Results and Discussion

In this section, we shall present experimental results for the pressure drop across woven-screen packed columns subjected to a periodically reversing flow. Experiments were carried out for three different mesh numbers (100, 150, 200) of the woven screens, three values of the fluid displacement x_{max} (80.98 mm, 111.12 mm, and 150.61 mm) which was varied by changing the stroke of oscillations, and at various kinetic Reynolds numbers $(Re_\omega)_{D_h}$ ranging from 0.001 to 0.13. A total of nine test cases with nine different values of $(A_o)_{D_h}$ are tabulated in Table 9.2.

Table 9.2: Experimental Conditions for the Tested Cases

($0.001 \leq (Re_{\omega})_{D_h} \leq 0.13$)

Case	Mesh Size	x_{max} (mm)	$(A_o)_{D_h}$
1	100	80.98	614.73
2	100	111.12	843.38
3	100	150.61	1143.25
4	150	80.98	879.99
5	150	111.12	1232.01
6	150	150.61	1645.54
7	200	80.98	1511.50
8	200	111.12	2073.71
9	200	150.61	2827.56

9.3.1 Temporal Variations of Pressure Drop

We now present the experimental data for the ensemble-averaged pressure drop which is given by Eq. (5.20a). Typical variations of the ensemble-averaged pressure drops across the tube packed with mesh 100 screens during a complete cycle at $(A_o)_{D_h}$ = 843.38 for $(Re_{\omega})_{D_h}$ =0.01005, 0.03770 and 0.05529 are illustrated in Fig. 9.3. At a fixed value of the dimensionless fluid displacement, it is seen that the pressure drop increases with the increase of the kinetic Reynolds number during most of the cycle. It is noted that for a small value of the kinetic Reynolds number, $(Re_{\omega})_{D_h}$ =0.01005, for example, the pressure drop varies sinusoidally almost without phase lags with respect to the cross-sectional mean fluid velocity as given by Eq. (9.11), with the maximum value occurring at $\phi = 90^{\circ}$. But for higher values of the kinetic Reynolds number, significant phase lags were observed. For example, the phase angle is delayed by 18° at $(Re_{\omega})_{D_h}$ = 0.03770 and is delayed by 24° at $(Re_{\omega})_{D_h}$ = 0.05529.

Fig. 9.4 shows typical temporal variations of the ensemble-averaged pressure drop across the tube packed with mesh 100 screens during a complete cycle at

$(Re_\omega)_{D_h} = 0.04524$ for $(A_o)_{D_h} = 614.73$, 843.38 and 1143.25. Again, it is apparent that the pressure drop increases with the increase of the dimensionless fluid displacement at a fixed value of the kinetic Reynolds number. However, it appears that the temporal variations of pressure drop are almost in phase with one another for the different three values of $(A_o)_{D_h}$. Therefore, we can conclude that the dimensionless oscillation amplitude of the fluid has no effect on the phase lag of pressure drop variations. From Figs. 9.3 and 9.4, we can conclude that the pressure drop in a packed column subject to an oscillatory flow increase with both the dimensionless oscillation amplitude of the fluid $(A_o)_{D_h}$ and the kinetic Reynolds number $(Re_\omega)_{D_h}$. The phase lag of the pressure drop with respect to the mean velocity increases with the increase of $(Re_\omega)_{D_h}$, but is relatively independent of $(A_o)_{D_h}$.

9.3.2 Maximum Pressure Drop Factor

The maximum pressure drop factor f_{max} was computed according to Eq. (9.5) based on the experimental data for the nine test cases listed in Table 9.2 and with $(Re_\omega)_{D_h}$ ranging from 0.001 to 0.13. The following correlation was obtained based on a least square fit of 92 experimental runs:

$$f_{max} = \frac{1}{(A_o)_{D_h}}\left[\frac{403.2}{(Re_\omega)_{D_h}} + 1789.1\right] \tag{9.16}$$

A comparison of Eq. (9.16) with the experimental data is presented in Fig. 9.5. The maximum relative error between Eq.(9.16) and the experimental data is about 15.1%.

As mentioned earlier, Eq. (9.4) is the correlation equation for the maximum pressure drop factor in an oscillatory flow through stacked screens, which was obtained

by Tanaka et al.(1990) at a fixed value of the dimensionless fluid displacement of $(A_o)_{D_h} = 829.4$. A comparison of Eq.(9.16) and Eq. (9.4) for different values of $(A_o)_{D_h}$ is presented in Fig. 9.6. It is shown that for the same value of $(A_o)_{D_h} = 829.4$, Eq.(9.1) obtained by Tanaka et al. (1990) is about 10% lower than the present results, which is within experimental errors. However, for the cases of $(A_o)_{D_h} = 614.7$ and 2827.6, the present results are substantially higher or lower than those given by Eq.(9.1). Therefore, Tanaka et al.'s correlation equation is only applicable to a specific value of the dimensionless oscillation amplitude of the fluid $(A_o)_{D_h}$, i.e., for $(A_o)_{D_h} = 829.4$.

9.3.3 Cycle-Averaged Pressure Drop Factor

We now define the cycle-averaged pressure drop factor $\bar{f}$ as follows:

$$\bar{f} = \frac{\Delta\bar{p} D_h}{\frac{1}{2}\rho(u_{max})_p^2 L} \tag{9.17}$$

where $\Delta\bar{p}$ is the cycle-averaged pressure drop which is determined from

$$\Delta\bar{p} = \frac{1}{N_i}\sum_{j=1}^{N_i}\sqrt{\Delta\tilde{p}_j^2} \tag{9.18}$$

with N_i being the total number of sampling intervals in one cycle and $\Delta\tilde{p}_j^2$ being the ensemble-averaged data at jth interval. Based on the experimental data, the cycle-averaged pressure drop factor $\bar{f}$ was computed according to Eq. (9.17) and presented in Fig. 9.7. It is shown that the experimental data are well fitted by the following correlation equation:

$$\bar{f} = \frac{1}{(A_o)_{Dh}}\left[\frac{247.3}{(Re_\omega)_{Dh}} + 1003.6\right] \tag{9.19}$$

Eq.(9.19) has a maximum relative error of 14% in comparison with experimental data.

Eq. (9.19) can be used to predict the cycle-averaged pressure drop in the design of the regenerator of a Stirling engine or a cryocooler. We now compare the pressure drops predicted by Eq. (9.1) for a steady flow and Eq. (9.19) for an oscillatory flow. The pressure drop ratio is given by

$$\frac{(\Delta\bar{p})_{pre}}{(\Delta p_{st})_{pre}} = \frac{\pi^2}{2}\left(\frac{D_w}{D_h}\right)\frac{\frac{1}{(A_o)_{Dh}}\left(\frac{247.3}{(Re_\omega)_{Dh}} + 1003.6\right)}{\frac{33.6}{Re_\beta} + 0.337} \tag{9.20a}$$

where we have made use of the relation $L = 2nD_w$. Eq. (9.20a) can be rewritten as

$$\frac{(\Delta\bar{p})_{pre}}{(\Delta p_{st})_{pre}} = \frac{\pi^2}{2}\left(\frac{D_w}{D_h}\right)\frac{\frac{247.3}{(Re_\omega)_{Dh}} + 1003.6}{\frac{33.6\pi D_h}{(Re_\omega)_{Dh}\beta} + 0.337(A_o)_{Dh}} \tag{9.20b}$$

since $Re_\beta = (Re_\omega)_{Dh}\frac{(A_o)_{Dh}\beta}{\pi D_h}$. Eq. (9.20b) shows that the pressure ratio depends on the similarity parameters $(A_o)_{Dh}$ and $(Re_\omega)_{Dh}$ as well as the geometry of the woven screens β, D_h and D_w. The data for Cases 3, 5 and 7 in the Table 9.2 were used to compute the pressure ratio given by Eq. (9.20b). The results are tabulated in Table 9.3, which shows that the oscillatory pressure drop is four to six times higher than that of the steady pressure drop at the same cross-sectional mean velocity. At small values of $(Re_\omega)_{Dh}$ where the first term in both upstairs and downstairs are small in comparison with the second term, Eq. (9.20b) reduces to

$$\frac{(\Delta\overline{p})_{pre}}{(\Delta p_{st})_{pre}} = 11.561\frac{\beta D_w}{D_h^2} \tag{9.21}$$

which depends only on the geometry of the woven-screens and independent of the similarity parameters $(A_o)_{D_h}$ and $(Re_\omega)_{D_h}$. The results of Eq. (9.21) for the three mesh screens are also listed in Table 9.3.

9.4 Summary

Experimental results on oscillatory pressure drops across a woven-screen packed column subjected to a periodically reversing flow have been reported in this paper. It is shown that the appropriate similarity parameters for the problem under investigation are the kinetic Reynolds number $(Re_{max})_{D_h}$ and the dimensionless oscillation amplitude of fluid $(A_o)_{D_h}$, both of which are based on the hydraulic diameter as the representative length. Correlation equations of both the maximum and the cycle-averaged pressure drop factors in terms of these two similarity parameters have been obtained. It was found that the values of the cycle-averaged pressure drop of an oscillatory flow in a packed column is several times higher than that of a steady flow at the same Reynolds number based on the cross-sectional mean velocity.

Table 9.3: Comparison of the pressure drop predicted by Eqs. (9.1) and (9.19)

Test cases	Re_β	$(Re_\omega)_{D_h}$	$\bar{f}$ given by Eq. (9.19)	f_{st} given by Eq.(9.1)	$(\Delta\bar{p})_{pre}/(\Delta p_{st})_{pre}$ given by Eq.(9.20b)	$(\Delta\bar{p})_{pre}/(\Delta p_{st})_{pre}$ given by Eq.(9.21)
Case 3 $(A_o)_{D_h}$=1143 mesh 100	6.986	0.025	9.484	5.147	4.661	4.526 for mesh 100
	13.972	0.050	5.181	2.742	4.780	
	20.958	0.075	3.747	1.940	4.885	
	27.944	0.101	3.029	1.539	4.978	
	34.930	0.126	2.599	1.299	5.061	
Case 5 $(A_o)_{D_h}$=1232 mesh 150	3.521	0.012	17.908	9.879	4.342	4.290 for mesh 150
	7.043	0.023	9.361	5.180	4.389	
	10.564	0.035	6.512	3.518	4.434	
	14.086	0.047	5.088	2.722	4.476	
	17.607	0.059	4.233	2.245	4.515	
Case 7 $(A_o)_{D_h}$=1511 mesh 200	1.875	0.005	33.211	18.256	5.850	5.481 for mesh 200
	3.750	0.010	16.937	9.297	5.859	
	5.625	0.015	11.513	6.310	5.868	
	7.500	0.020	8.801	4.817	5.876	
	9.376	0.025	7.173	3.921	5.884	

CHAPTER 10

CONCLUDING REMARKS

10.1 Summary and Conclusions

The present work is concerned with the fluid flow and heat transfer characteristics in a pipe subjected to a periodically oscillatory and reversing flow. The related problem of pressure drops in an oscillatory flow through a woven-screen packed column has also been investigated experimentally. Various analytical, numerical and experimental findings and conclusions reached during the course of this study have been detailed in Chapters 4-9. Salient results are summarized below:

1. An examination of the governing equations and boundary conditions shows that the governing similarity parameters for the fluid flow in a pipe of finite length subjectedto sinusoidally oscillatory flow are the kinetic Reynolds number Re_ω, the dimensionless oscillation amplitude of fluid A_o, and the length to diameter ratio of the pipe L/D. For the corresponding heat transfer problem, the governing parameters are the same with the Prandtl number being the additional parameter.

2. The change in the sign of the pressure gradient is found to be directly responsible for the occurrence of instability in an oscillatory and reversing pipe flow. The criteria for the onset of turbulence in terms of two independent similarity parameters, the kinetic Reynolds number and the dimensionless oscillation amplitude of the fluid, has been obtained.

3. Analytical expressions to the instantaneous and cycle-averaged friction coefficients for a fully developed laminar oscillating and reversing pipe flow have been obtained and confirmed by experimental data. A correlation equation for the cycle-averaged friction coefficient of a cyclically turbulent flow has also been obtained based on experimental data.

4. For a sinusoidally oscillatory and reversing flow in a finite pipe, it is shown that at any instant of time, there exists three flow regimes in the pipe: an entrance regime, a fully developed regime, and an exit regime. This phenomena is unique for a periodically oscillatory and reversing flow. Based on the numerical results, a correlation equation of the space-cycle averaged friction coefficient for an incompressible, laminar, hydrodynamically developing oscillatory pipe flow has been obtained.

5. The numerical results reveal that annular effects also exist in the temperature profiles of an oscillatory flow at high kinetic Reynolds numbers near the entrance and exit locations of the pipe. Based on the numerical results, an expression for the space-cycle averaged Nusselt number of air (with $Pr = 0.7$) in terms of the three dimensionless parameters (A_o, Re_ω, and L/D) has been obtained for the laminar oscillatory heat convection in a pipe heated at constant temperature.

6. Based on the experimental data, a correlation equation for the space-cycle averaged Nusselt number in terms of A_o and Re_ω has been obtained for oscillatory heat transfer in a long pipe with uniform heat flux.

7. A correlation equation for the pressure drop in an oscillatory flow through a packed-screen column has been determined.

10.2 Future Work

The following recommendations are offered for future work:

1. Extend the present study of laminar oscillatory heat convection to the turbulent flow regime.
2. Investigate the problem of heat transfer in a packed column and obtain the interfacial heat transfer coefficient between solid and fluid.
3. Study the problems of oscillatory fluid flow and heat transfer in a pipe with the compression and expansion effects taken into consideration.

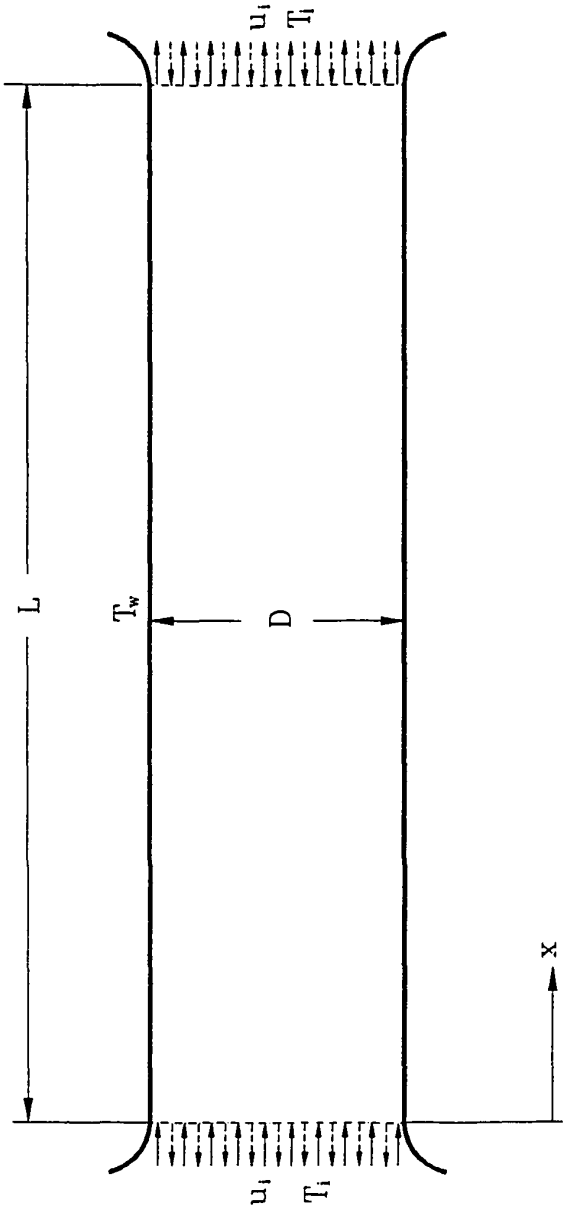

Fig. 2.1 Schematic diagram of the flow geometry

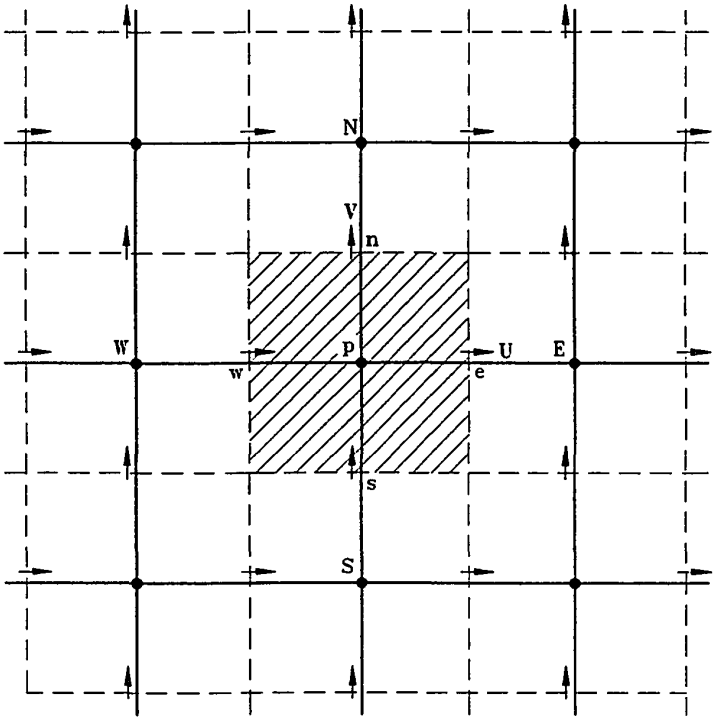

Fig. 2.2 Control volumes

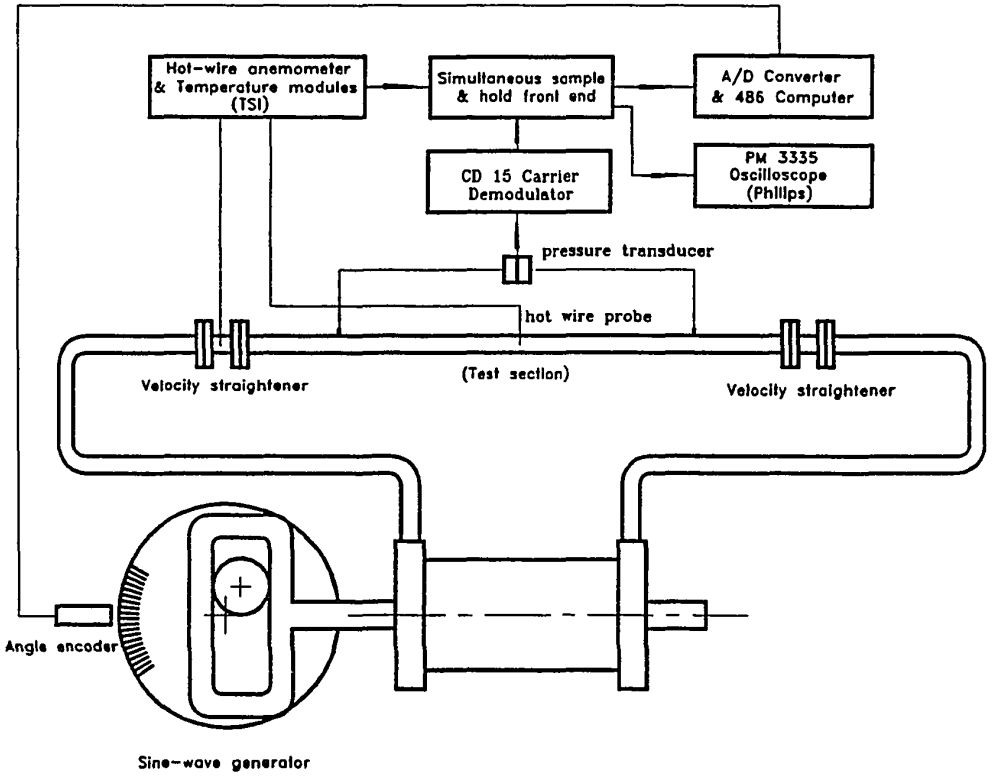

Fig. 3.1 Apparatus of the measurement of fluid flow characteristics

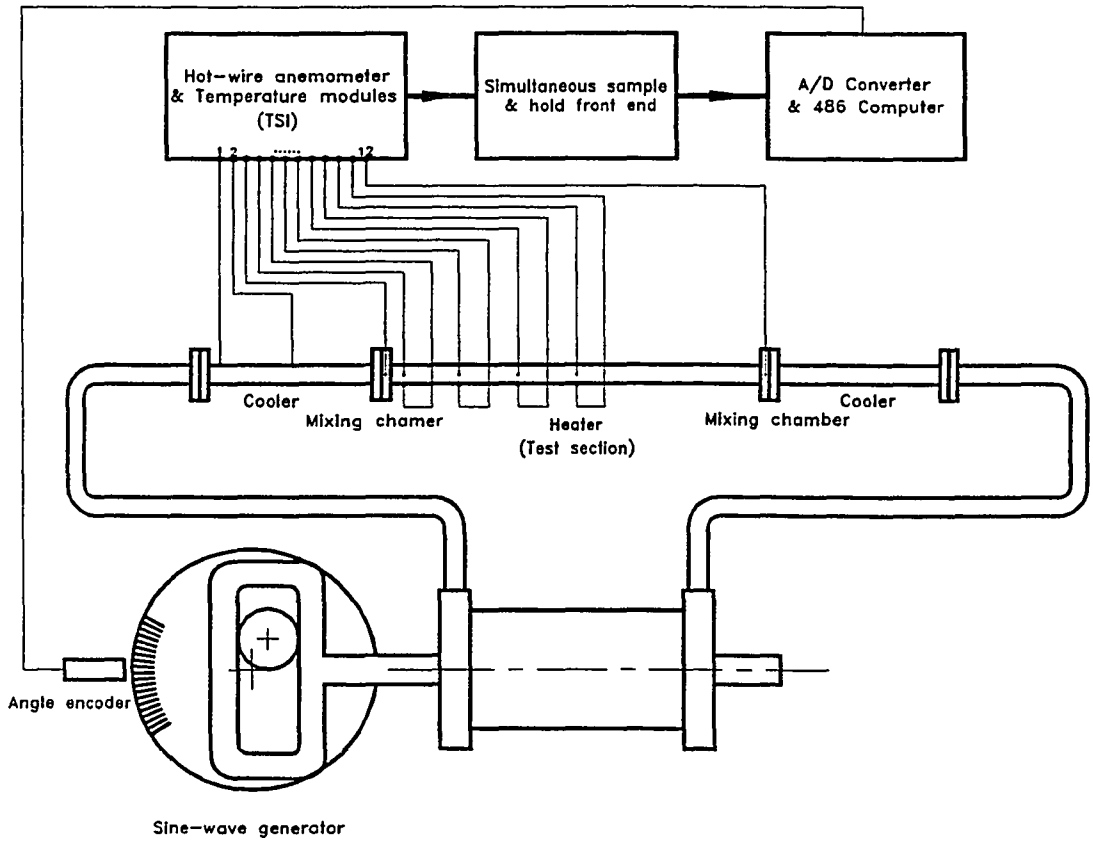

Fig. 3.2 Apparatus of the measurement of heat transfer characteristics

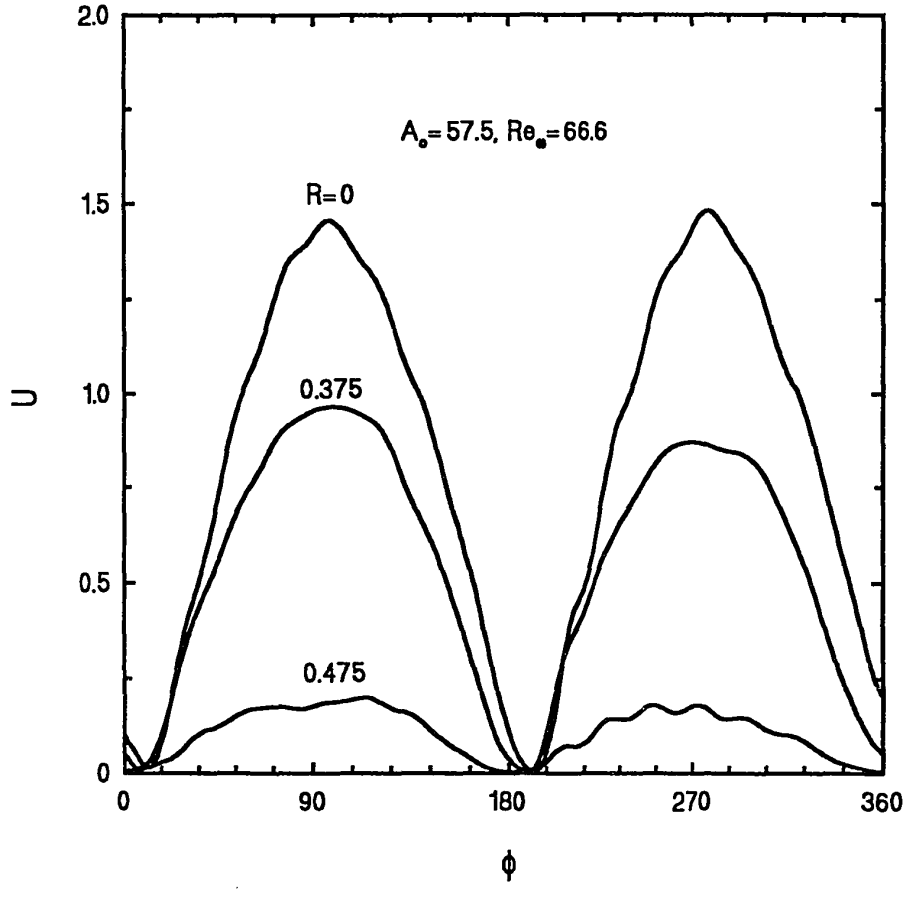

Fig. 4.1a Temporal axial velocity variations of a laminar flow for A_o= 57.5 and Re_ω = 66.6

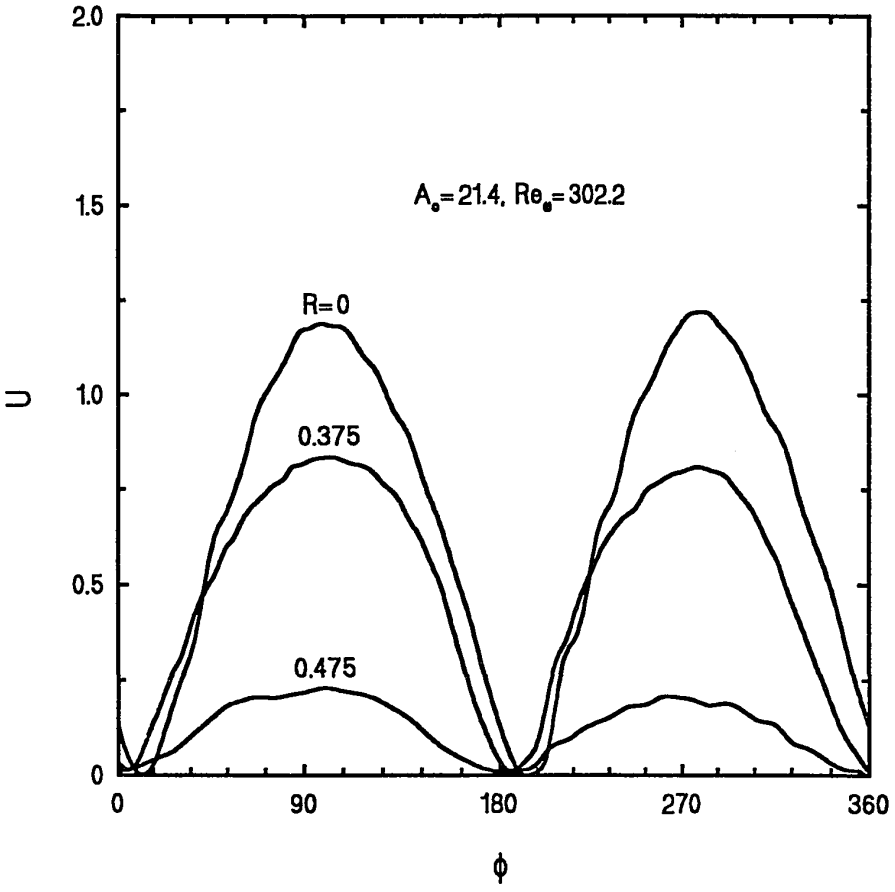

Fig. 4.1b Temporal axial velocity variations of a laminar flow for A_o= 21.4 and Re_ω=302.2

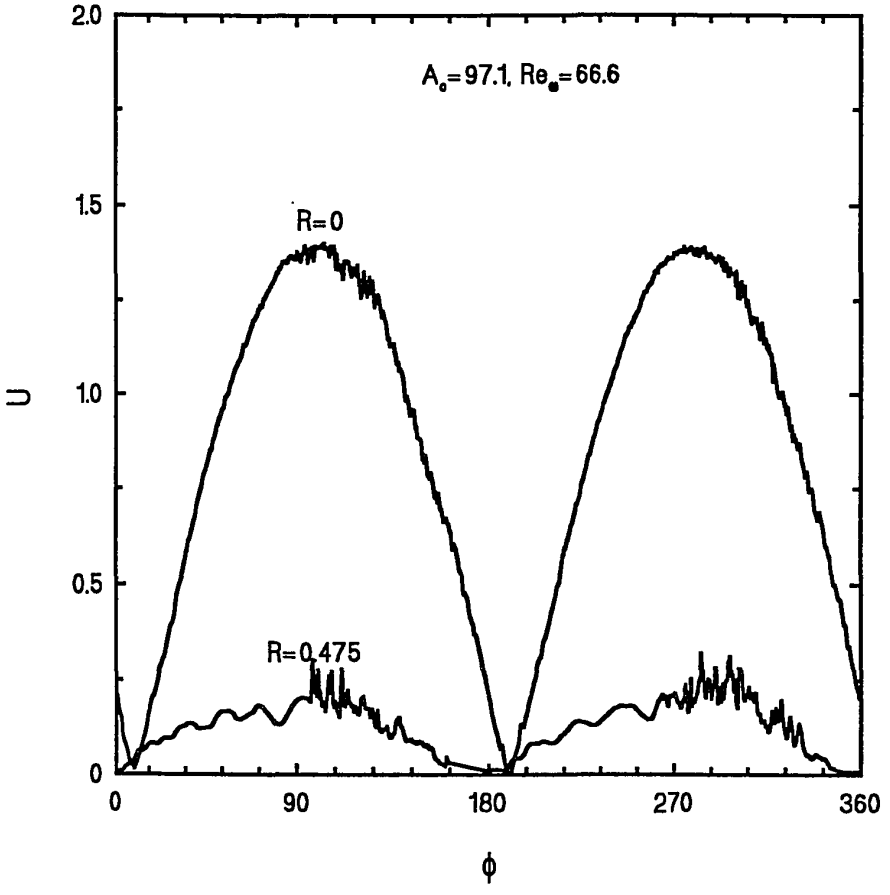

Fig. 4.2a Temporal axial velocity variations at the onset of transition to turbulence: A_o= 97 and Re_ω = 66.6

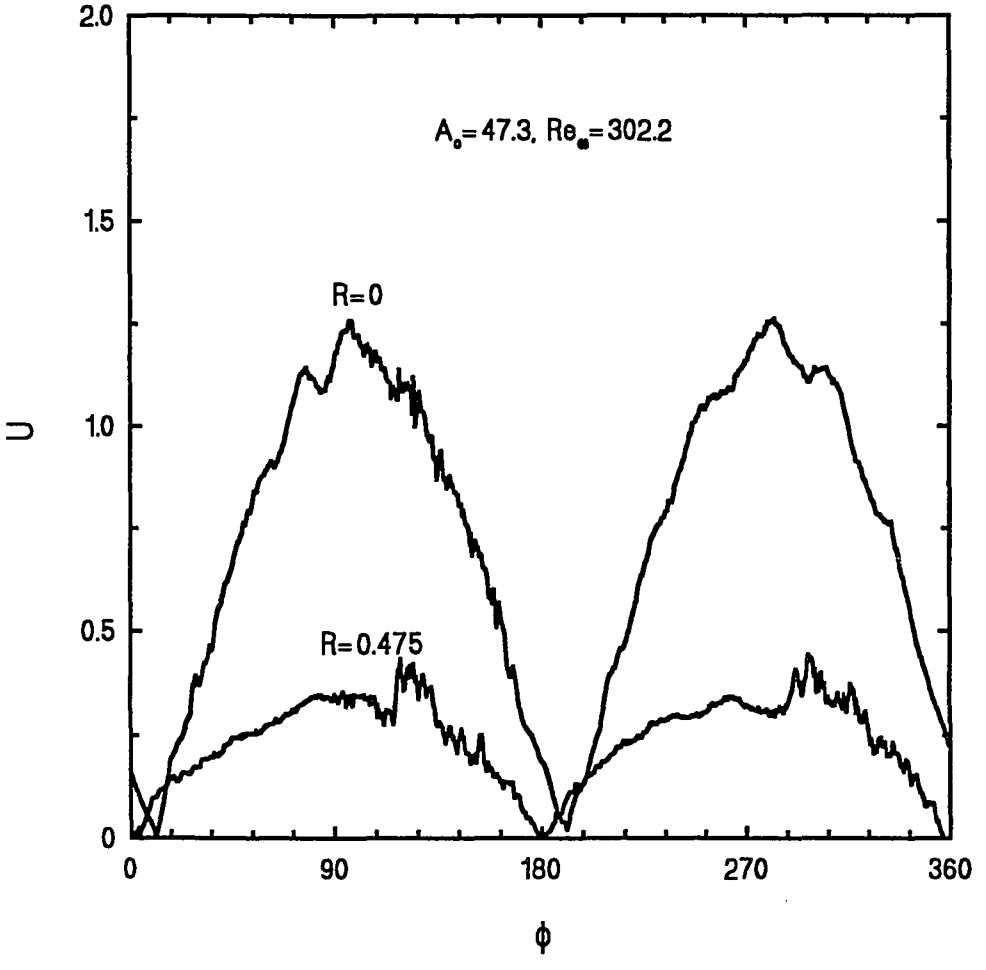

Fig. 4.2b Temporal axial velocity variations at the onset of transition to turbulence: A_o= 47.3 and Re_ω=302.2

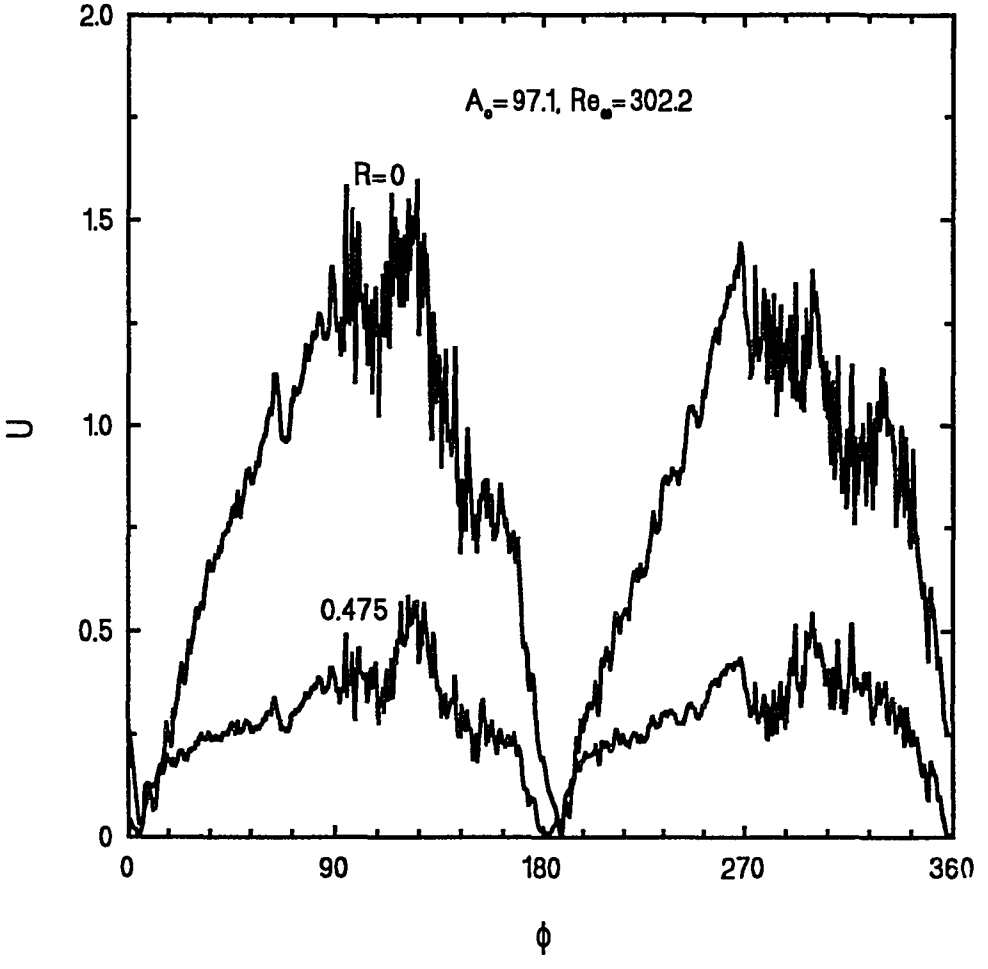

Fig. 4.3 Temporal axial velocity variations of a turbulent flow for A_o= 97.1 and Re_ω = 302.2

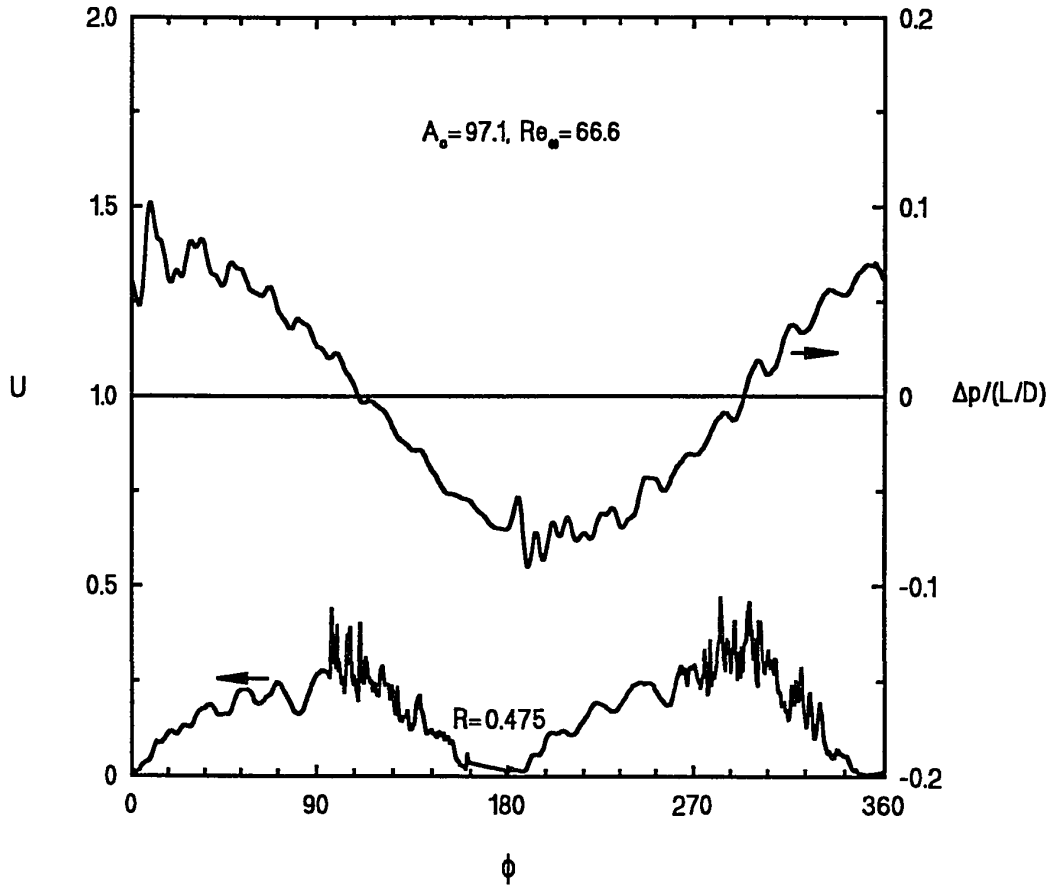

Fig. 4.4a Temporal variations of axial velocity and pressure drop at the onset of transition to turbulence: $A_o = 97.1$ and $Re_\omega = 66.6$

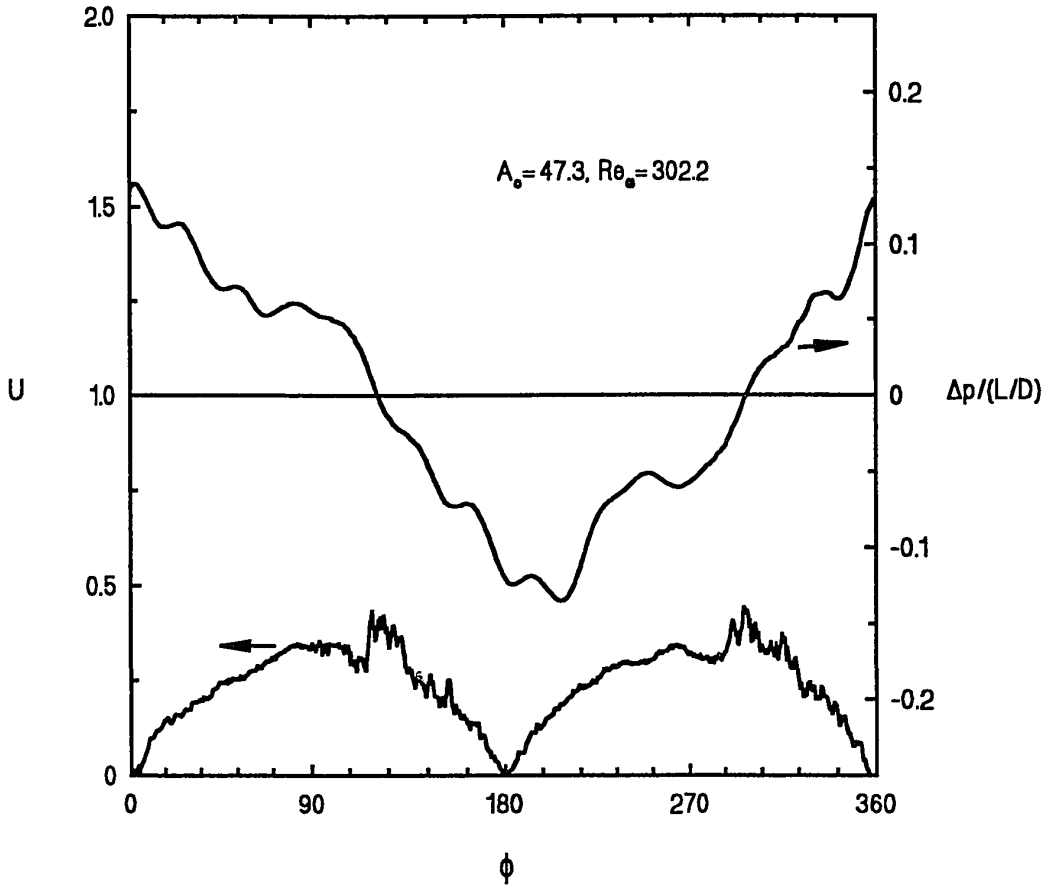

Fig. 4.4b Temporal variations of axial velocity and pressure drop at the onset of transition to turbulence: $A_o = 47.3$ and $Re_\omega = 302.2$

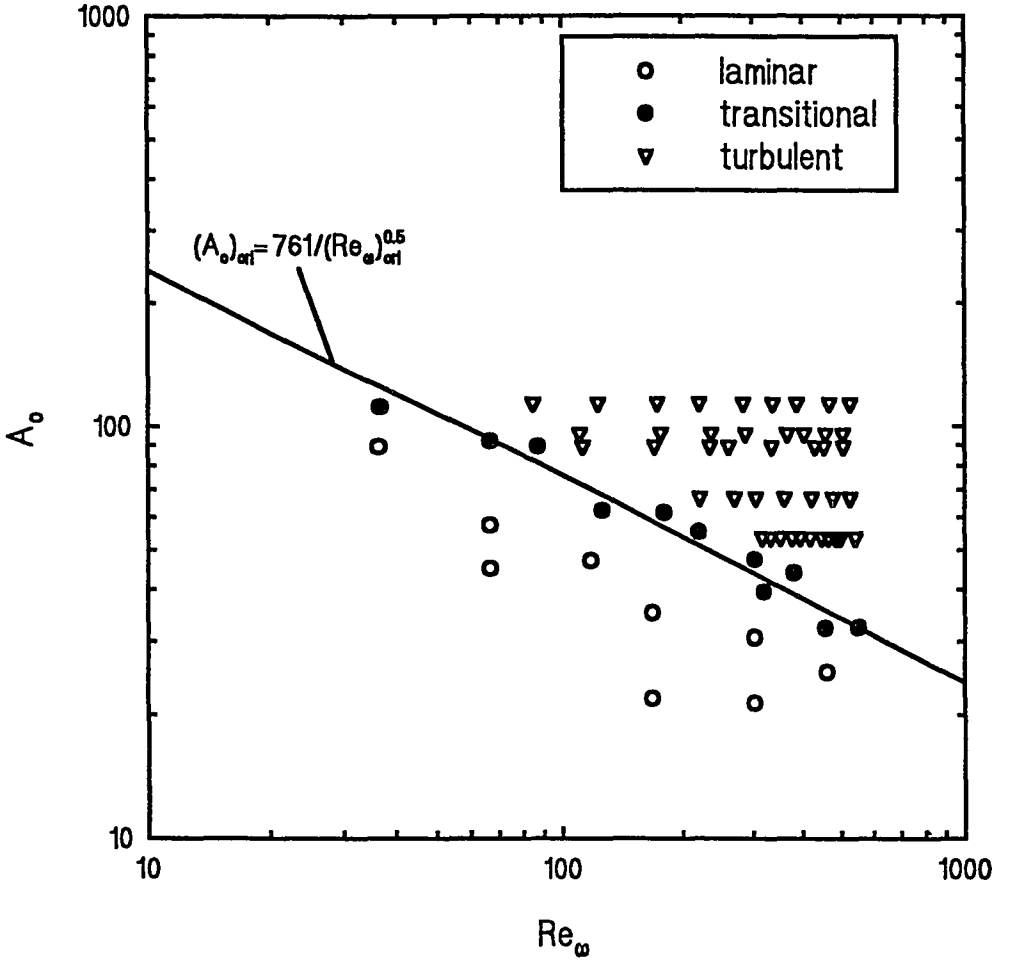

Fig. 4.5 Correlation equation of the critical dimensionless oscillation amplitude of fluid A_o and the kinetic Reynolds number Re_ω

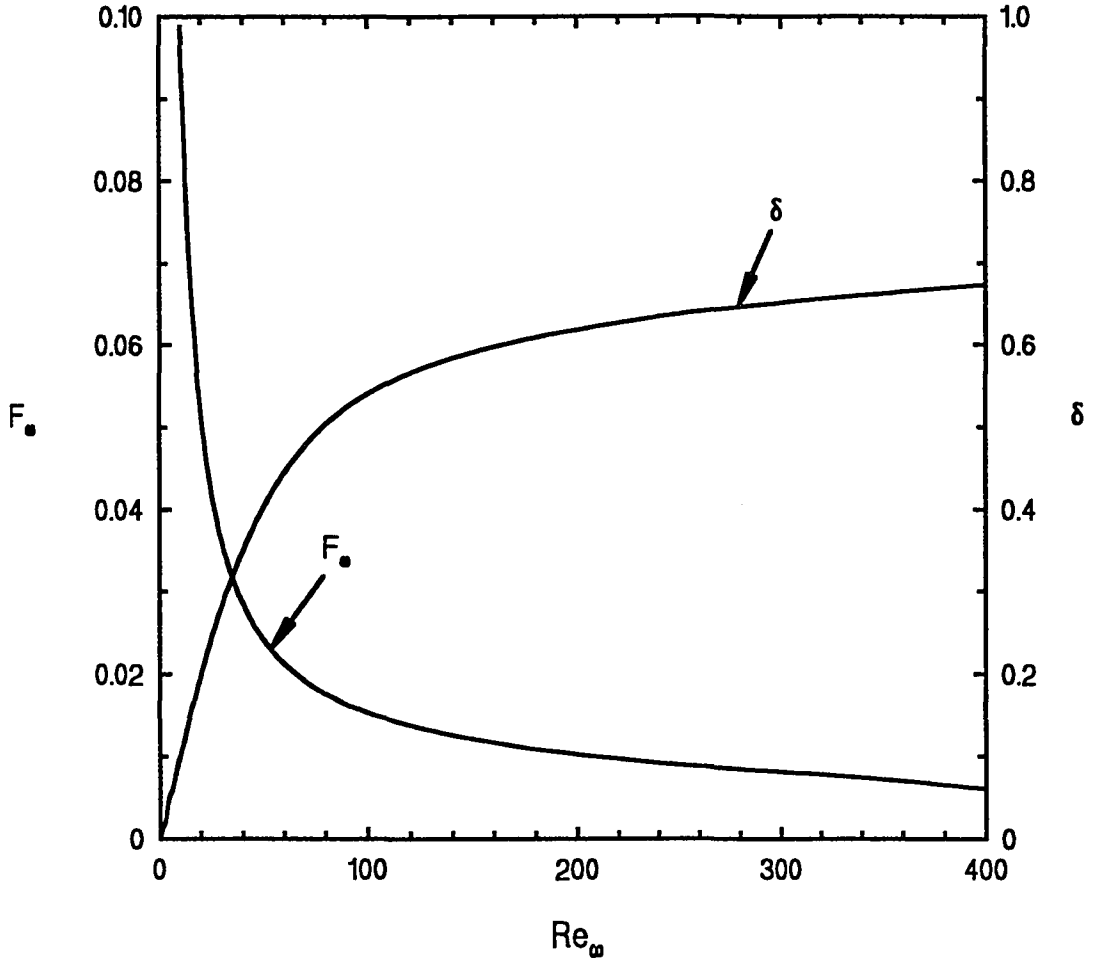

Fig. 5.1 F_ω and δ versus the kinetic Reynolds number Re_ω

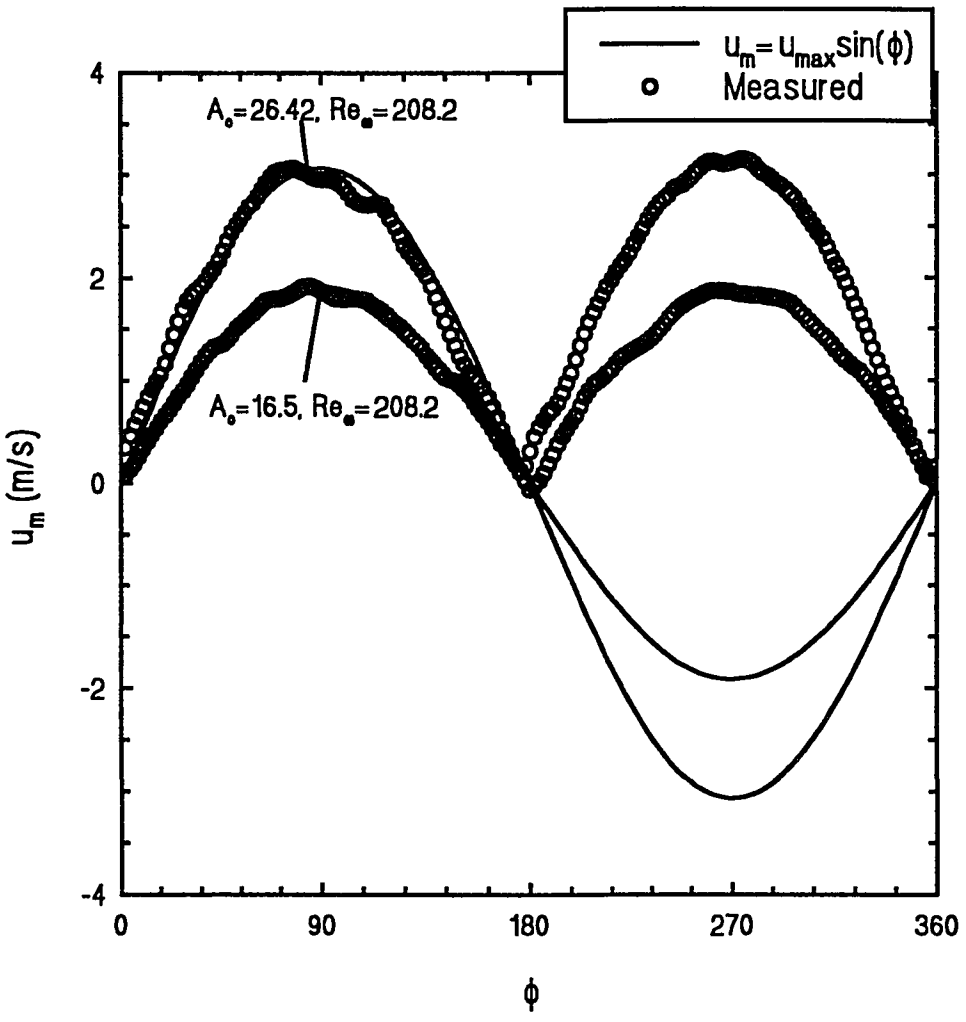

Fig. 5.2 Comparison of the ensemble-averaged traces of the cross-sectional mean velocity at the inlet and the assumed sinusoidal inlet mean velocity variation

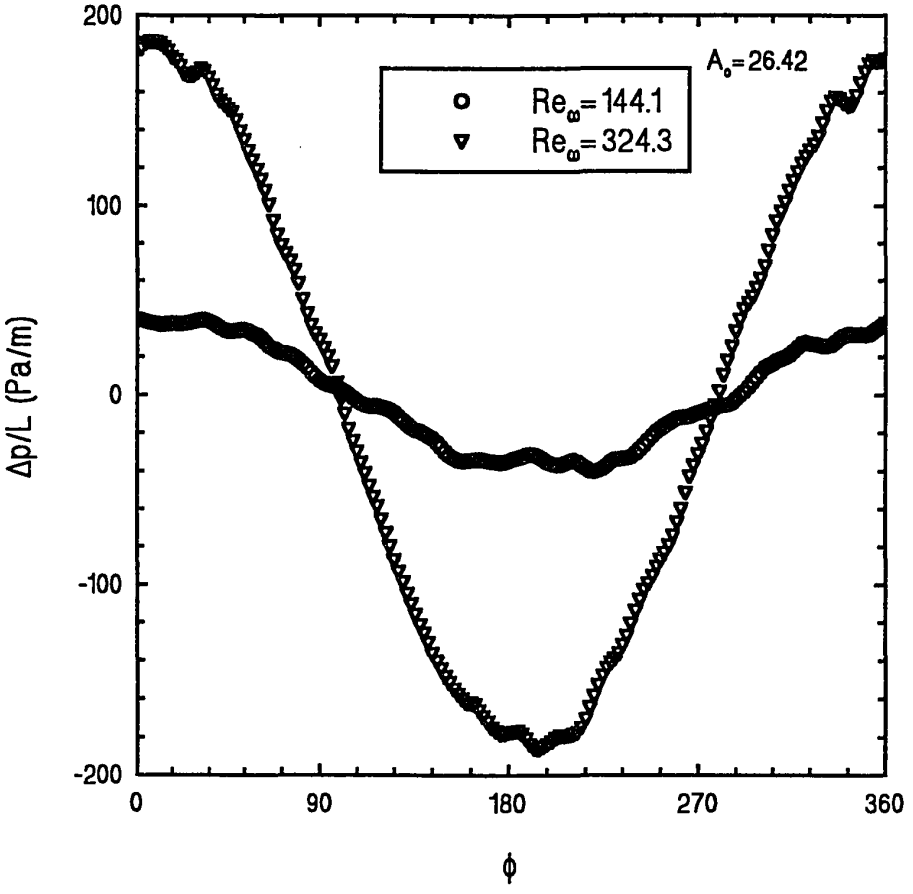

Fig. 5.3 Typical variations of the ensemble-averaged pressure drops for Re_ω =144.1 and 324.3 at A_o=26.42

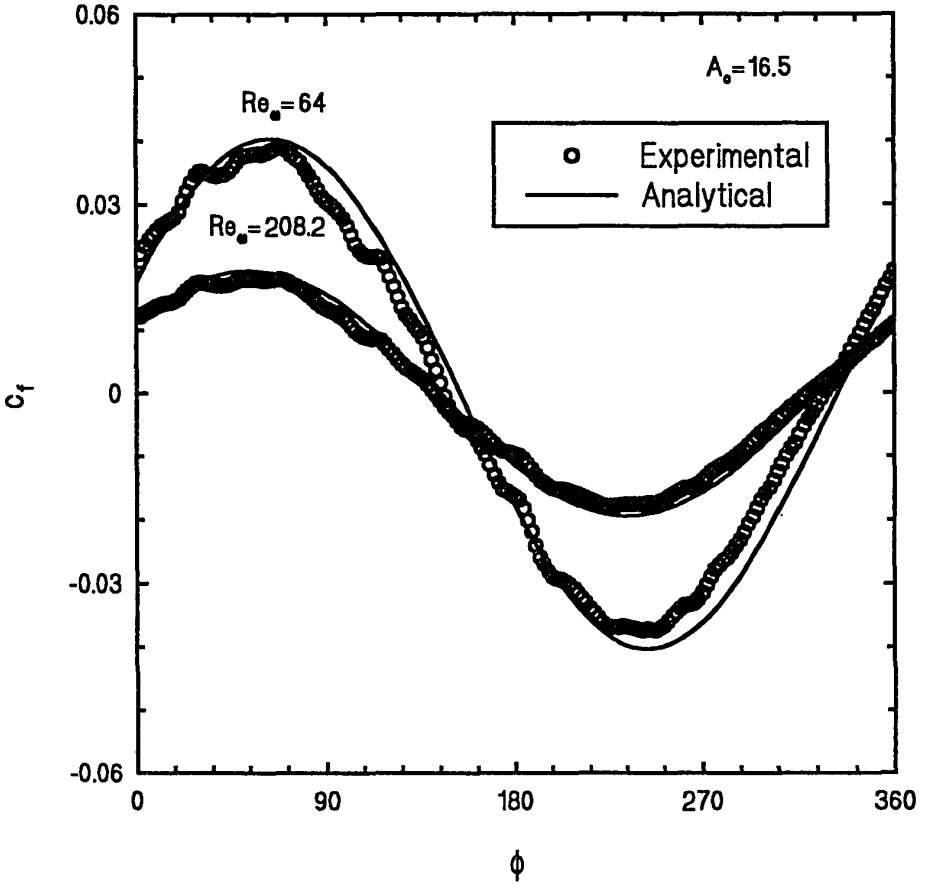

Fig. 5.4a Comparison of the instantaneous friction coefficient of the fully developed flow between analytical and experimental results for Re_ω=64 and 208.2 at A_o=16.5

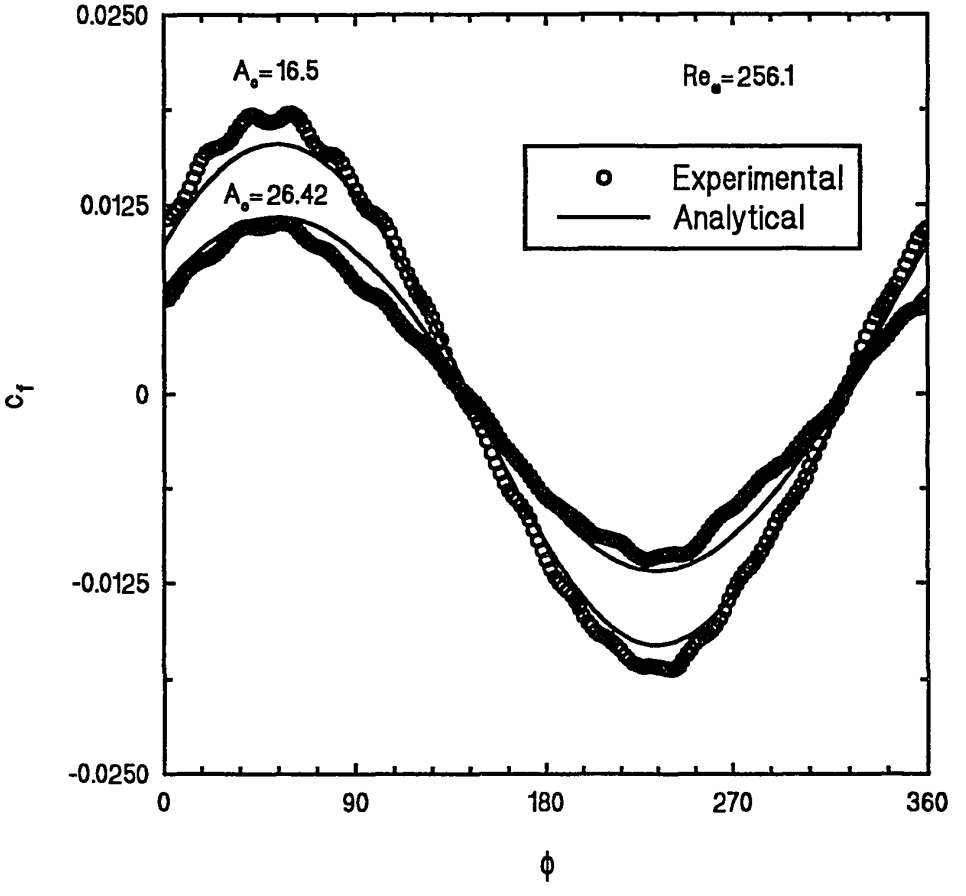

Fig. 5.4b Comparison of the instantaneous friction coefficient of the fully developed flow between analytical and experimental results for A_o=16.5 and 26.42 at Re_ω=256.1

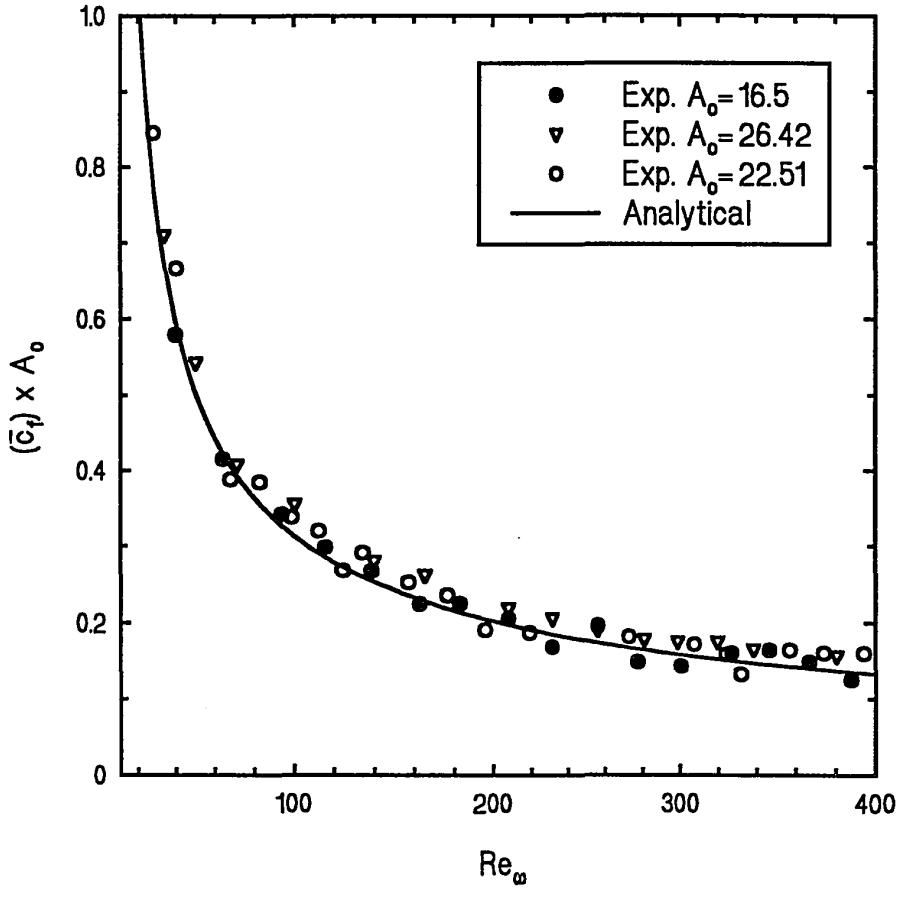

Fig. 5.5 Comparison of the cycle-averaged friction coefficient between analytical solution and experimental data

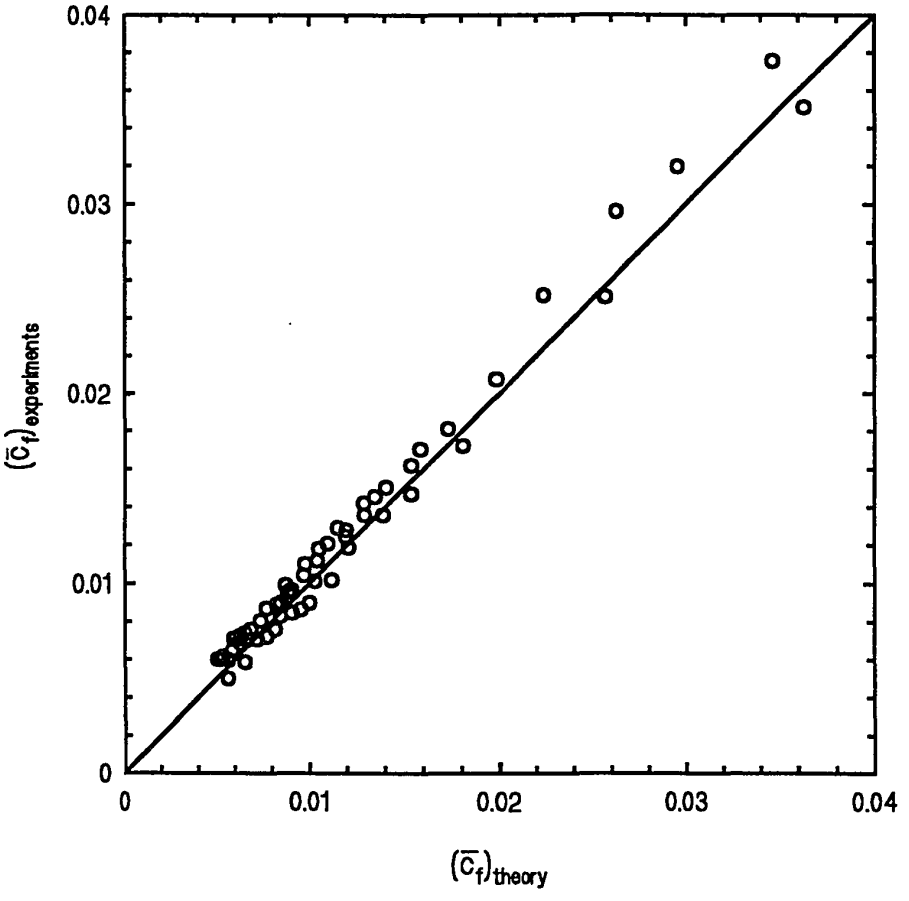

Fig. 5.6 The accuracy of the predication equation of the cycle-averaged friction coefficient

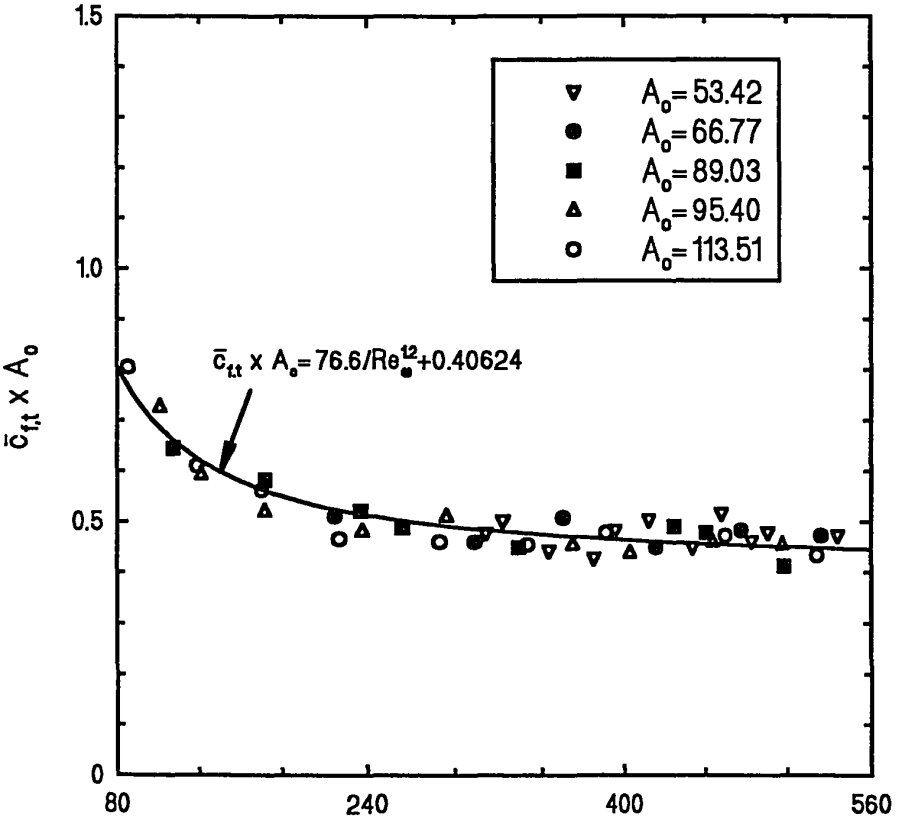

Fig. 5.7 Correlation equation of the cycle-averaged friction coefficient in terms of A_o and Re_ω for oscillatory turbulent flow

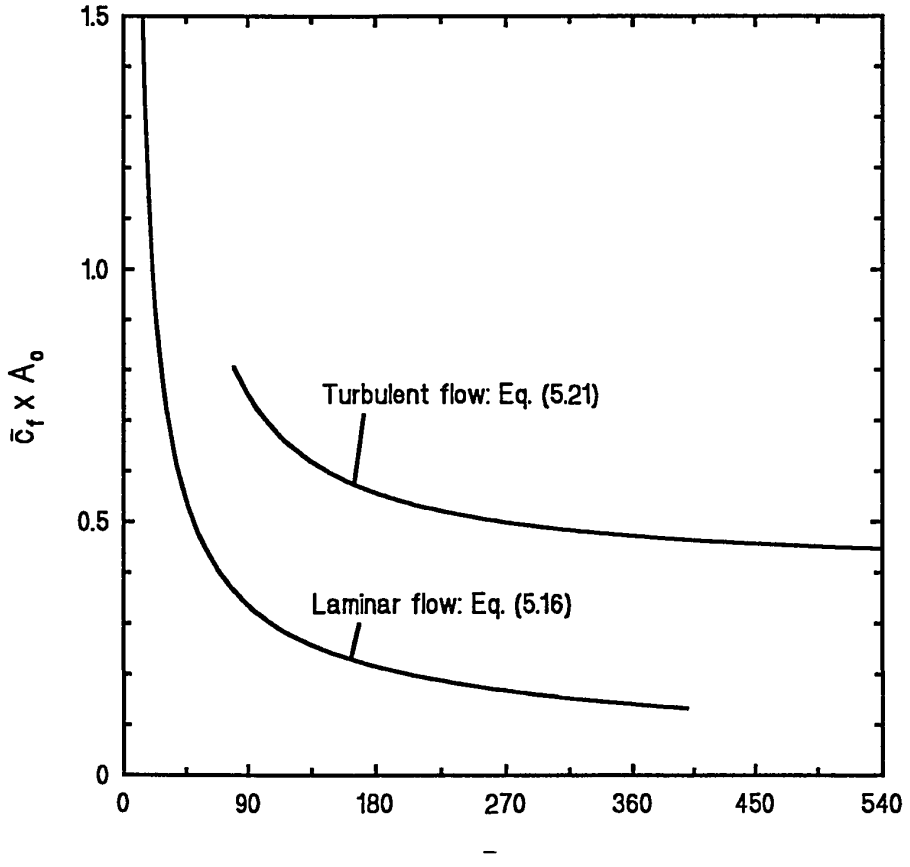

Fig. 5. 8 Comparison of the correlation equations of the cycle-averaged friction coefficient between the oscillatory laminar flow and turbulent flow

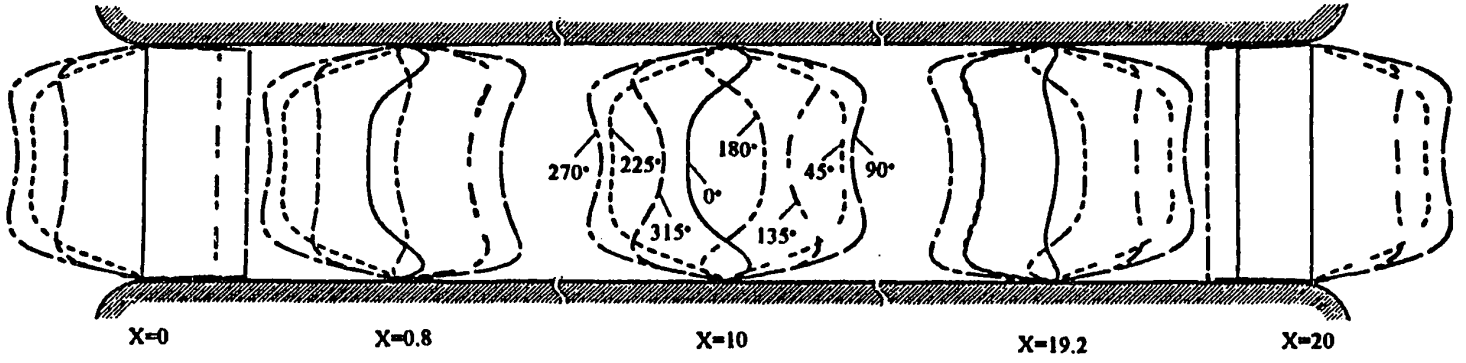

Fig. 6.1 Transient velocity profiles at different locations along the pipe for A_o=10, Re_ω=100 and L/D=20

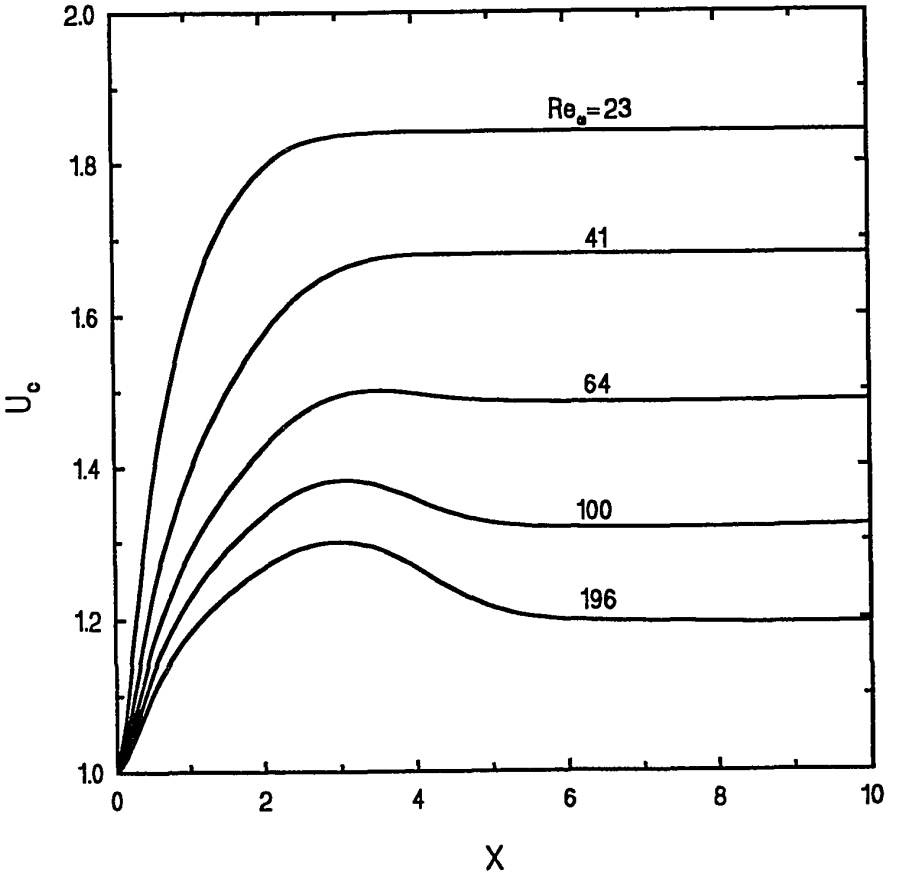

Fig. 6.2a Effects of Re_ω on the centerline axial velocity variations along axial location in the entrance region at ϕ=90°

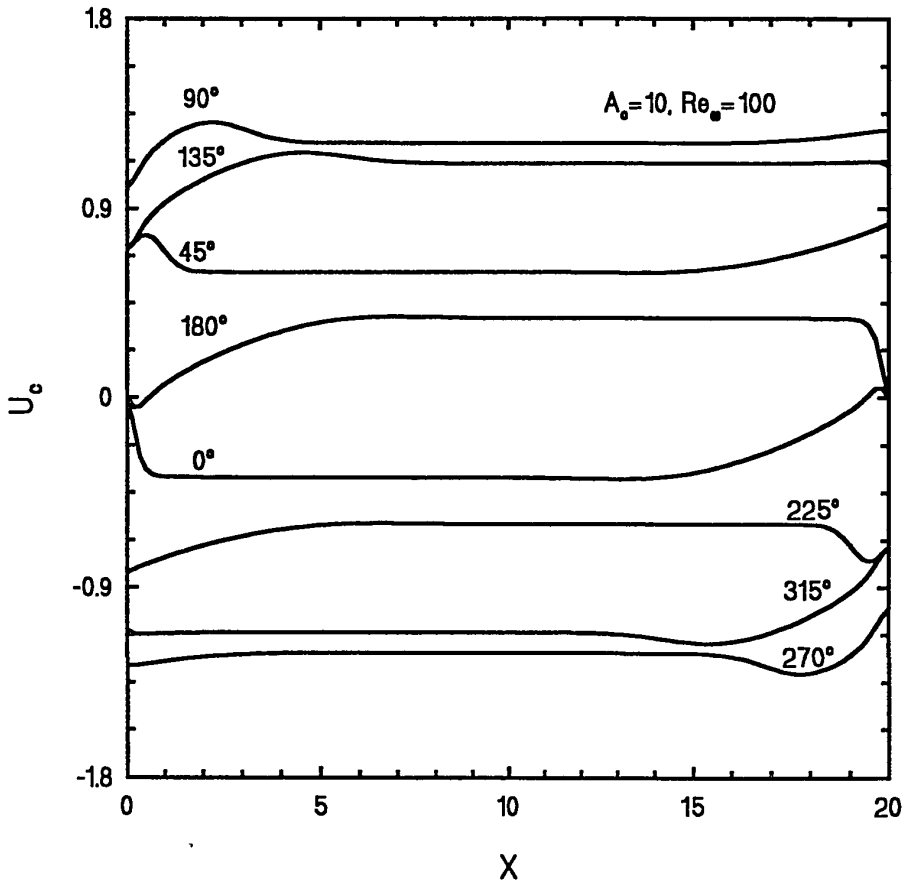

Fig. 6.2b Variations of the centerline velocity along the tube at different instants of times for A_o=10, Re_ω=100 and L/D=20

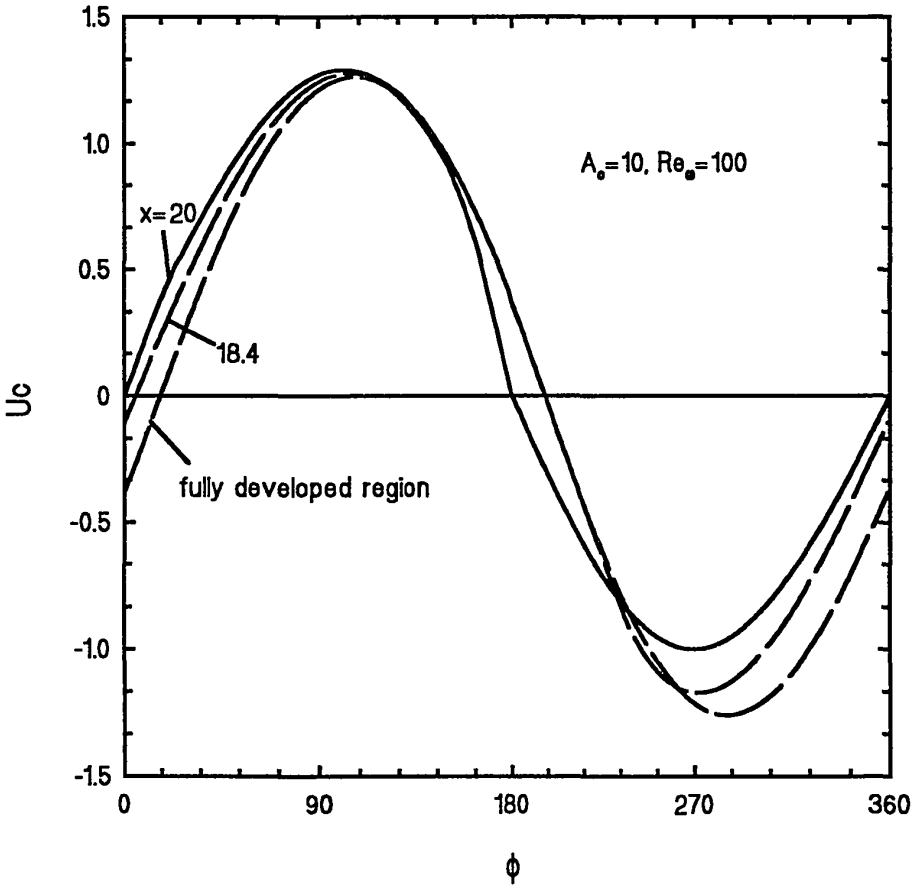

Fig. 6.2c Transient centerline axial velocity near the exit for A_o=10, Re_ω=100, and L/D=20

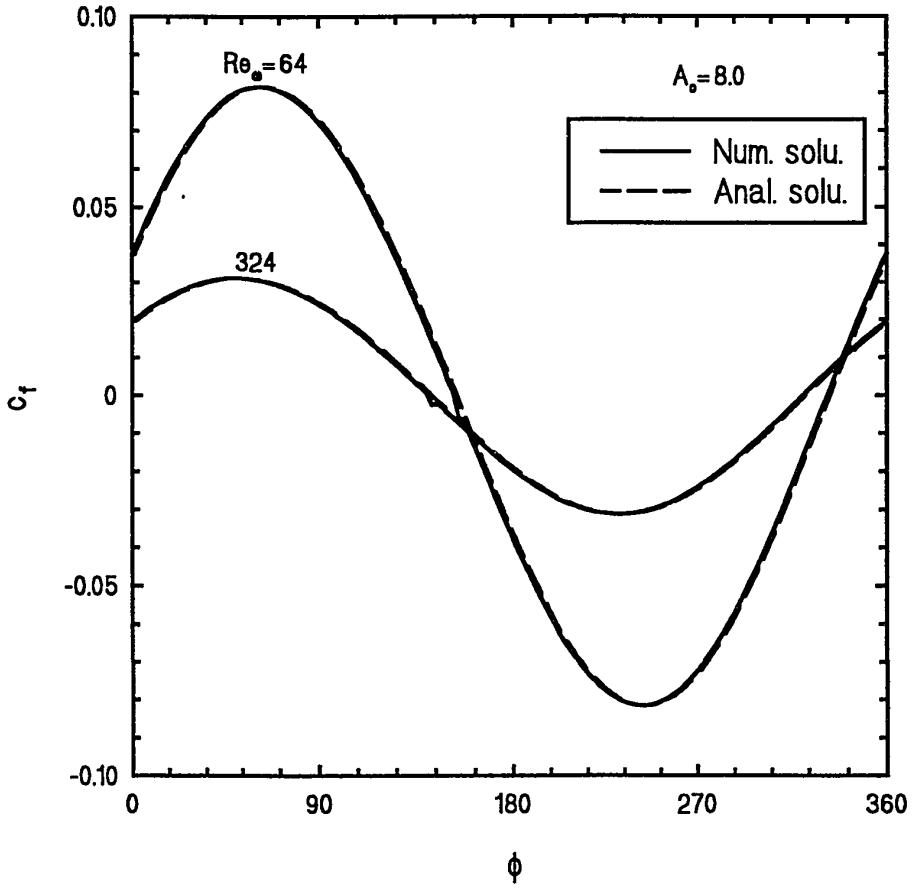

Fig. 6.3a Comparison of the instantaneous friction coefficient of the fully developed flow between numerical and analytical solutions

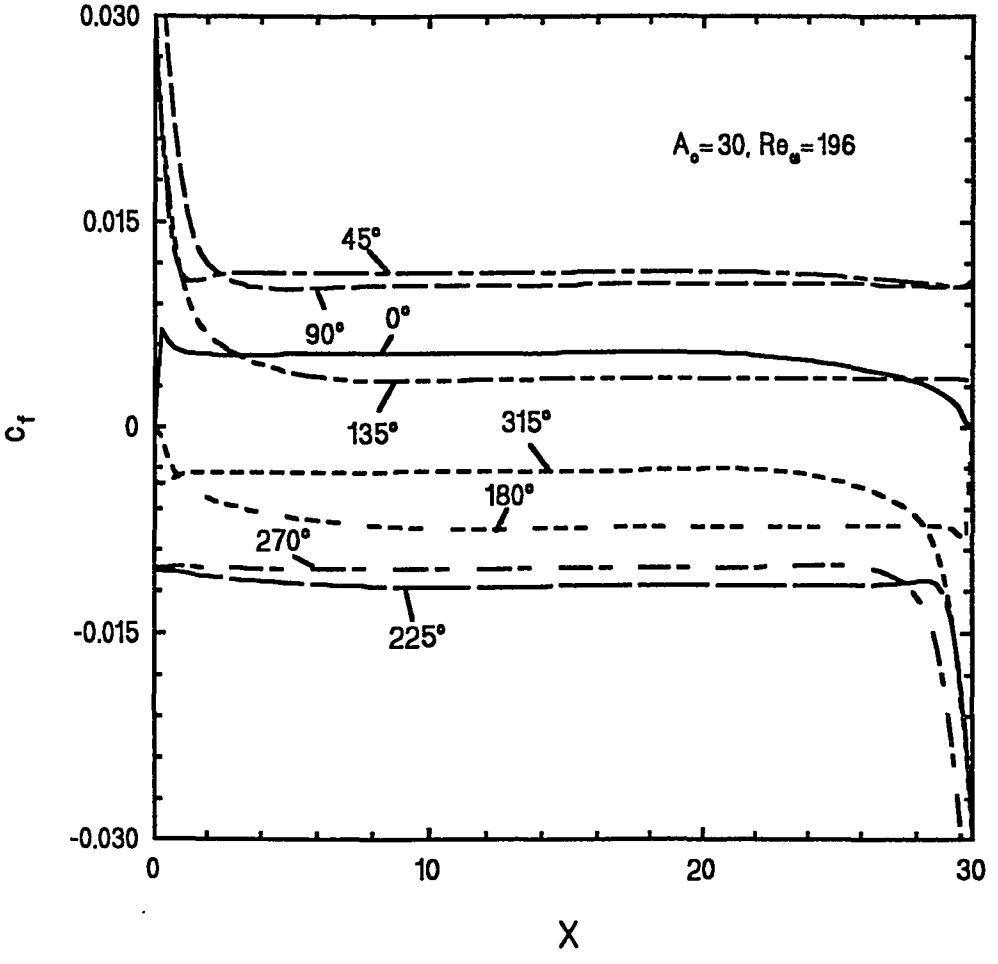

Fig. 6.3b Variations of the friction coefficient along the tube at different instants for A_o=30, Re_ω=196 and L/D=30

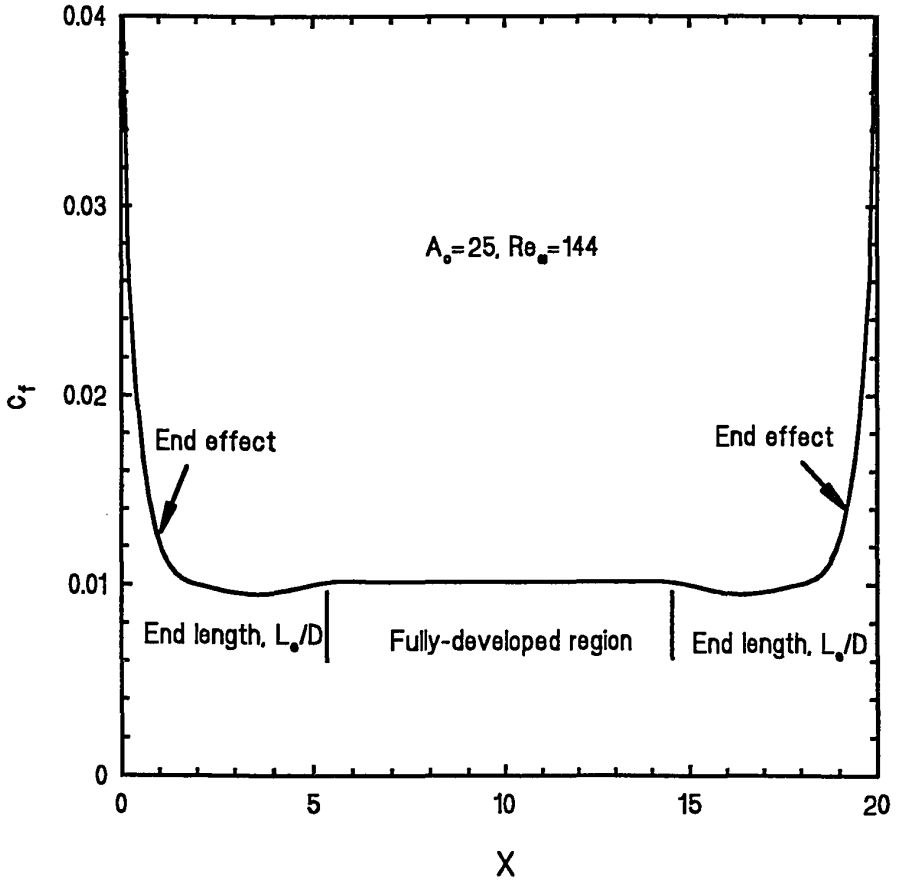

Fig. 6.3c The end effect and the end length

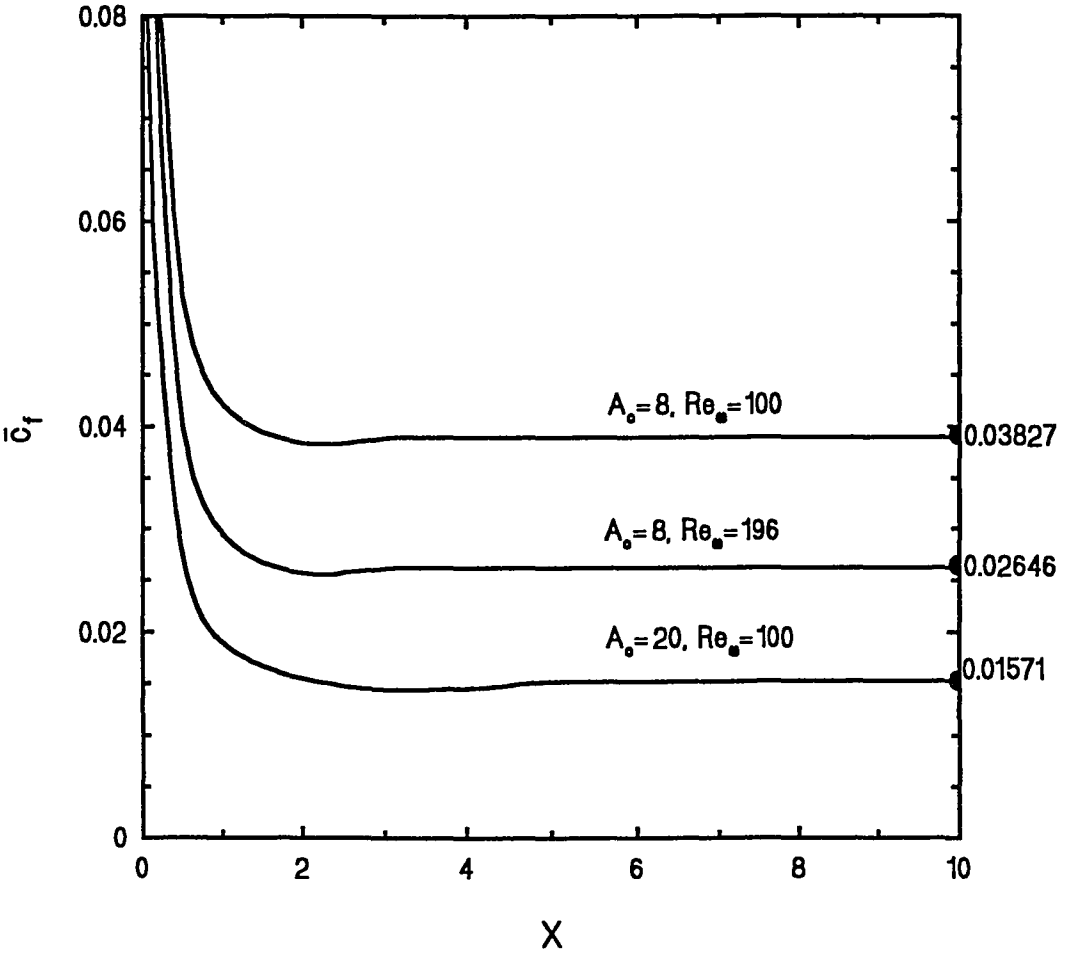

Fig. 6.3d Effects of A_o and Re_ω on variations of the cycle-averaged friction coefficient along the axial location in the left end of the pipe

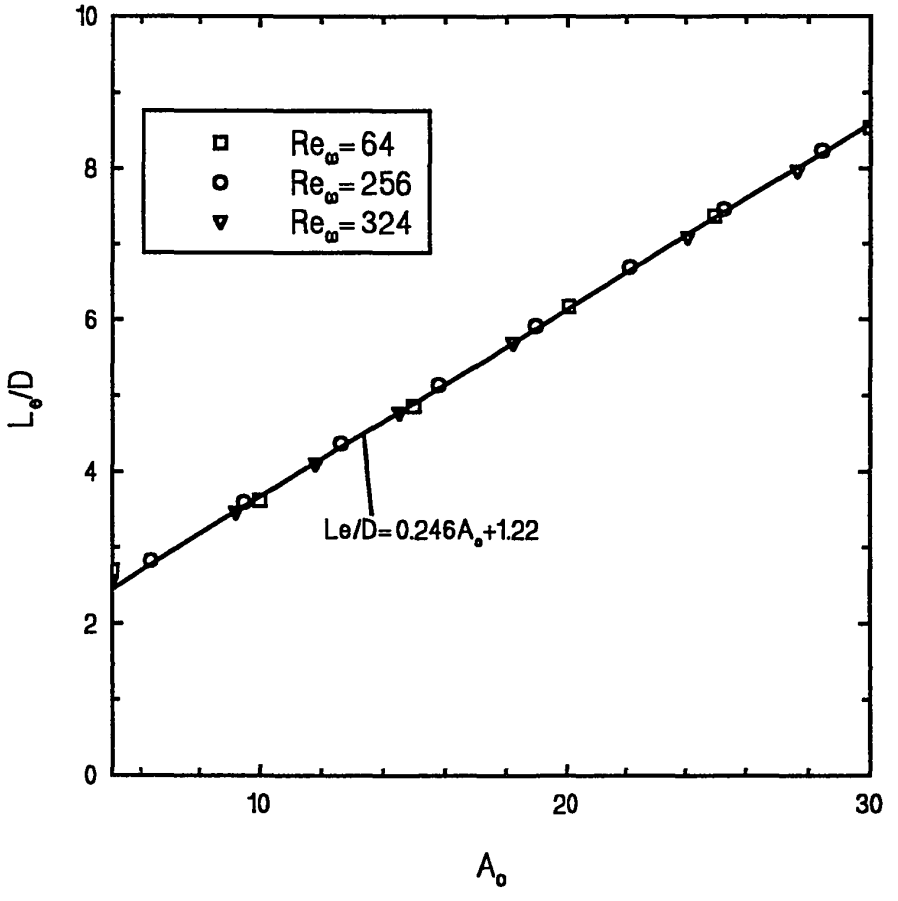

Fig. 6.4 Correlation equation for end length in terms of A_o

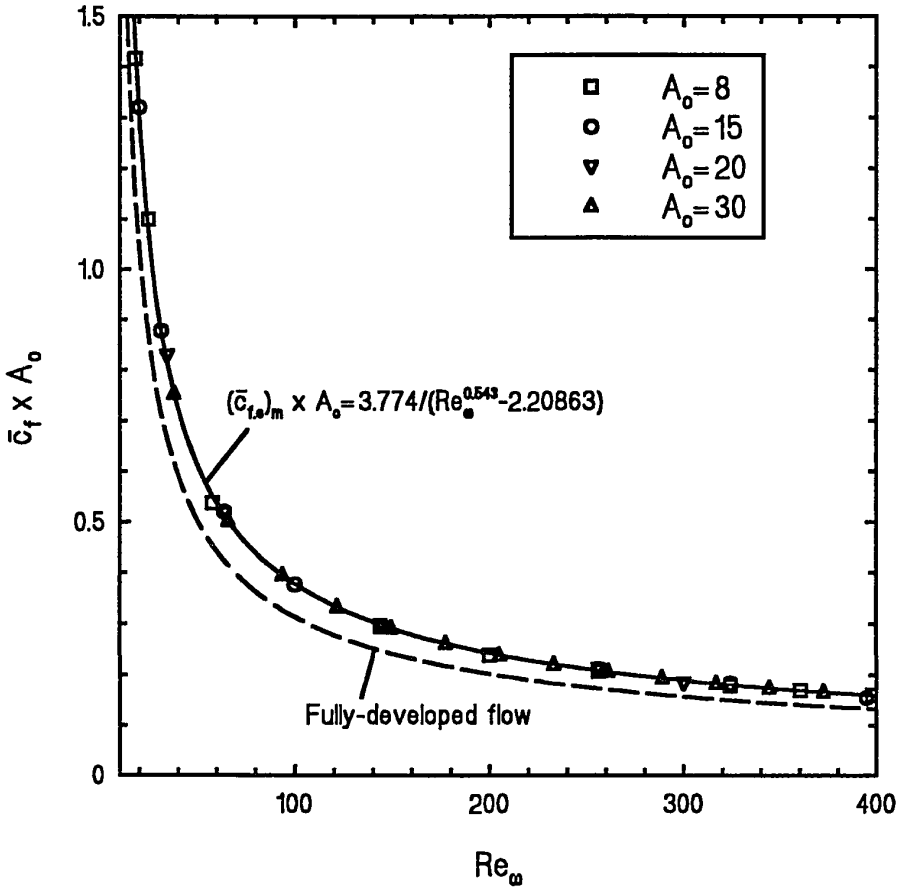

Fig. 6.5 Correlation equation for the space-cycle averaged frictioncoefficient in the end region

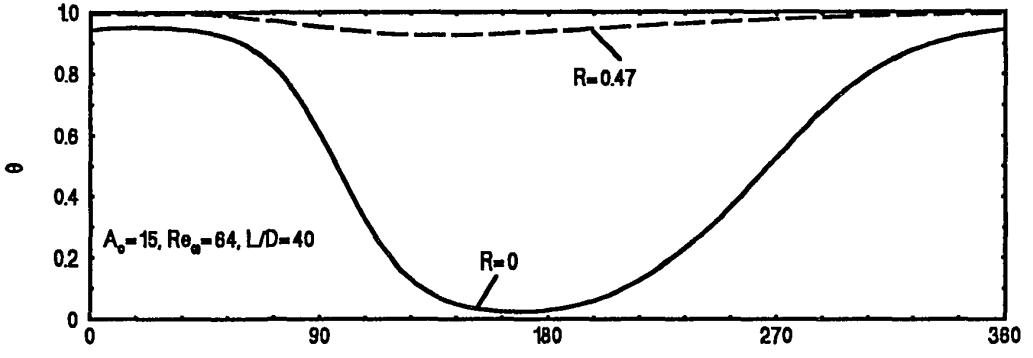

7.1a Temporal temperature variations at X=6.2 and at different radial positions for A_o=15, Re_ω=64, and L/D=40

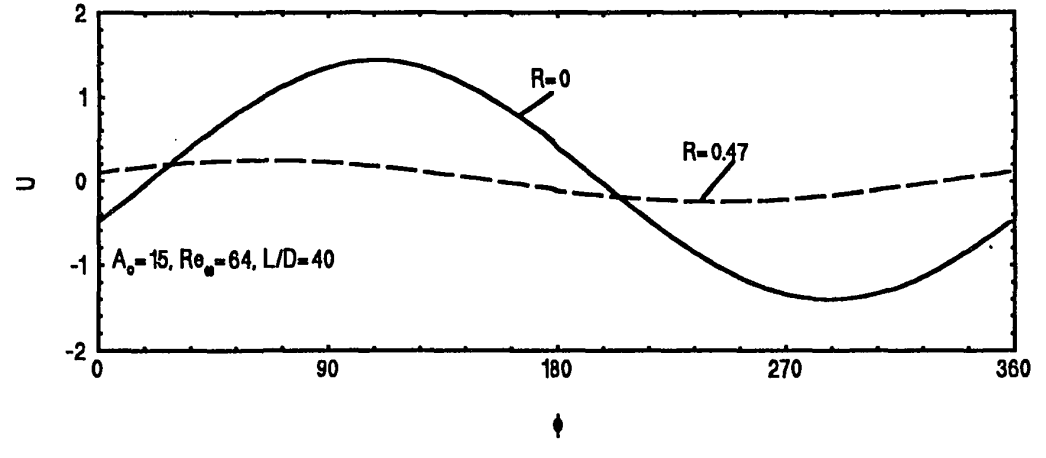

7.1b Temporal velocity variations at X=6.2 and at different radial positions for A_o=15, Re_ω=64, and L/D=40

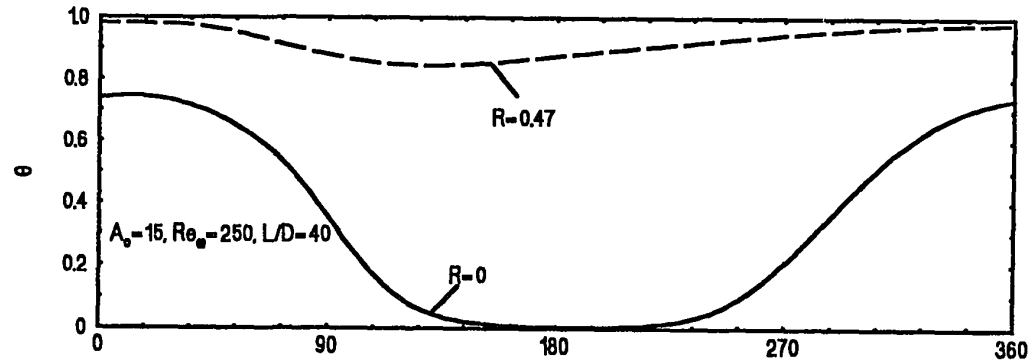

7.2a Temporal temperature variations at X=6.2 and at different radial positions for A_o=15, Re_ω=250, and L/D=40

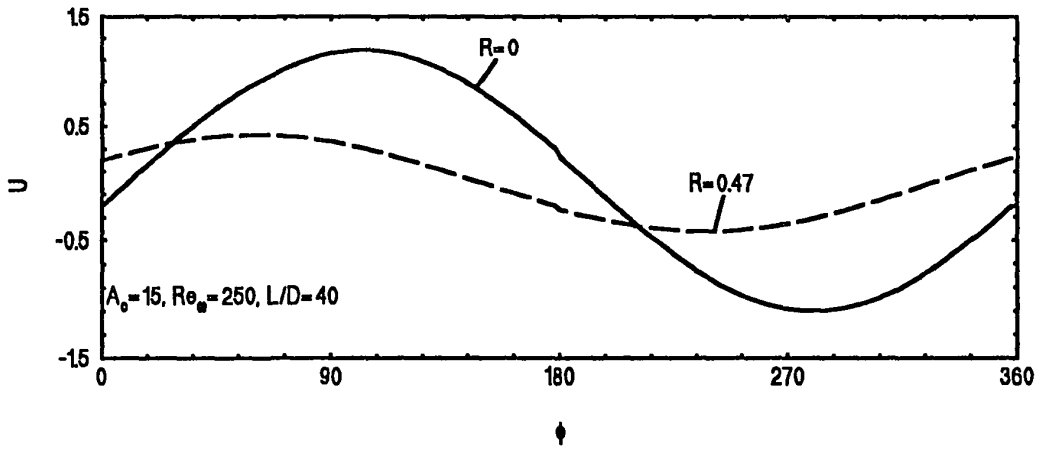

7.2b Temporal velocity variations at X=6.2 and at different radial positions for A_o=15, Re_ω=250, and L/D=40

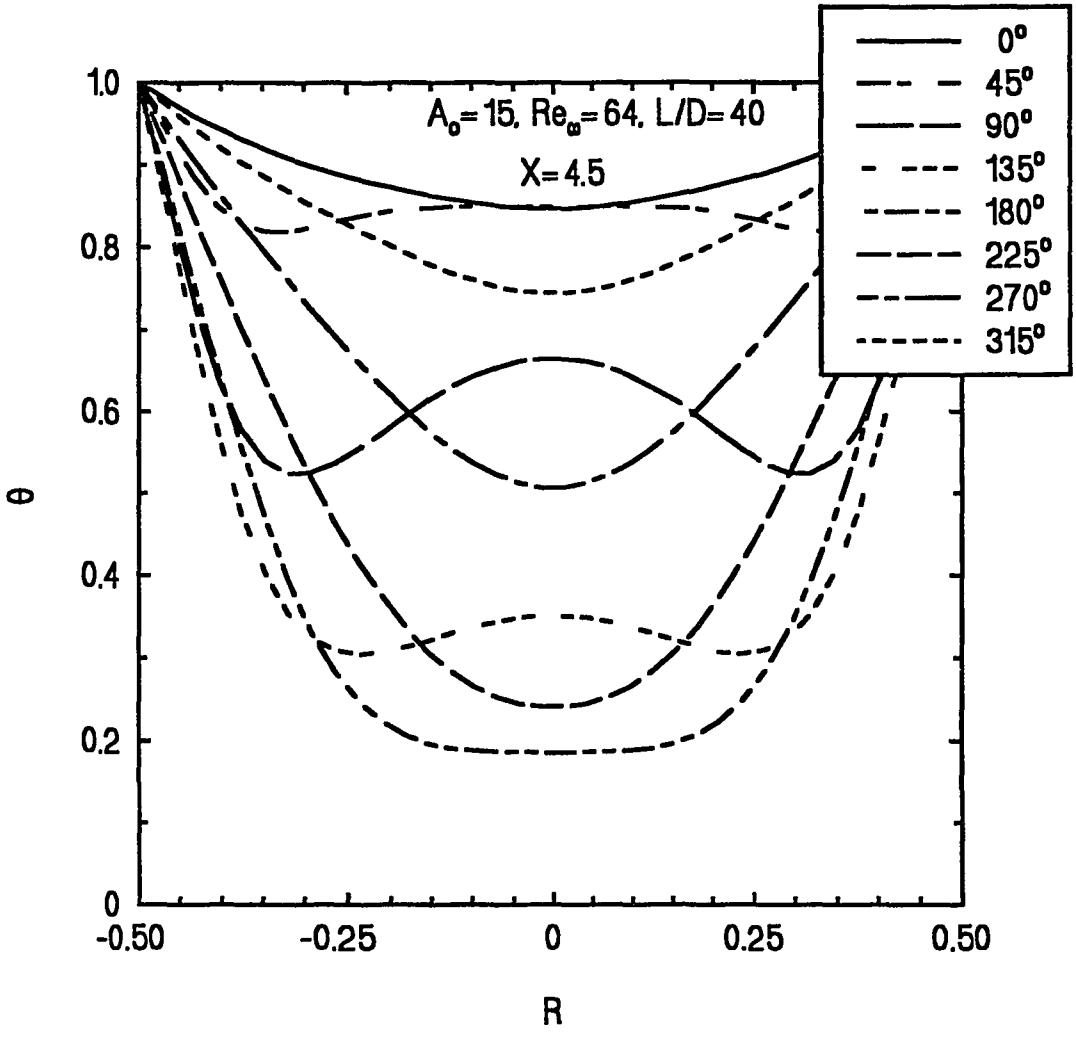

Fig. 7.3a Development of temperature profiles at X=4.5 for A_o=15, Re_ω=64, and L/D=40

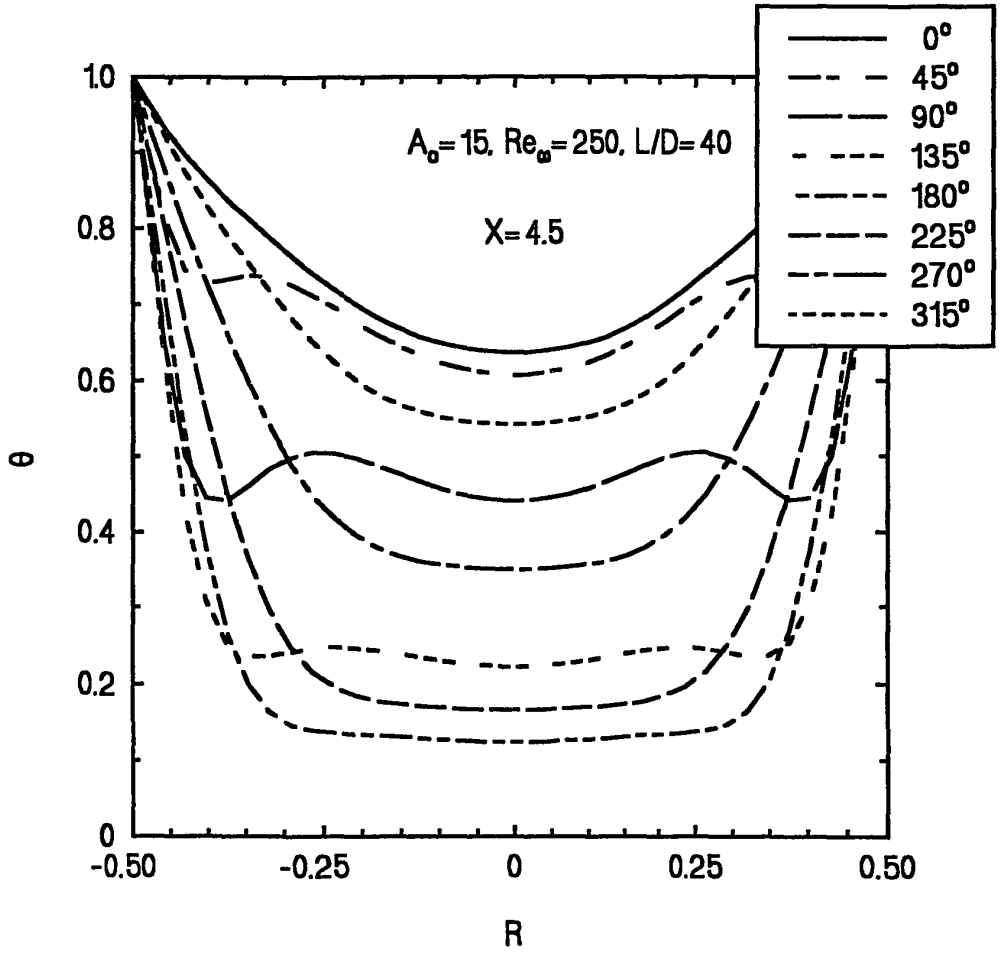

Fig. 7.3b Development of temperature profiles at $\dot{X}$=4.5 for A_o=15, Re_ω=250, and L/D=40

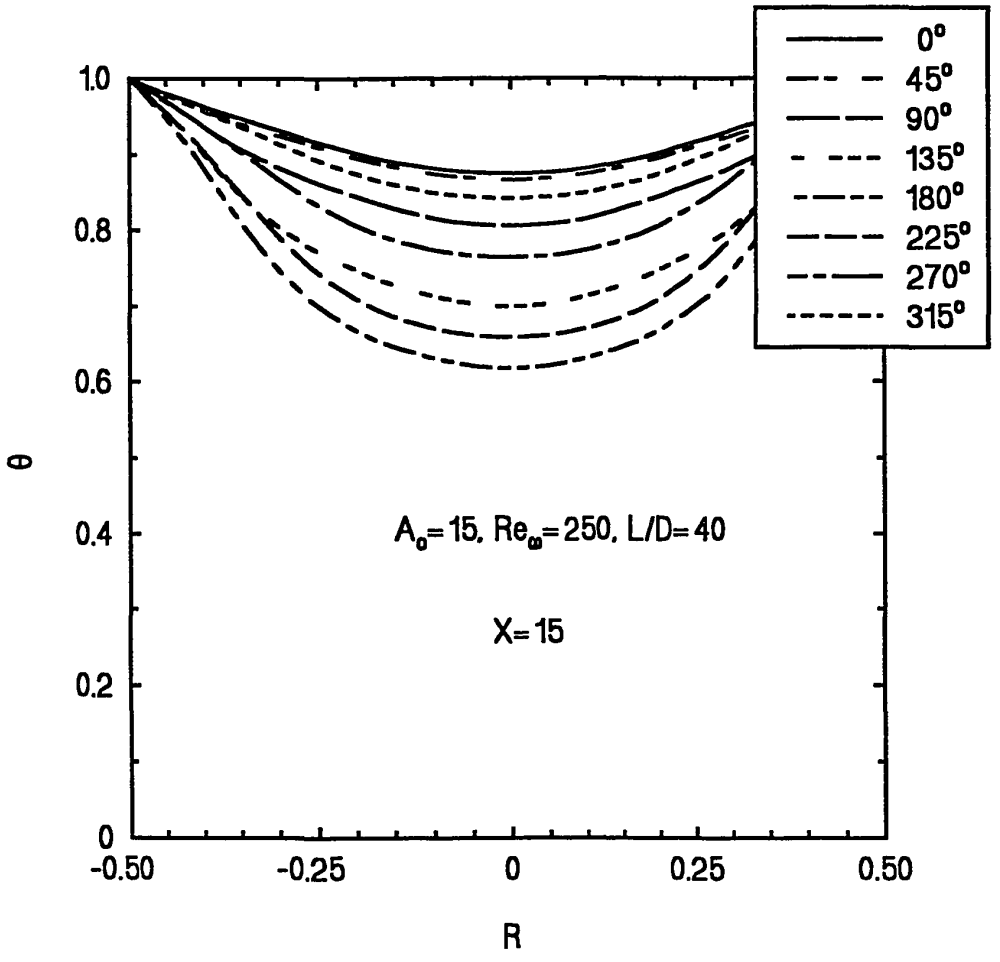

Fig. 7.4a Development of temperature profiles at X=15 for A_o=15, Re_ω =250, and L/D=40

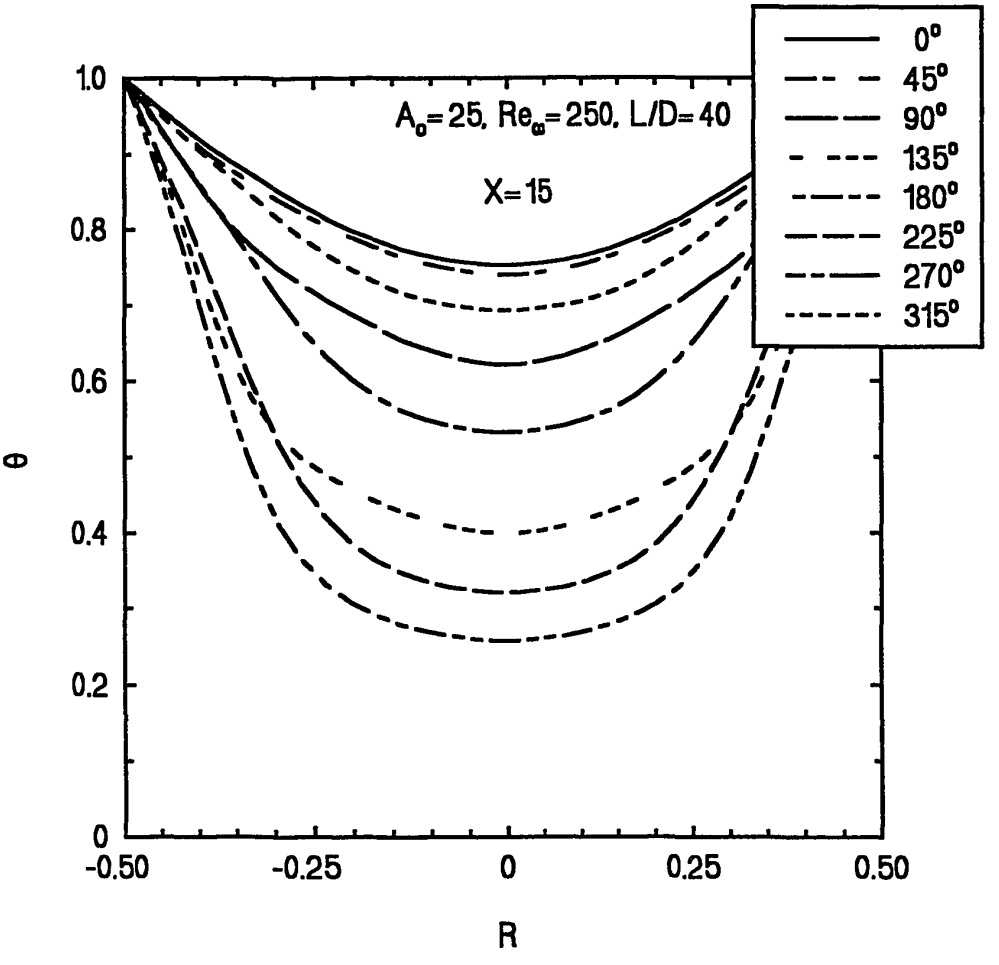

Fig. 7.4b Development of temperature profiles at X=15 for A_o=35, Re_ω=250, and L/D=40

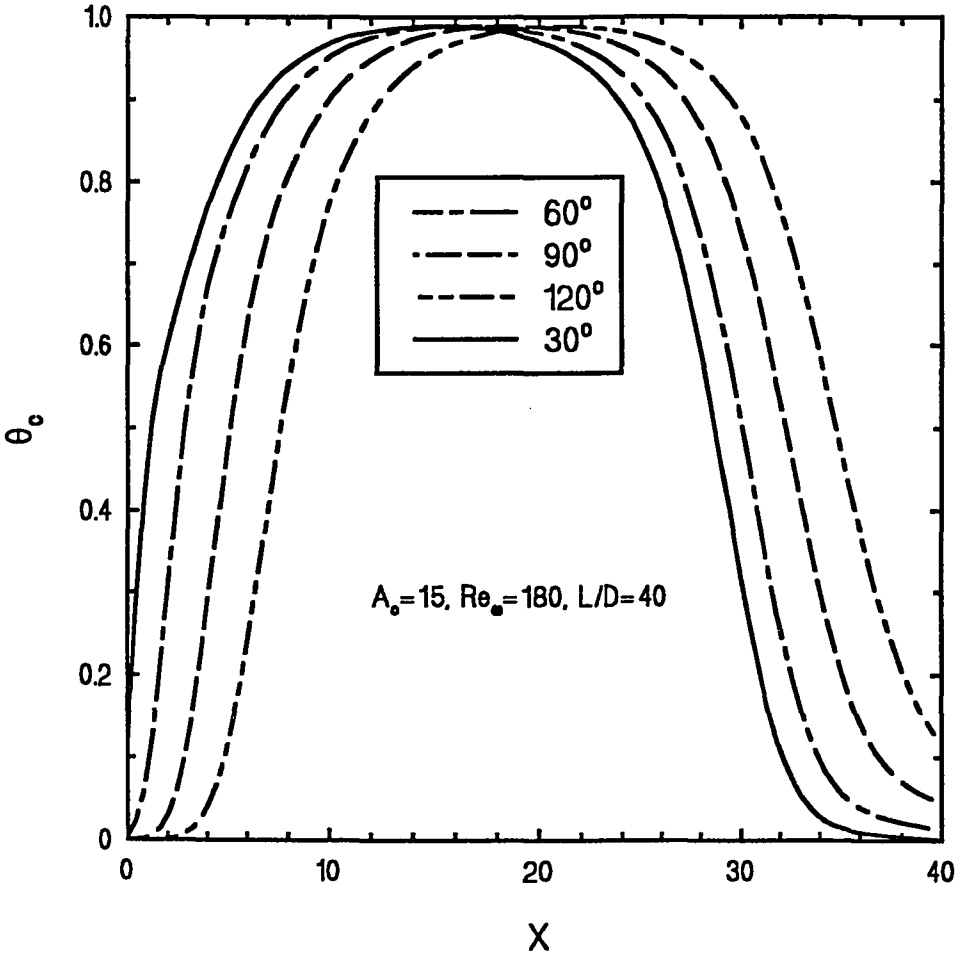

Fig. 7.5 Variations of the centerline temperature along the axial position at different phase angles for A_o=15, Re_ω =180, and L/D= 40

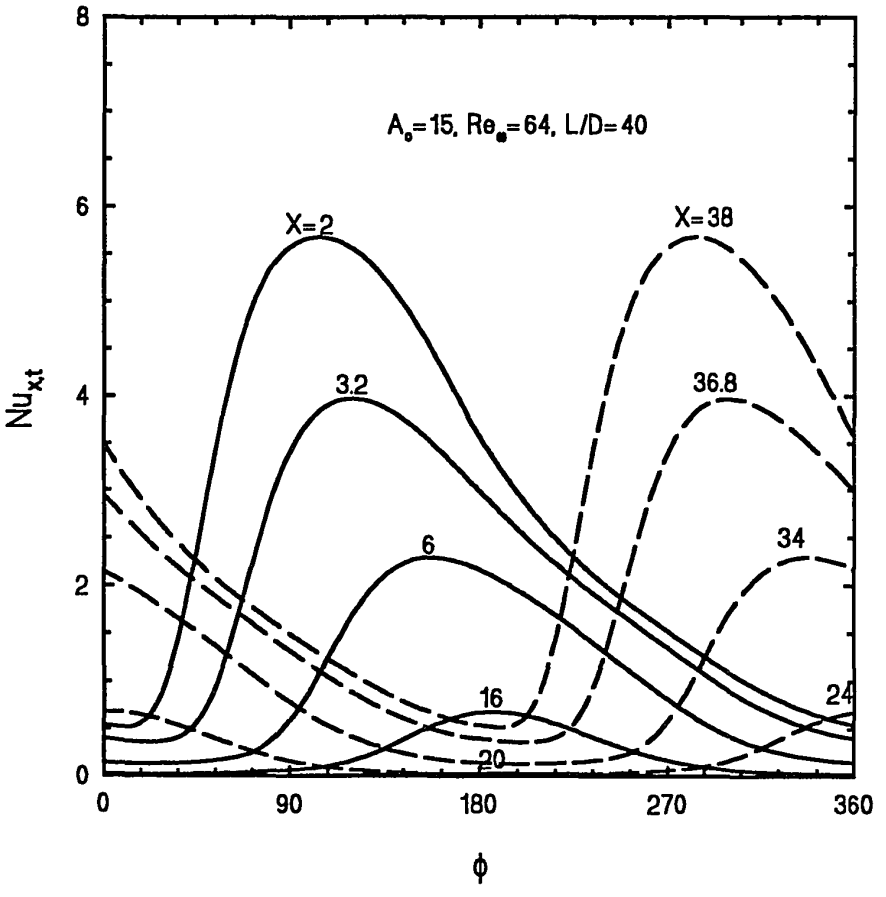

Fig. 7.6a Temporal variations of the local instantaneous Nusselt number at different axial locations for A_o=15, Re_∞ =64, and L/D=40

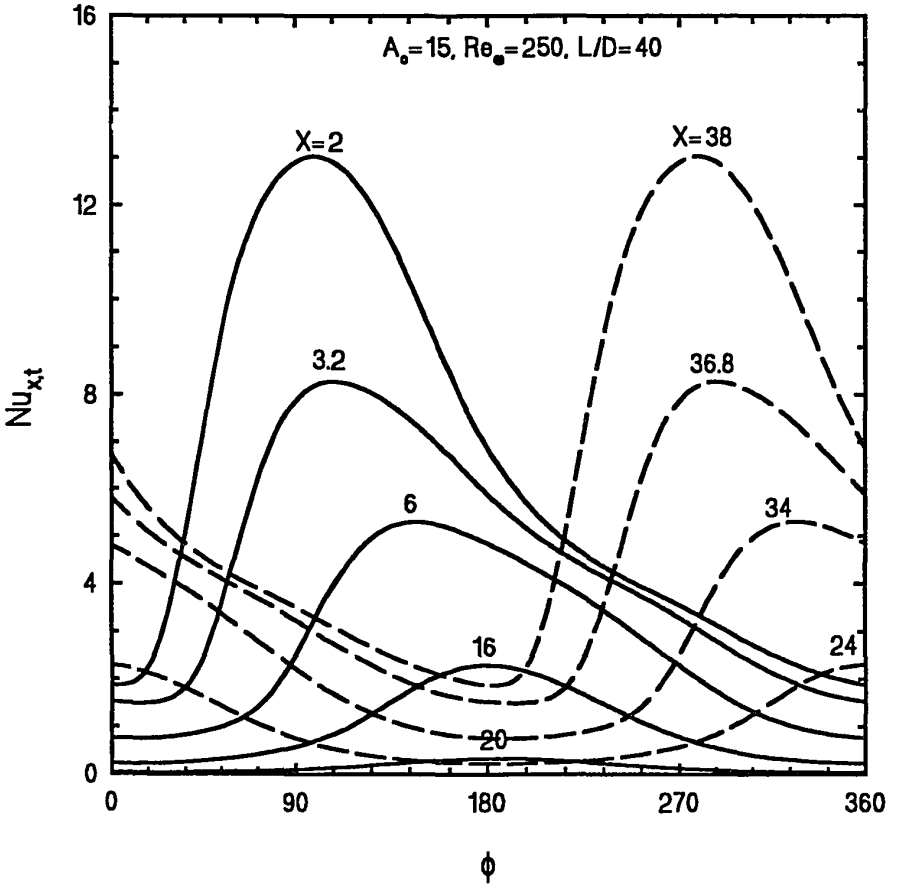

Fig. 7.6b Temporal variations of the local instantaneous Nusselt number at different axial locations for A_o=15, Re_ω=250, and L/D=40

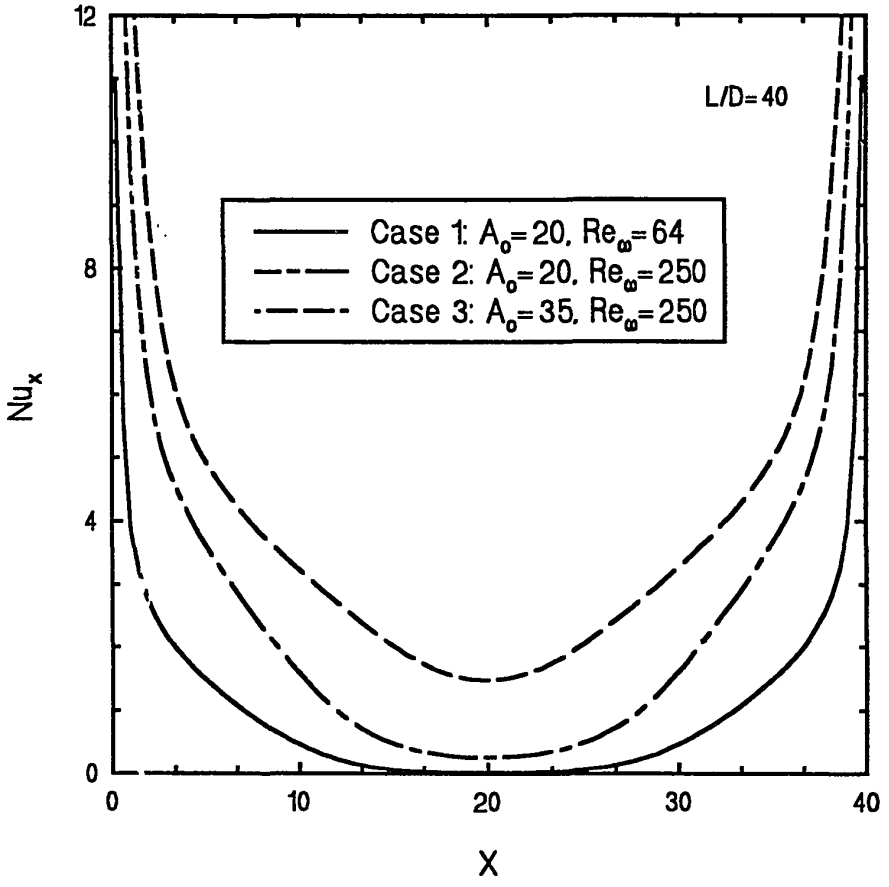

Fig. 7.7 Effects of the dimensionless oscillation amplitude of fluid A_o and the kinetic Reynolds number Re_ω on the cycle-averaged local Nusselt number at L/D=40

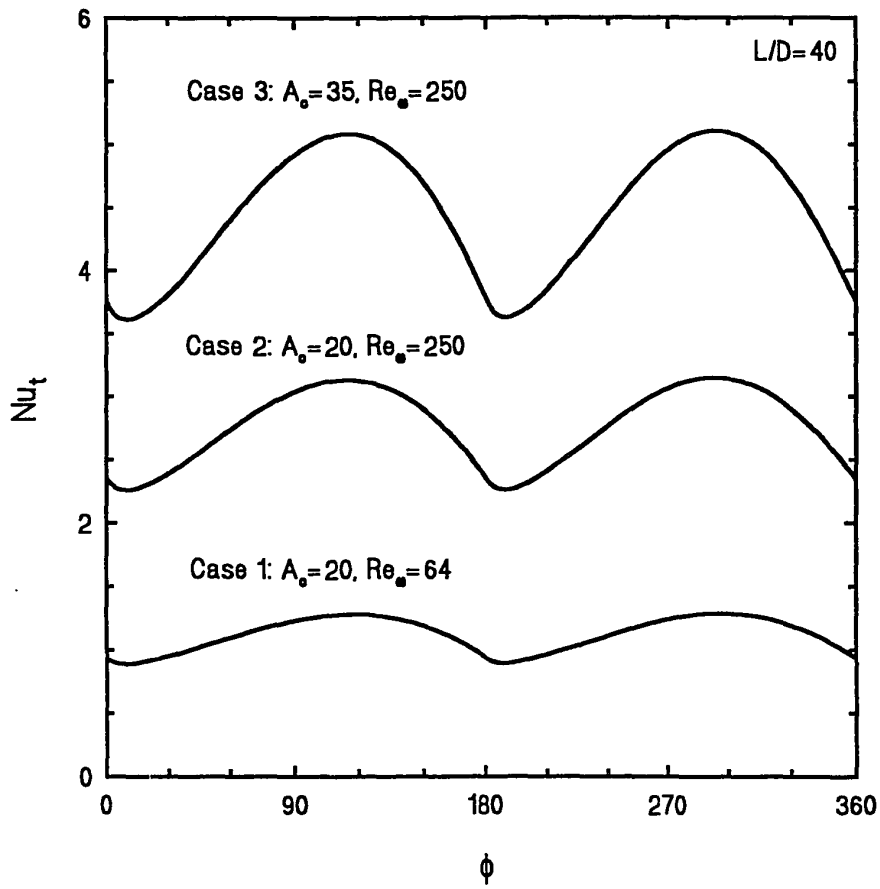

Fig. 7.8 Effects of the dimensionless oscillation amplitude of fluid A_o and the kinetic Reynolds number Re_ω on space-averaged instantaneous Nusselt number for L/D=40

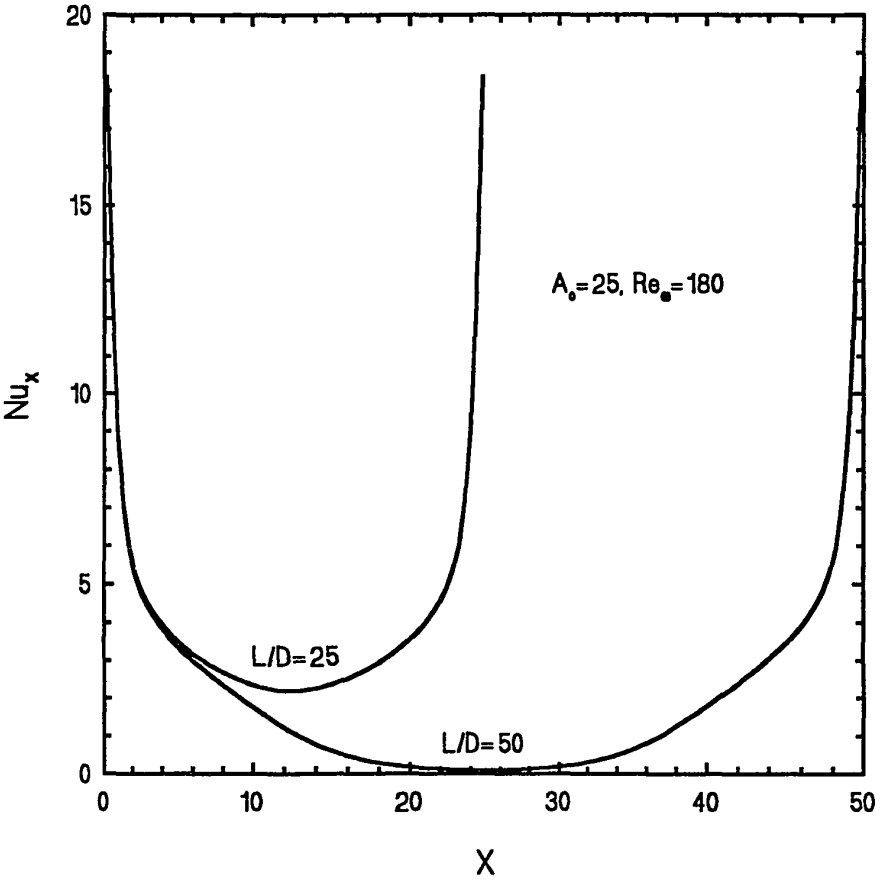

Fig. 7.9 Effects of length/diameter of the pipe on the cycle-averaged local Nusselt number for A_o=25 and Re_ω =180

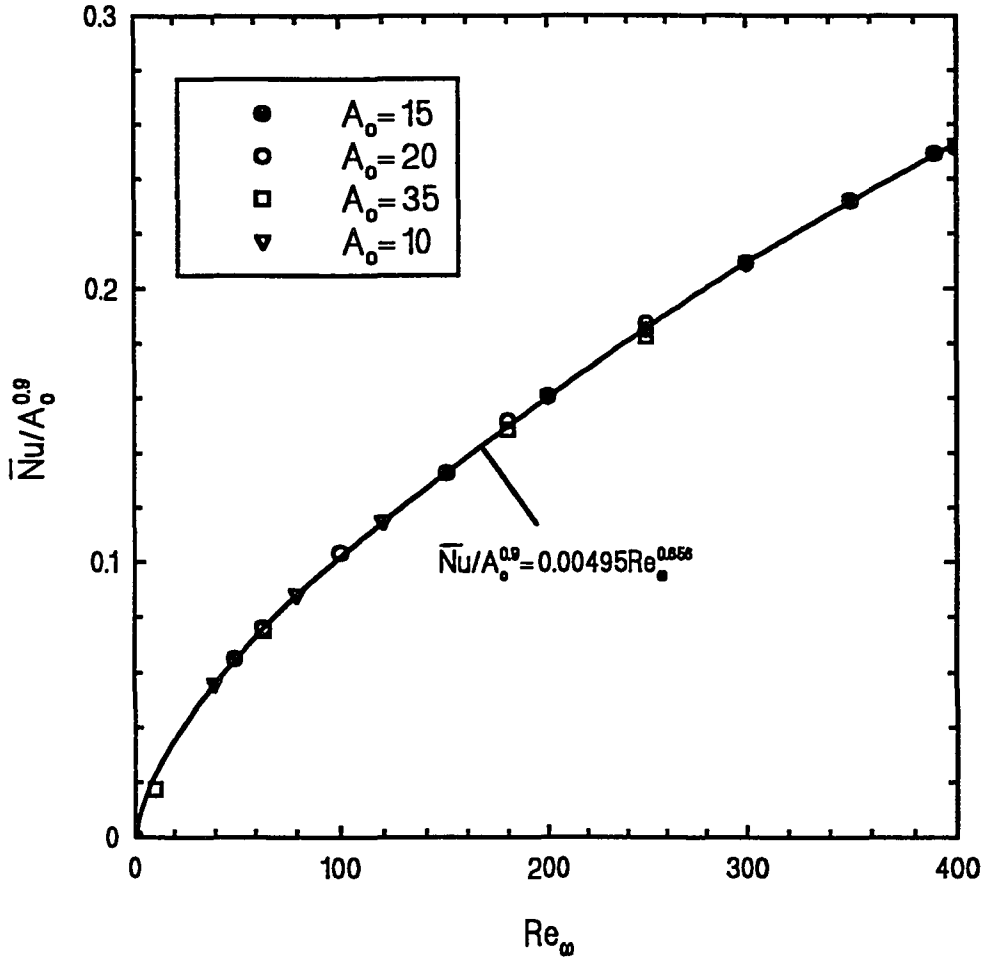

Fig. 7.10 Correlation equation of the space-cycle averaged Nusselt number for air in terms of A_o and Re_ω at L/D=40

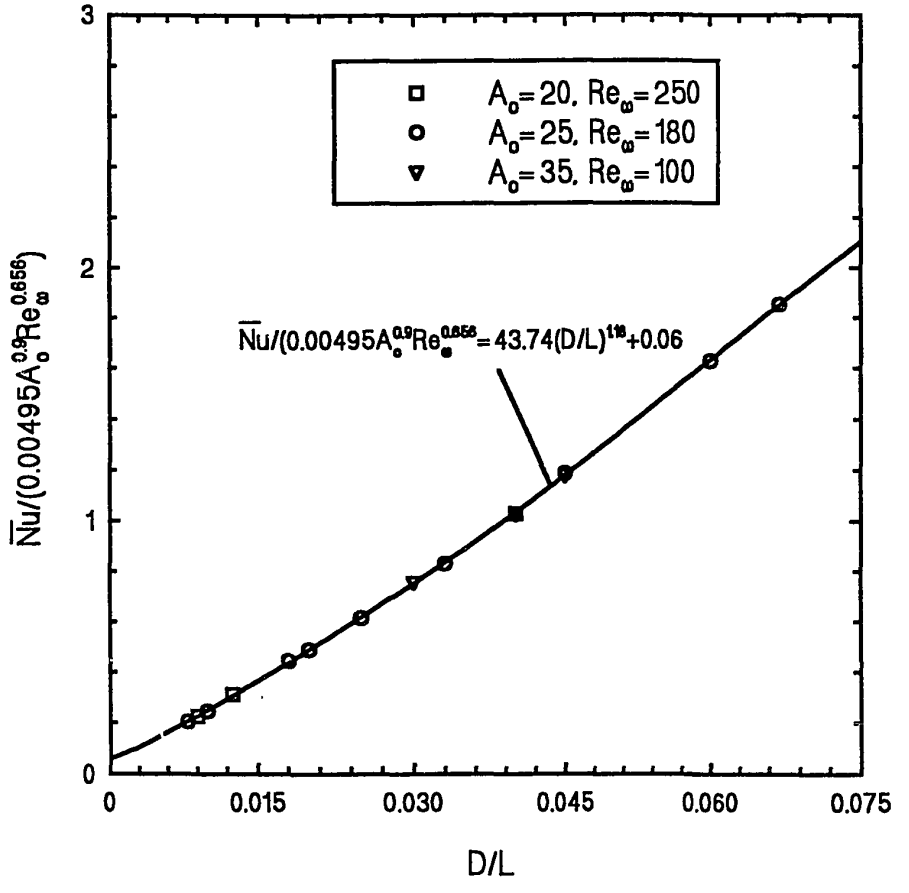

Fig. 7.11 Correlation equation of the space-cycle averaged Nusselt number for air in terms of A_o, Re_ω and L/D

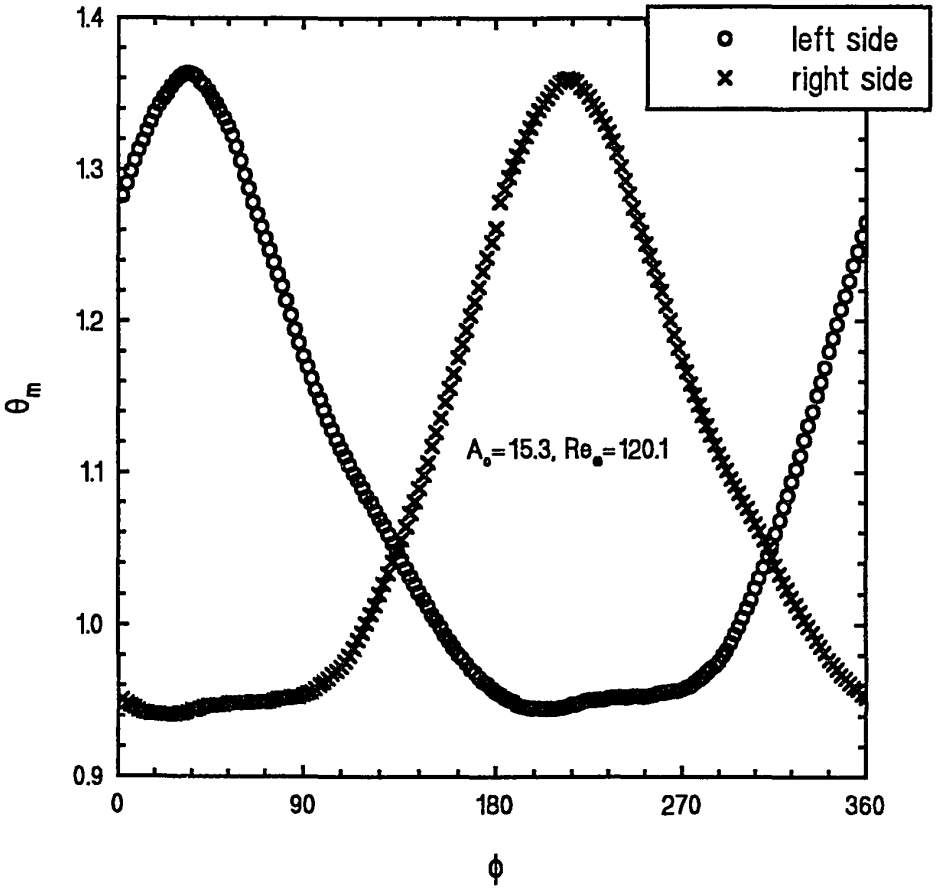

Fig. 8.1a Temporal fluid temperature variations in the left and right mixing chambers for A_o=15.3, Re_ω =120.1, and L/D=44.8

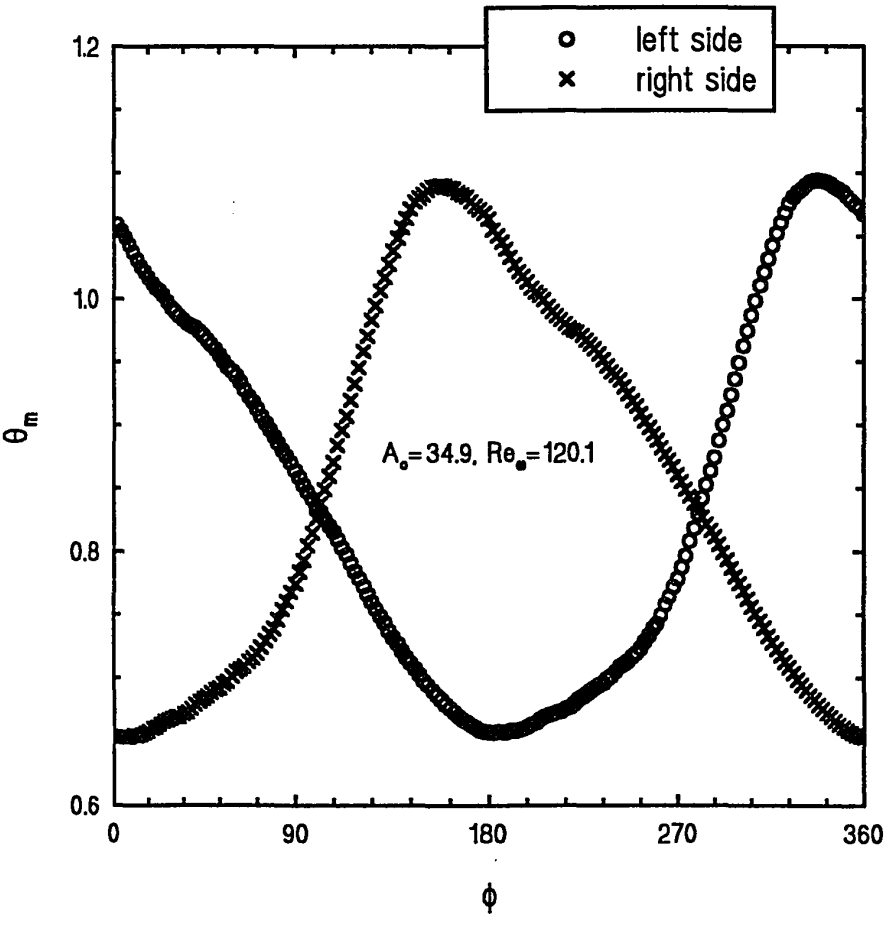

Fig. 8.1b Temporal fluid temperature variations in the left and right mixing chambers for A_o=34.9, Re_ω=120.1, and L/D=44.8

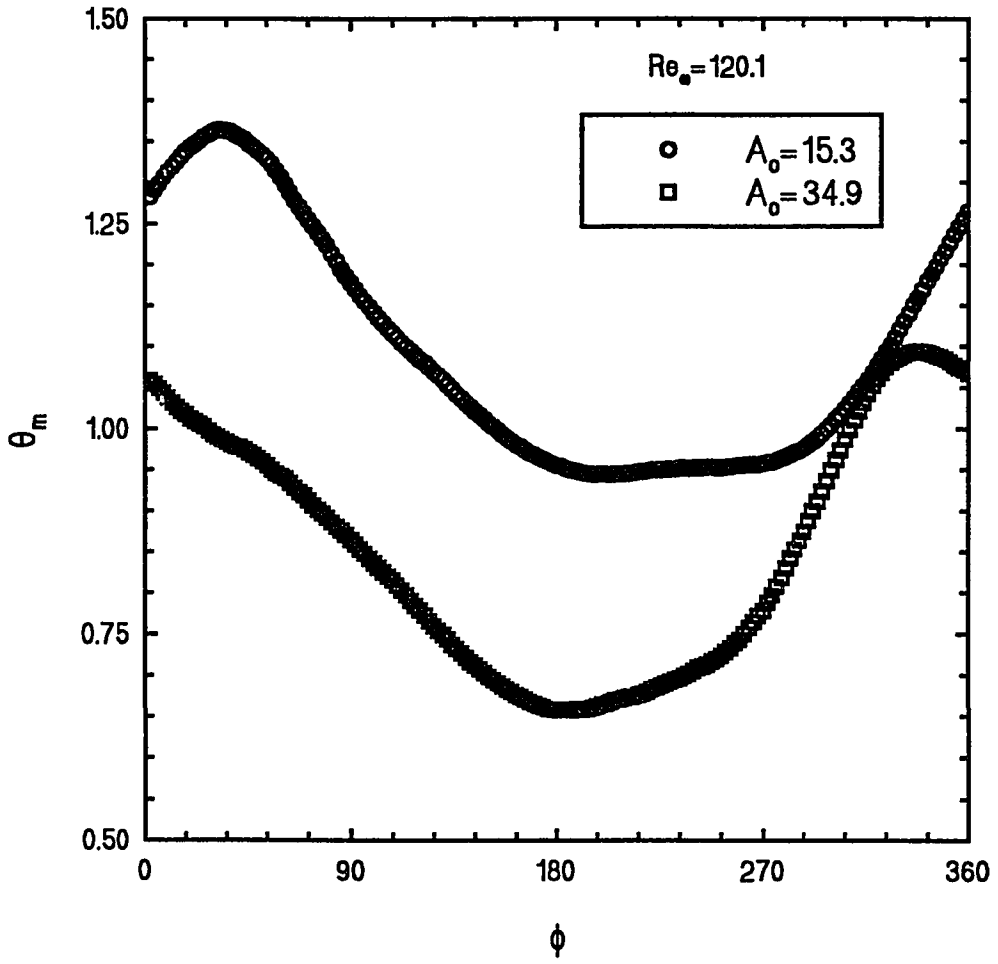

Fig. 8.2 Effects of the dimensionless oscillation amplitude of fluid A_o on the temporal fluid temperature variations in the left mixing chamber for Re_ω=120.1 and L/D=44.8

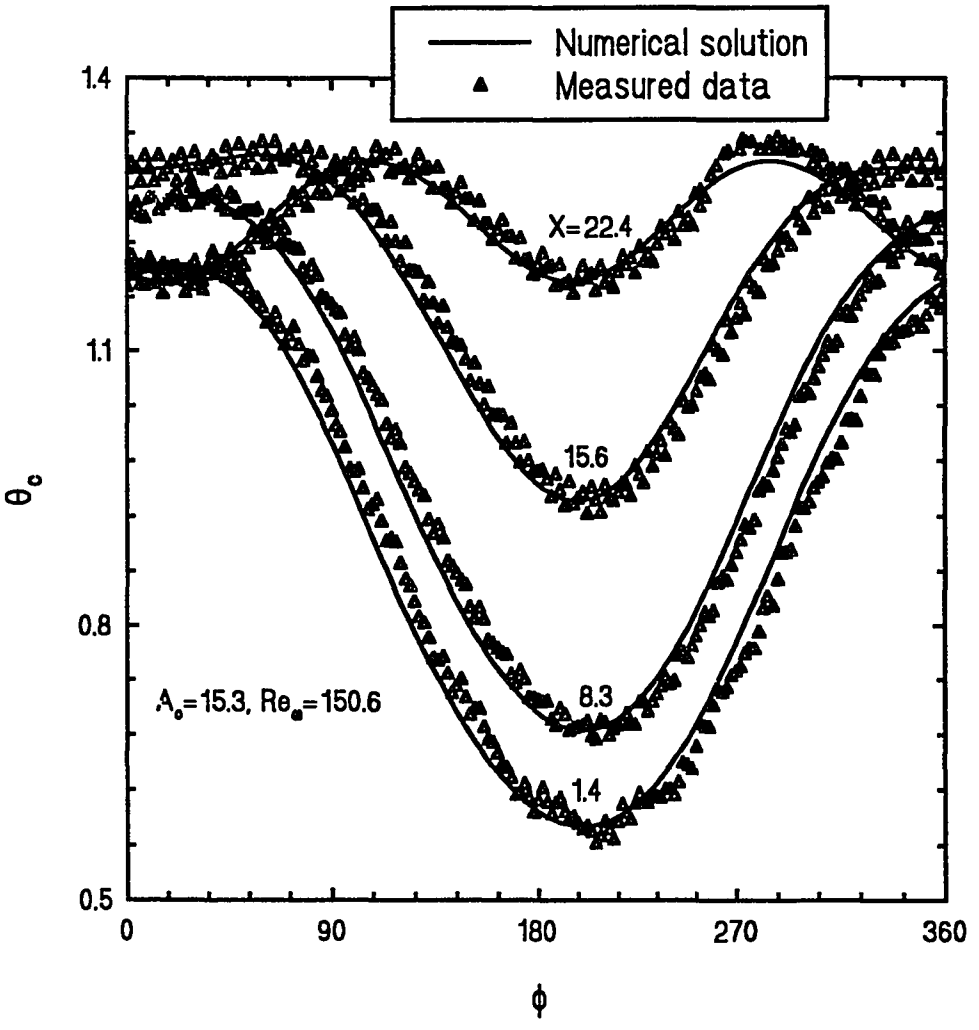

Fig. 8.3 Variations of the centerline temperature along the axial position at different phase angles for A_o=15.3, Re_ω=150.6, and L/D= 44.8

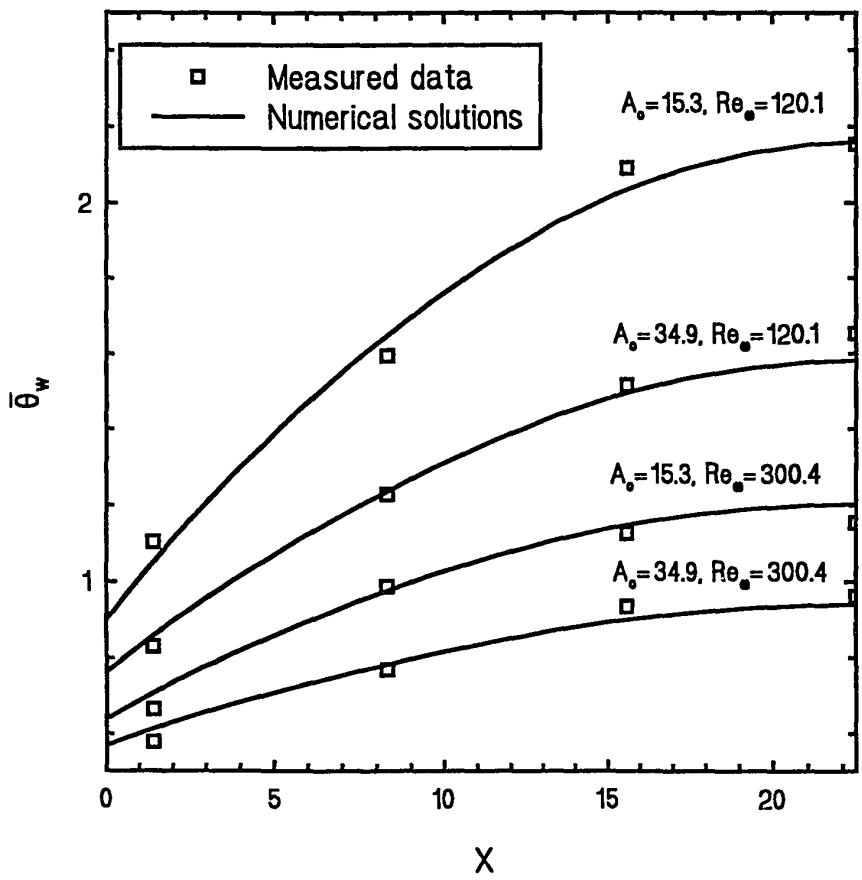

Fig. 8.4 Effects of the dimensionless oscillation amplitude of fluid A_o and the kinetic Reynolds number Re_ω on the cycle-averaged wall temperature at L/D=44.8

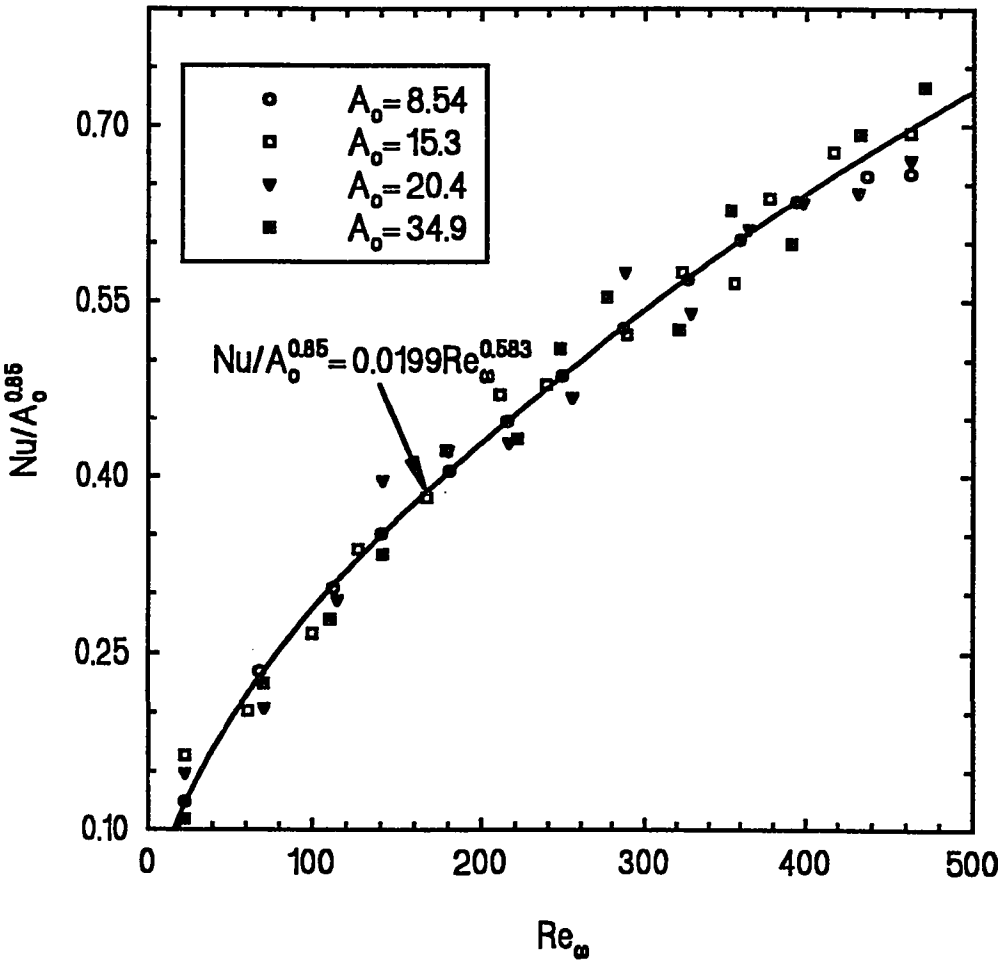

Fig. 8.5 A correlation equation based on the experimental data for the cycle-space averaged Nusselt number

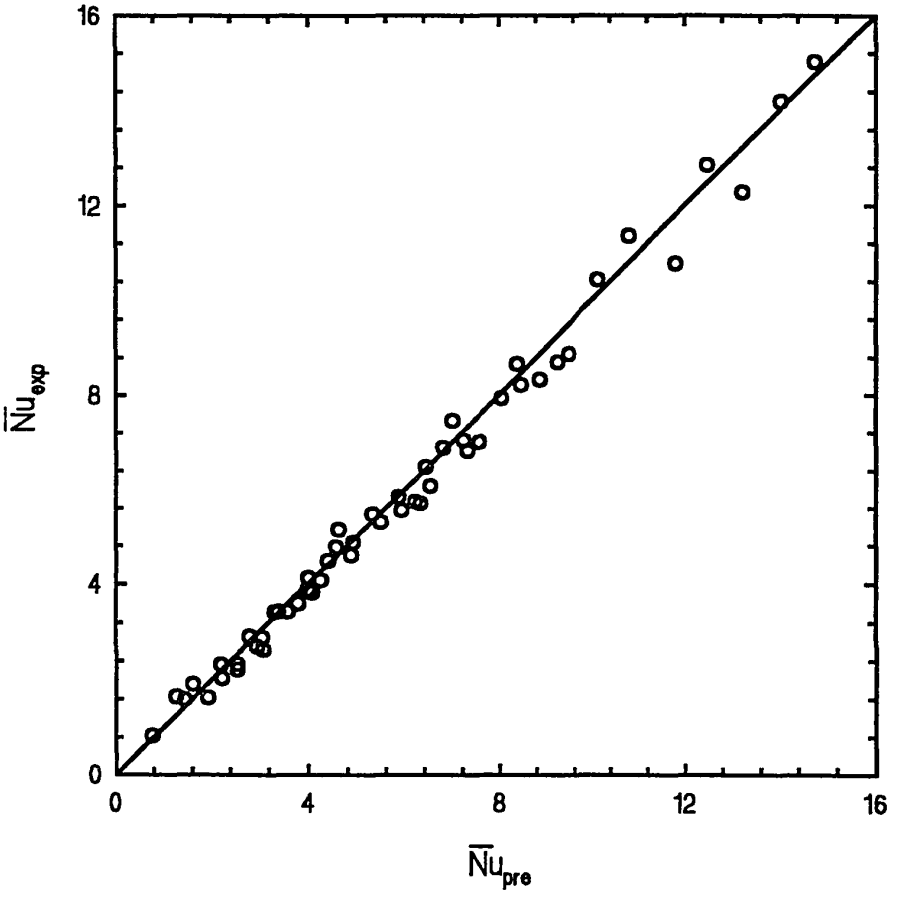

Fig. 8.6 The accuracy of the correlation equation

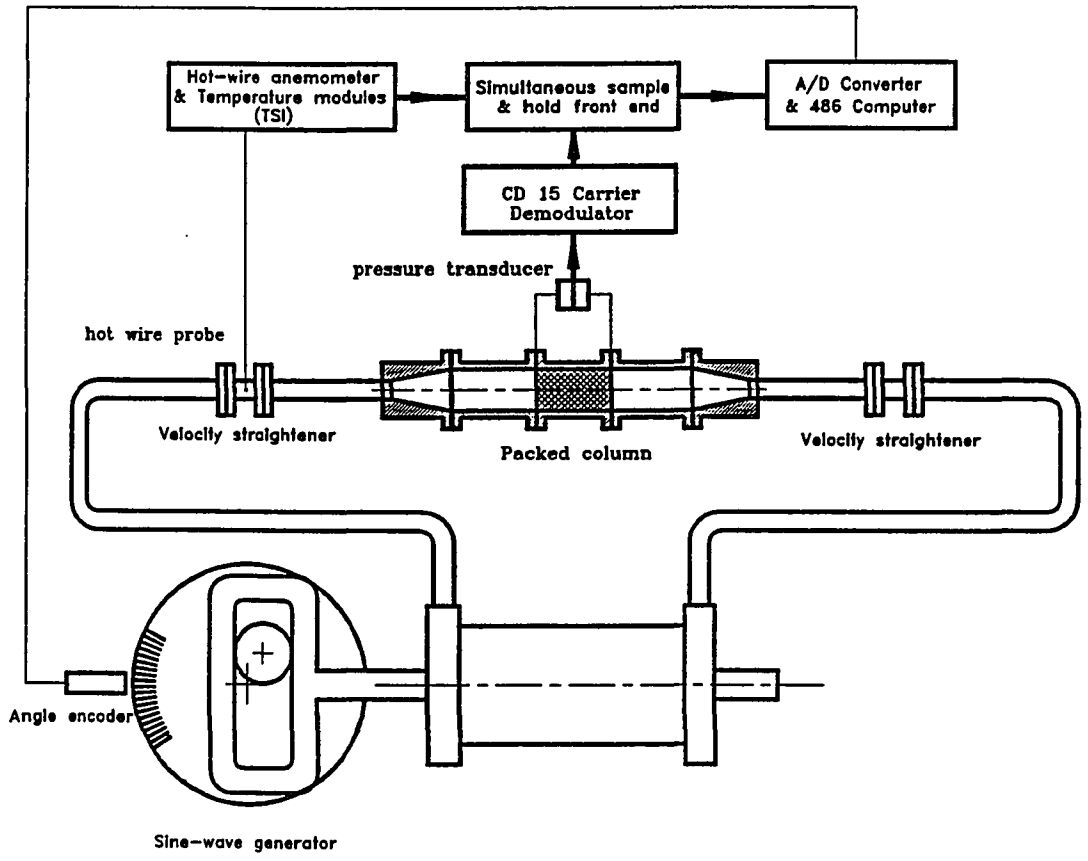

Fig. 9.1 Schematic diagram of experimental apparatus

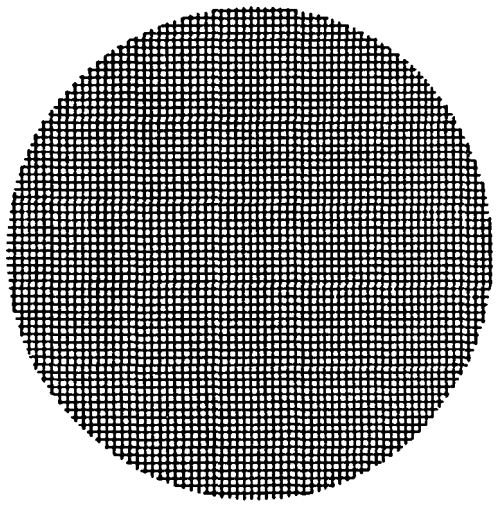

Fig. 9.2a Woven-screens

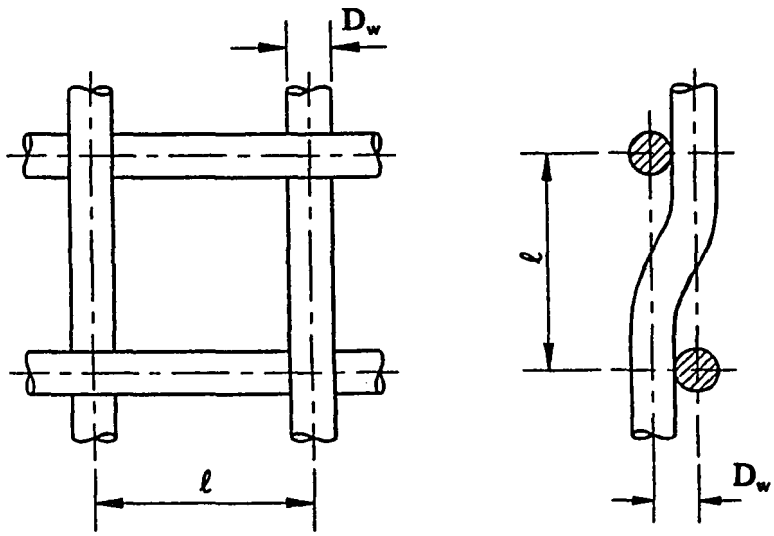

Fig. 9.2b Mesh unit geometry

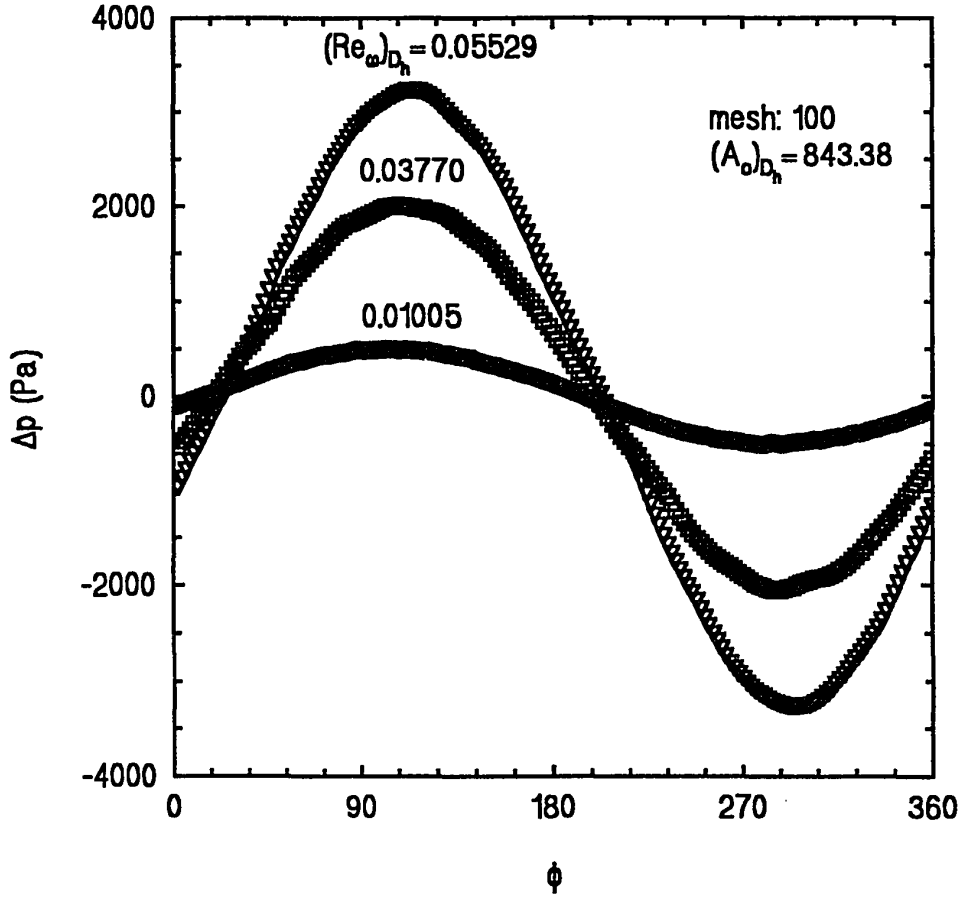

Fig. 9.3 Typical variations of the ensemble-averaged pressure drop for $(A_o)_{D_h}$ =843.38 and at $(Re_\omega)_{D_h}$ =0.01005, 0.03770, and 0.05529

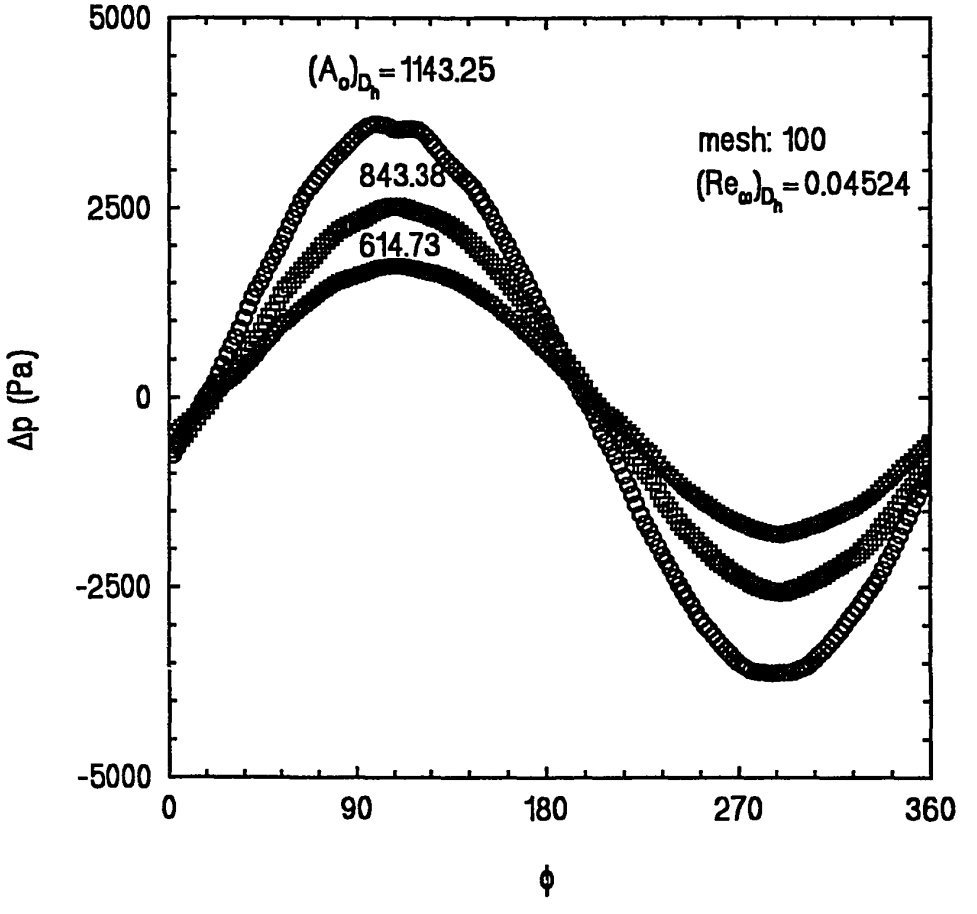

Fig. 9.4 Typical variations of the ensemble-averaged pressure drop for $(Re_\omega)_{D_h}$ =0.04524 and at $(A_o)_{D_h}$ =614.73, 843.38, and 1143.25

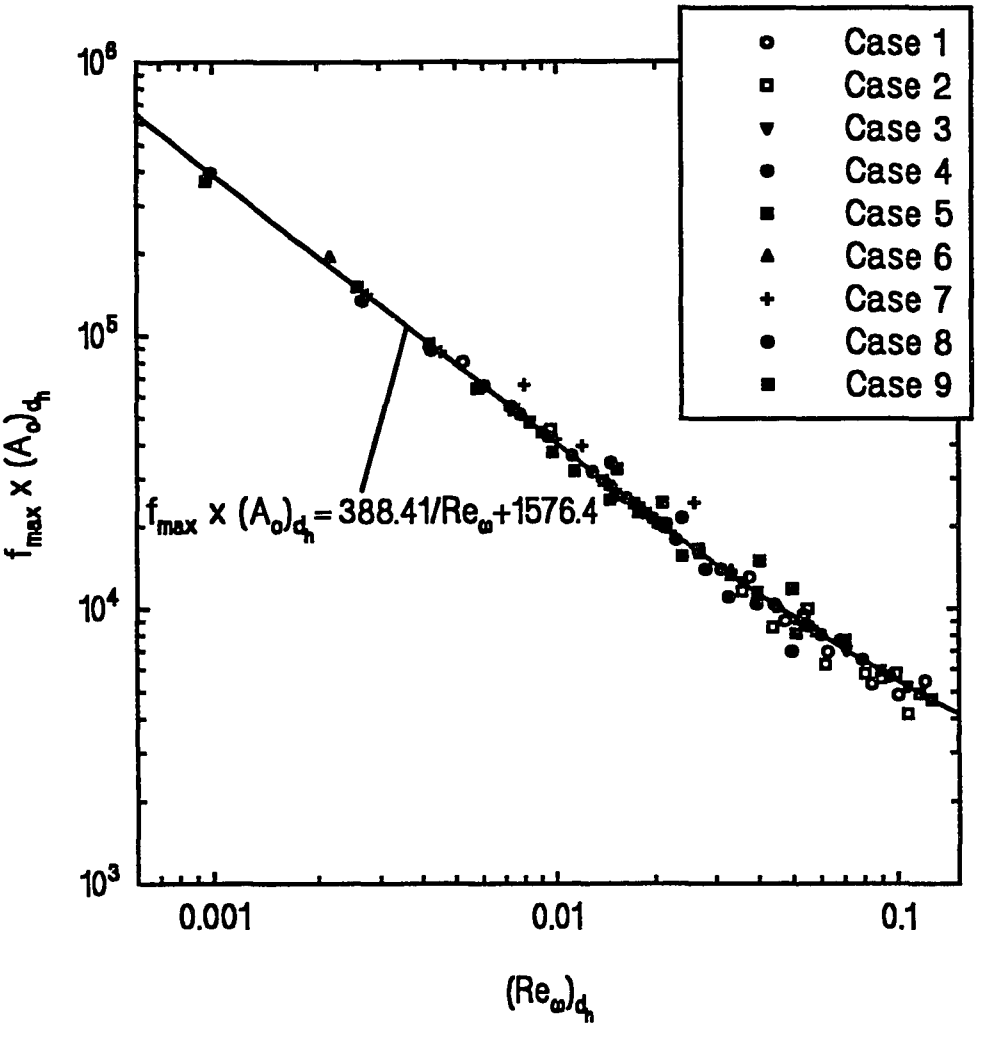

Fig. 9.5 A correlation equation of the maximum pressure drop factor interms of $(A_o)_{D_h}$ and $(Re_\omega)_{D_h}$

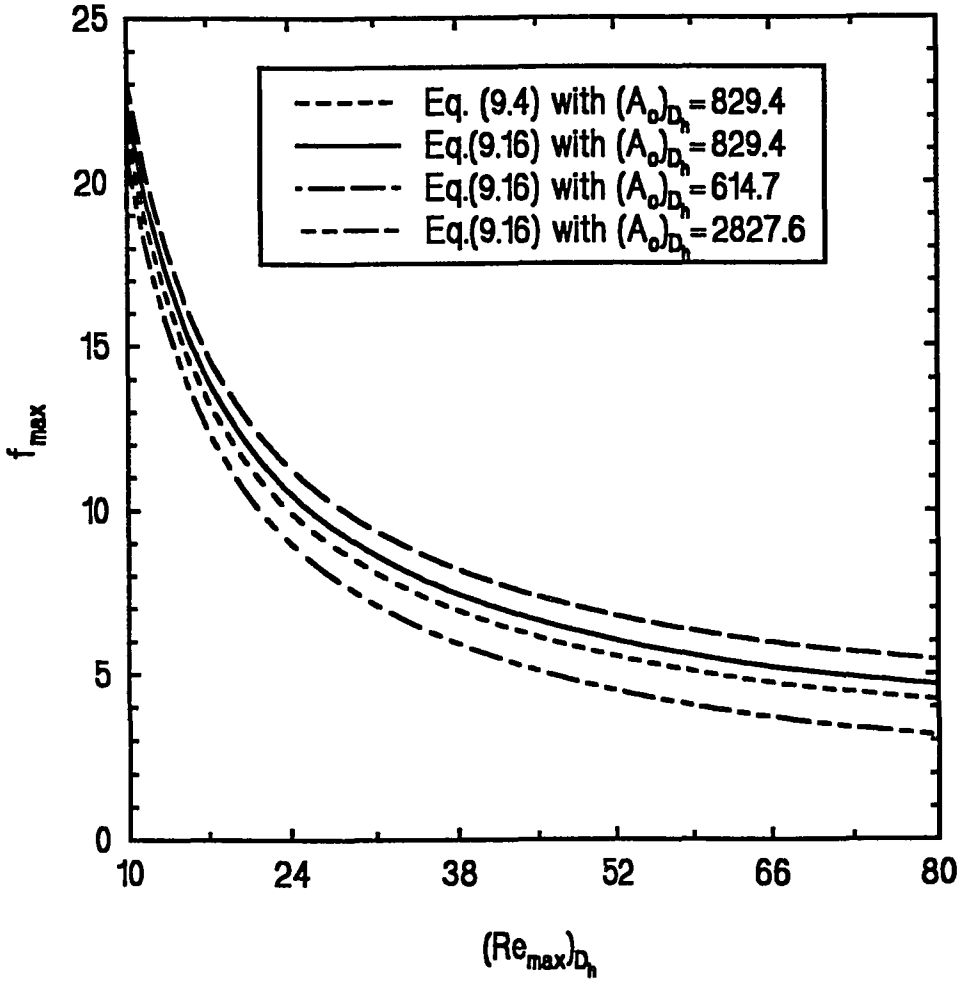

Fig. 9.6 Comparison of the present correlation equation of the maximum pressure drop factor with that obtained by Tanaka et al. (1990)

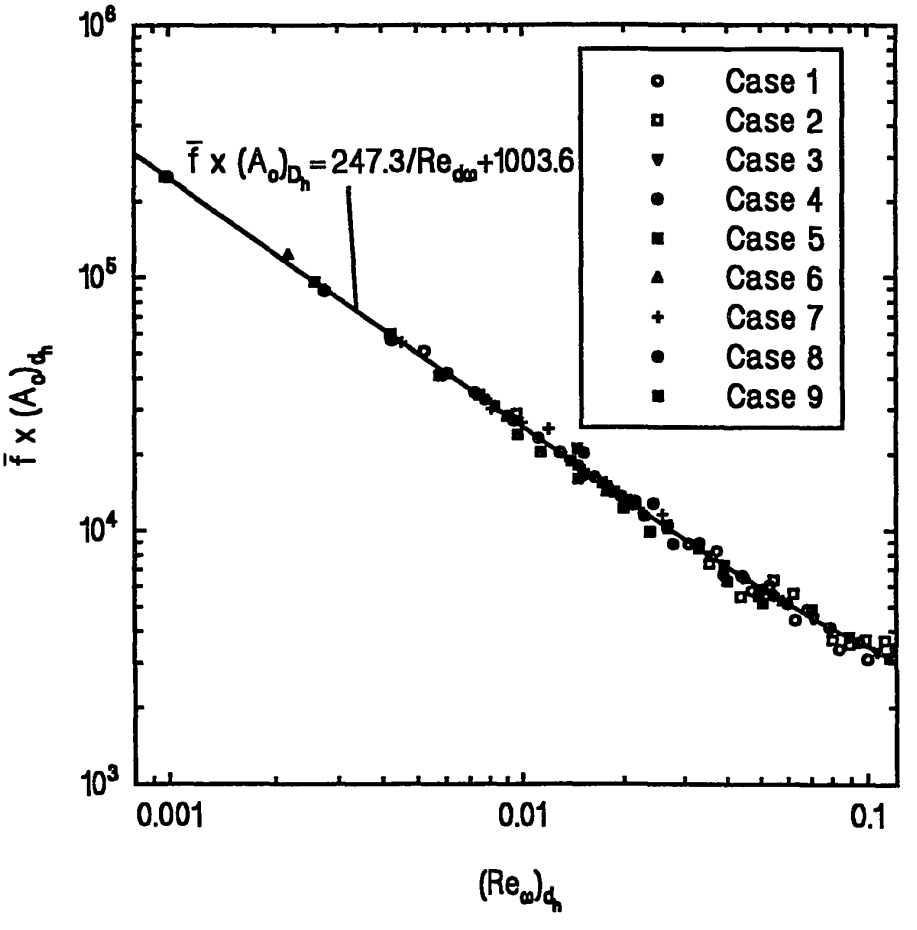

Fig. 9.7 A correlation equation of the cycle-averaged pressure drop factor in terms of $(A_o)_{D_h}$ and $(Re_\omega)_{D_h}$

APPENDIX A

BLOCK DIAGRAM OF THE DATA ACQUISITION AND PROCESSING SOFTWARE

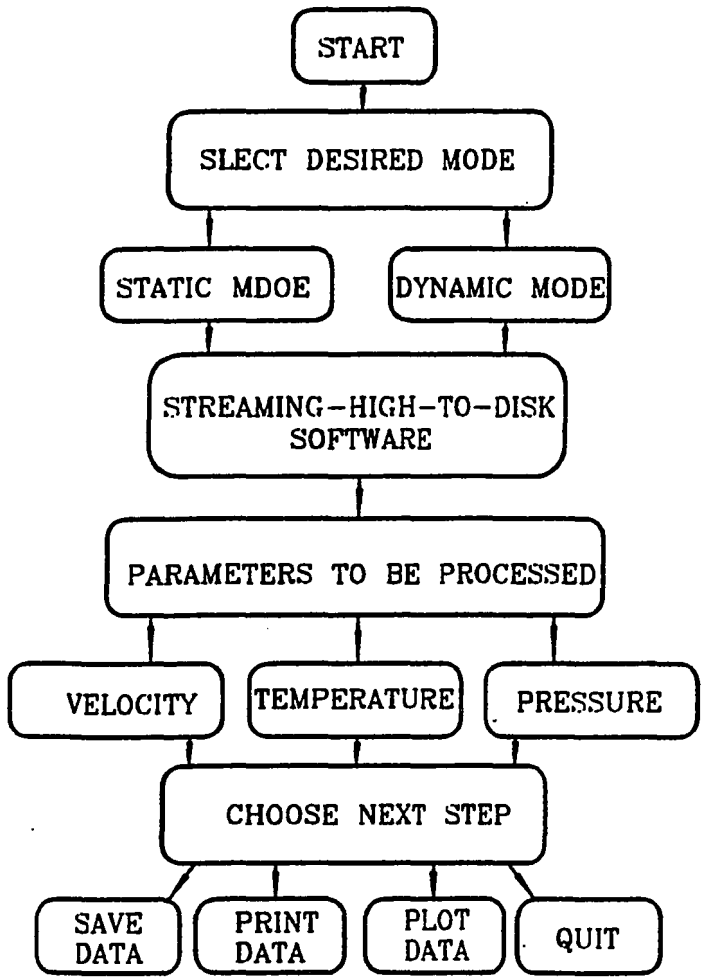

APPENDIX B

MEASUREMENT UNCERTAINTIES

An uncertainty analysis based on the method described by Moffat 1988 was performed. Uncertainty in the kinetic Reynolds number Re_ω or $(Re_\omega)_{D_h}$ was dominated by the measurement of oscillation frequencies, and was estimated at 2.3 %. Uncertainty in the dimensionless oscillation amplitude of the fluid A_o or $(A_o)_{D_h}$ was computed to be less than 0.5%, which was primarily influenced by errors in measuring the stroke and the diameter of the air pump. The statistical uncertainty in the ensemble-averaged velocity is estimated to be 2.5%, assuming uncorrelated, normally distributed measurements with a 95% confidence level. Similarly, the statistical uncertainty in the ensemble-averaged pressure drops varies from 6 to 9%. The main source of error in the reported results on the friction coefficient and the pressure drop factor is statistical uncertainty in the ensemble-averaged quantities of velocities and pressure drops. The largest uncertainties in the measurements the cycle-averaged friction coefficient $\bar{c}_{f,exp}$ and the cycle-averaged pressure drop factor $\bar{f}$ were computed to be about 11.5% and12.5%, respectively. The experimental errors associated with the Nusselt numbers were limited primarily by the measurements of temperatures and heat flux. The largest uncertainties in the space-cycle averaged Nusselt numbers $\overline{Nu}$ were estimated to be about 9%.

REFERENCES

Akhavan, R., Kamm, R. D. and Shapiro, A. H., 1991, "An Investigation of the Transition to Turbulence in Bounded Oscillatory Stokes Flows, Part 1: Experiments," *Journal of Fluid Mechanics*, Vol. 225, pp. 423-444.

Charrenyon, P. O., 1984, "Convective Heat Transfer Enhancement in Unsteady Channel Flow - A Review," in P. H. Roethe (ed.): *Forum on Unsteady Flows*, ASME FED- Vol. 15, presented at the winter annual meeting of the ASME, New Orleans, LA, Dec. 9-13.

Chen, N. C. J. and Griffin, F. P., 1983, " Effects of Pressure Drop Correlations on Striling Engine Predicted Performance.", *18th IECEC*, PP 708-713.

Cooper, W. L., Yang, K. T. and Nee, V. W., 1993, "Fluid Mechanics of Oscillatory and Modulated Flows and Associated Applications in Heat and Mass Transfer-A Review," *Journal of Energy, Heat and Mass Transfer*, Vol. 15, 01-19.

Drake, D. G., 1965, "On the Flow in a Channel Due to a Periodic Pressure Gradient," *Quarterly Journal of Mechanics and Applied Mathematics*, Vol. 18, Part 1, pp. 1-10.

Gedeon, D., "Mean-Parameter Modeling of Oscillating Flow," *Journal of Heat Transfer*, Vol. 1087, pp.513-518, 1986.

Goldaberg, P., 1958, "A Digital Computer Simulation for Laminar Flow Heat Transfer in Circular Tubes," *J. Heat Transfer*, Vol. 108,

Greeard, J. H., 1971, "An Experimenatl Investigation of Pulsating Turbulent Water Flow in a Tube," *J. Fluid Mech.*, Vol. 46, pp. 43-64.

Hino, M., Sawamoro, M. Takasu, S., 1976, "Experiments on the Transition to Turbulence in an Oscillating Pipe Flow," *J. Fluid Mech.* Vol. 75, Part 2, pp 193-207.

Hino, M., Kashiwayanagi, A., Hara, T., 1983, "Experiments on the Turbulence Statistics and the Structure of a Reciprocating Oscillatory Flow," M. S. Thesis, Department of Mechanical Engineering, MIT, Cambridge, MA.

Hwang, M. F. and Dybbs, A., 1983, "Heat transfer in a tube with oscillatory flow," *ASME Paper* #83-WA/HT-90.

Iguchi, M. Ohmi, M., 1983, "Analysis of Free Oscillating Flow in a U-Shaped Tube," *Bull. JSME,* Vol. 25, pp 1398-1405.

Iwabuchi , M. and Kanzaka, M. , 1982, "Experimental investigation into heat transfer under the periodically reversing flow condition in a heated tube," *J. Mech. Engineers,* C24/82, pp.135-139.

Kurzweg, U. H., Lindgren, E. R., and Lothrop, B., 1989, "Onset of Turbulence in Oscillating Flow at Low Womersley Number," *Phys. Fluids,* V. A1.

Mao, Zhuo-Xiong and Hanratty, Thomas J., 1986, "Studies of the Wall Shear Stress in a Turbulent Pulstaing Pipe Flow," *J. Fluid Mech.*, Vol. 170, pp. 545-564.

Martini, W. R., 1978, "Design Manual for Stirling Engines," *DOE/NASA Report.*

Miyabe, H., Takahashi, S., Hamaguchi, K., 1982, "An Approach to the Design of Stirling Engine Regenerator Matrix Using Packs of Wire Gauzes.", *Proc. 17th IECEC*, pp. 1839-1844.

Ohmi, M. Iguchi, M., Urahata, I., 1982, "Flow Patterns and Frictional Losses in an Oscillating Pipe Flow," *Bulletin of JSME,* Vol. 25, No. 202, pp 536-543.

Park, J. and Baird, M., 1970, "Transition to Turbulence in an Oscillating Manometer," *Canadian Journal of Chemical Engineering*, Vol. 48, pp 491-495.

Patankar, S. V., 1980, *Numerical Heat Transfer and Fluid Flow*, Hemisphere, Washington, D. C..

Radebaugh, R., 1991, "Progress in Cryocoolers", *Application of Cryogenics Technology,* Vol. 10, pp. 1-14.

Ramaprian, B. R. and Tu, S. W., 1983, "Fully Developed Periodic Turbulent Pipe Flow, Part 2. The Detailed Structure of the Flow," *J. Fluid Mech.*, Vol. 137, pp. 59-81.

Richardson, E. G. and Tyler, E., 1929, "The Transverse Velocity Gradient near the Mouths of Pipes in Which an Alternating or Continuous Flow of Air is Established," *Proceedings. Physics Society. London*, Vol. 42, Part 1, pp.1-15.

Rix, D. H., 1984, "Gas Process Asymmetry in Stirling Cycle Machines, ", Ph. D Thesis, Engineering Dept., Cambridge University.

Roach , P. D. and Bell, K. J., 1988, "Analysis of pressure drop and heat transfer data from the reversing flow test facility," *Rept. # ANL/MCT-88-2*, Argonne National Laboratory, Argonne, Illinois.

Sergreev, S., 1966, "Fluid Oscillations at Moderate Reynolds Numbers," *Fluid Dynamics*, Vol. 1, No. 1, pp 121-122.

Seume, J. R., 1988, "An Experimental Investigation of Transition in an Oscillating Pipe Flow," Ph. D dissertation, University of Minnesota, Minneapolis, Minnesota, USA.

Sexl, T., 1930, "Uber den von entdeckten Annulareeffekt," *Zeitschrift fuer Physik*, Vol. 61, pp.349-362.

Siegel, R., 1987 "Influence of Oscillation-Induced Diffusion on Heat Transfer in a Uniformly Heated Channel," *ASME Transactions.*, Vol.109, pp.244-247.

Simon, T. W. and Seume, J. R., 1988, "A survey of oscillating flow in Stirling engine heat exchanger," *NASA Contract Report* 182108.

Tanaka, M. Yamshita, I. and Chrisaka, F., 1990, "Flow and Heat Transfer Charaterisctics of the Stirling Engine Regenerator in an Oscillating Flow," *JSME International J.* Vol. 33, pp 283-289.

Tang, X. G., 1992, "An Experimental Study on Oscillatory Heat Transfer in a Circular Tube with Periodically Reversing Flow,", M. S. Thesis, Univ. of Hawaii, Honolulu, Hawii.

Taylor, D. R. and Aghili, H., 1984, "An Investigation of Oscillating Flow in Tubes, 19th Intersociety Energy Conversion Engineering Conference," *Proceedings (IECEC Paper 849716)*, pp. 2033-2036. American Nuclear Society.

Tong, L. S., and London, A. L., 1957, "Heat-Transfer and Flow-Friction Charateristics of Woven-Screen and Cross-Rod Matrices," *Trans. ASME*, pp 1558-1570.

Uchida, S., 1950,"The Pulsating Viscous Flow Superposed on the Steady Laminar Motion of an Incompressible Fluid in a Circular Pipe,"*ZAMP*, Vol. 7, pp.403-422.

Urielli, I., 1977, "A Computer simulation of Stirling Cycle Machies, Ph. D Thesis, Univ. Witwatersrand, Johannesburg, S. A..

Walker, G. and Vasishta, V., 1971, "Heat Transfer and Friction Charateristics of Wire-Screen Stirling Engine Regenerators," *Adv. Cryog. Engng.*,Vol. 16, pp. 324-332.

Walker, G. and Wan, W. K., 1972, "Heat Transfer and Fluid Friction Charateristics of Dense-Mesh Wire Screen Regenerator Matrices at Cryogenics Temperatures," *Proc. 4th Int. Cryog. Engng. Conf.*, Eindhoven, Netherland, pp. 93-96.

Wommersley, J. R., 1955, "Method for the Calculation of Velocity, Rate of the Flow and Viscous Drag in Arteries When the Pressure Gradient is Known," *Journal of Physiology*, Vol. 127, pp.553-563.

Wu, P. , Lin, B., Zhu, S., He, Y., Ren C., and Wang, F., 1990, "Investigation of oscillating flow resistance and heat transfer in the gap used for cryocoolers," *13th IECEC Proceedings*.

Zhao, T. and Cheng, P. , 1994, "The Friction Coefficient of A Fully-Developed Laminar Oscillatory and Reversing Flow in a Circular Pipe," submitted for publication